Habilitation à Diriger des Recherches

Présentée et soutenue publiquement le

Spécialité : Mathématiques

Présenté par

Thibault LIARD

Monitoring and Management of Traffic flow

Devant le jury composé de :

M.	Samir Adly	Chargé de suivi
M.	Boris Andreianov	Rapporteur
M.	Franck Boyer	Rapporteur
M.	Jean-Michel Coron	Examinateur
Mme	Carlotta Donadello	Examinatrice
M.	Pierre Lissy	Examinateur
M.	Vincent Perrollaz	Examinateur
M.	Emmanuel Trélat	Rapporteur

Thibault LIARD :

XLIM - Université de Limoges

Adresse électronique : thibault.liard@unilim.fr

Remerciements

Je voudrais tout d'abord remercier chaleureusement Samir Adly d'avoir accepté d'être le chargé de suivi de cette HDR et de m'avoir accompagné et conseillé depuis mon arrivée à XLIM. Je tiens également à remercier Boris Andreianov, Franck Boyer et Emmanuel Trélat d'avoir accepté de rapporter cette HDR. Je leur suis très reconnaissant pour l'intérêt qu'ils ont porté à ce manuscrit ainsi que pour leurs remarques et commentaires. Je remercie aussi Jean-Michel Coron, Carlotta Donadello, Pierre Lissy et Vincent Perrollaz de me faire l'honneur de participer à ce jury et d'assister à cette soutenance. C'est pour moi un grand plaisir de pouvoir présenter ce travail devant vous.

Depuis mon arrivée à XLIM, j'ai la chance de travailler au sein du laboratoire dans une ambiance à la fois agréable et conviviale. Merci à Emmanuel, Cyrille, Mercedes, Ilaria, Laure-Anne, Nicolas, Olivier et Tristan avec qui je partage de nombreux repas du midi, souvent suivis de siestes plus ou moins longues en écoutant les histoires d'Emmanuel sur les brocantes ou encore celles de Cyrille sur l'histoire et le tennis. Merci aussi à Ilaria qui arrive à me supporter malgré la présence envahissante de ma trottinette, de mes affaires de sport et le joyeux désordre qui règne sur mon bureau, sans parler du temps perdu à faire de petites sessions potins autour d'un bon café. Je voudrais également remercier tout particulièrement Maxime pour avoir largement contribué à mon intégration à Limoges, en me faisant découvrir la ville et quelques-uns de ses QGs. Je suis aussi très content que Laure-Anne soit arrivée à Limoges : même si les discussions entre un mathématicien et une biologiste ne sont pas toujours simples, on progresse, et je suis convaincu que cela mènera à de très belles recherches. Un grand merci enfin à Julie et Debora pour leur efficacité redoutable et leur aide précieuse dans toutes les démarches administratives.

Je veux aussi remercier Yannick, qui a toujours été présent et à l'écoute lorsque j'en ai eu besoin, et surtout pour m'avoir préparé au monde de la recherche et permis d'arriver là où j'en suis aujourd'hui. Je remercie également Vincent pour son aide mathématique, même s'il me faut parfois plusieurs jours pour tout comprendre. Je termine avec Pierre, mon directeur « spirituel », avec qui je continue à collaborer, à échanger sur les mathématiques et sur la vie, et avec qui j'ai le plaisir de co-encadrer avec Amaury la thèse de Nail.

En dehors du cadre académique, je souhaite aussi remercier mes amis qui m'accompagnent depuis de nombreuses années, et plus particulièrement Flo (pour la découverte culinaire de la Belgique, les discussions de fins de soirées et les nombreuses parties de TFT), Antoine (pour la découverte culinaire de la Guadeloupe et les cartes postales) et Pierre (pour la découverte culinaire de la place d'Italie et Veigar/Syndra mid). Je remercie également la Team Rocket avec qui nous pourchassons les vilains en voiture de police tous les lundis et jeudis, avec quelques accidents à rapporter ; un vrai bol d'air qui permet de décompresser de la semaine. Merci aussi à Gianni et Chloé, toujours prêts à partir en voyage, même si cela m'oblige parfois à enchaîner les fast-foods ou à jouer le vendeur/bricoleur.

Je terminerai ces remerciements en évoquant les personnes qui comptent le plus dans ma vie : ma famille. Sans vous, sans votre soutien constant et votre amour, rien de tout cela n'aurait été possible. Je vous dois énormément. Merci du fond du cœur. Je vous aime.

Contents

Chapter 1

Introduction

1.1 Presentation of the thesis

The objective of this manuscript is to monitor and manage vehicular traffic flow on highways or road networks using sensors and controllers such as toll gates or/and autonomous vehicles (AVs). To this end, we rely on dynamical models to capture the evolution of vehicular traffic. At macroscopic scale, it is modeled by Partial Differential Equations (PDEs) [77, 87] having the following form

$$\partial_t \rho(t,x) + \partial_x f(\rho(t,x)) = 0, \ (t,x) \in \mathbb{R}_+^* \times \mathbb{R}, \tag{1.1.1}$$

where the function $(t,x) \mapsto \rho(t,x)$ stands for the density of cars at time t and at position x. PDEs of this form are called conservation laws since the variation of the quantity ρ is given only by the amount of flux going through its boundary. Such models are well suited to describe large-scale traffic phenomena but they also have intrinsic mathematical difficulties, such as the development of discontinuities in finite time and the need to select a unique physical weak solution of (1.1.1). The most standard criteria for selecting a unique weak solution are the so-called entropy conditions introduced by Kruzhkov [65], which are inspired by fluid dynamics. However, weak-entropy solutions alone do not capture the effects of tollgates or AVs on traffic flow. To account for these features, alternative notions of weak solutions of (1.1.1) will be considered, based either on a flux-constrained PDE or on coupled PDE–ODE systems. The flux-constrained PDE models the presence of tollgates along a highway, while the coupled PDE–ODE model describes the impact of AVs on traffic flow. In the PDE–ODE framework, the Ordinary Differential Equations (ODEs) represent the trajectories of the AVs. They impact the traffic flow, modeled by the PDE, through moving flux constraints, that locally reduce the road capacity.

Our goal is to design controllers so as to positively influence traffic flow, for instance by reducing total travel time or overall fuel consumption. The controllers act on the traffic flow through the reduction of road capacity at tollgate locations and/or by modifying the maximum speed of AVs. To construct controllers, we have to study optimal control and stabilization problems for systems of conservation laws. Due to the presence of discontinuities in the road density ρ, the cost functions associated with optimal control problems are generally non-differentiable, making the derivation of first-order optimality conditions challenging. Moreover, these discontinuities, together with switching and delay phenomena, significantly complicate stability analysis and the derivation of stabilization results.

There exist a large variety of controllers dealing with stabilization of hyperbolic systems as Proportional controller, Proportional-Integral controller [69] or Sliding Mode Controller [70]. These laws require a good and accurate knowledge of road density ρ in (1.1.1). In [83, 94], the mass of the weak-entropy solution of (1.1.1) over the segment $[0,L]$ is needed to stabilize (1.1.1) around a stationary point. This highlights the need for efficient state reconstruction algorithms using measurements from fixed sensors but also capable of dealing with GPS measurements. Accurate macroscopic state reconstruction from probe vehicle data requires a clear understanding of the relationship between microscopic and macroscopic models.

In Part I, we develop efficient traffic state reconstruction methods capable of exploiting heterogeneous data sources, including fixed sensors and sparse GPS measurements from probe vehicles. More precisely, in Chapter 2, we give a short review of microscopic and macroscopic traffic models, including Follow-the-Leader systems, the LWR model, and second-order models as ARZ and GARZ. We also explain how the impact of AVs on traffic flow can be modeled throught moving flux constraints. Chapter 2 also discusses the challenges of reconstructing macroscopic traffic density from limited microscopic data and motivates the use of learning approaches based on rigorous micro-to-macro convergence results. In Chapter 3, we prove existence, uniqueness, and stability results for coupled PDE–ODE traffic models that model the impact of AVs on traffic flow. The main difficulty lies in the presence of non-classical shock waves, shocks that violate the Lax entropy condition. As a consequence, standard weak-entropy frameworks for conservation laws cannot be applied directly. Chapter 3 also focuses on the reconstruction of states from sparse data. It includes a detailed study of inverse problems for scalar conservation laws and introduces a machine-learning-based reconstruction framework with theoretical convergence proofs to weak-entropy solutions of (1.1.1). In Chapter 4, we extend the discussion to traffic flow on road networks. We recall how to construct consistent coupling conditions at junctions using the theory of generalized germs ($\mathcal{G}$-solution from [4, 5, 79]) and realistic junction configurations (merges, priority, spillover effects). Then, we formulate open problems related to the construction of physically realistic germs, existence theory on networks, and micro-to-macro limits for networked traffic models.

In Part II, we develop control strategies for conservation laws to have a positive impact on traffic flow. In chapter 5, we discuss the limitations of applying existing stabilization techniques in the presence of discontinuous waves, entropy boundary conditions, and finite propagation speed. In Chapter 6, we present the main results on stabilization of $\mathcal{G}$-solutions of conservation laws using maximum flow controllers at junction, such as toll gates. We also analyze optimal control problems aimed at reducing total fuel consumption. We show numerically that controlled autonomous vehicles can have a positive impact on overall traffic flow. In Chapter 7, we extend the discussion to the construction of open-loop optimal controllers and feedback controllers for traffic networks.

Overall, the manuscript provides a unified framework for modeling, monitoring, and controlling traffic flow, based on rigorous mathematical analysis. It establishes well-posedness results for coupled PDE–ODE models with autonomous vehicles, proposes reconstruction methods with theoretical guarantees under sparse data, and develops robust control strategies for traffic management. The work also opens several perspectives on traffic flow on networks, contributing to the development of realistic and mathematically consistent traffic control systems, see figure below for a schematic view of the thesis.

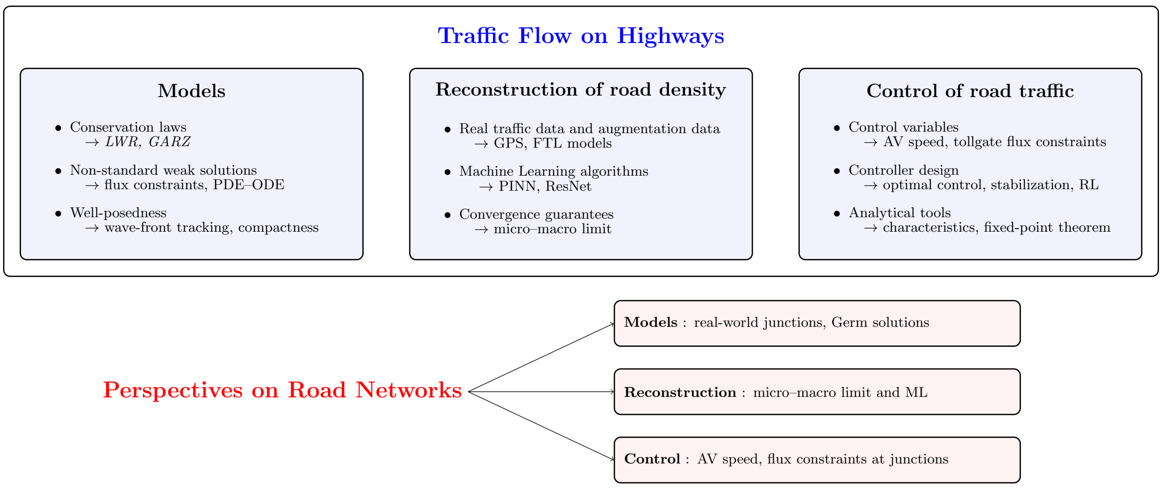

1.2 Publication, supervision and funding received

1.2.1 List of publications

Publications and pre-publications presented in this thesis

1. A multiscale second order model for the interaction between AV and traffic flows: analysis and existence of solutions; A. Hayat, T. Liard, B. Piccoli, preprint 2025.
2. Stabilization of conservation laws for G-solutions with application to traffic flow; T. Liard and V. Perrollaz, preprint 2025.
3. Traffic Flow Reconstruction from Limited Collected Data; N. Baloul, A. Hayat, T. Liard and P. Lissy, accepted to 2025 IEEE 64th Conference on Decision and Control (2025).
4. A PDE-ODE model for traffic control with autonomous vehicles; T. Liard, R. Stern and M.L Delle Monache, Networks and Heterogeneous Media 2023, Volume 18, Issue 3: 1190-1206 (2023).
5. Analysis and numerical solvability of backward-forward conservation laws; T.Liard and E. Zuazua, SIAM Journal on Mathematical Analysis, Vol. 55, No. 4. pp. 1949-1968, doi:10.1137/22M147872 (2023).
6. Initial data identification for the one-dimensional Burgers equation; T.Liard and E. Zuazua, IEEE Transactions on Automatic Control, doi: 10.1109/TAC.2021.309621 (2021).
7. On entropic solutions to conservation laws coupled with moving bottlenecks; T.Liard and B.Piccoli, Communications in Mathematical Sciences, Vol. 19, No. 4. pp. 919-945 (2021).
8. A controlled multiscale model for traffic regulation via autonomous vehicles; M. Garavello, P. Goatin, T. Liard and B. Piccoli, J. Differential Equations, https://doi.org/10.1016/j.jde.2020.04.031 (2020).
9. Optimal driving strategies for traffic control with autonomous vehicles; T.Liard, R.Stern and M.L Delle Monache. IFAC World Congress, Berlin, Germany, IFAC-PapersOnLine, 53(2), 5322-5329 (2020).
10. Traffic reconstruction using autonomous vehicles; M.L. Delle Monache, T.Liard, B. Piccoli, R. Stern, D. Work. SIAM Journal on Applied Mathematics, Vol. 79, No. 5. pp. 1748-1767 (2019).
11. Well-posedness for scalar conservation laws with moving flux constraints; T. Liard and B. Piccoli, SIAM Journal on Applied Mathematics. No. 2. pp 641–667 (2019).
12. The Riemann Problem for the GARZ Model with a moving constraint; T. Liard, F. Marcellini, B. Piccoli. XVII International Conference (HYP2018) on Hyperbolic Problem, vol 10, pages 524-530 (2018).

Publications and pre-publications posterior to the PhD thesis, but not presented in this thesis.

1. Super-twisting sliding mode control for the stabilization of a linear hyperbolic system; I. Balogoun, S. Marx, T. Liard, F. Plestan, IEEE Control Systems Letters, vol. 7, pp. 1-6, doi: 10.1109/LCSYS.2022.3186230 (2023).
2. Boundary sliding mode control of a system of linear hyperbolic equations: a Lyapunov approach; T. Liard, I. Balogoun, S. Marx, F. Plestan, Automatica, Volume 135, 109964 (2022).

PhD Publications

1. Non-localization of eigenfunctions for Sturm-Liouville operators; T. Liard, P. Lissy and Y. Privat, J. Differential Equations 264, no. 4, 2449–2494 (2018).
2. A Kalman rank condition for the indirect controllability of coupled systems of linear operator groups; T. Liard and P. Lissy, P. Math. Control Signals Syst. 29: 9. https://doi.org/10.1007/s00498-017-0193-x (2017).
3. How to estimate observability constants of one-dimensional wave equations? Propagation versus Spectral methods; A. Haraux, T. Liard and Y. Privat, J. Evol. Eq. 16, 825–856 (2016).

1.2.2 Supervisions

Internships and master students

- Shun Arakawa, 2025-2026, 6 months, co-advised with Olivier Ruatta and Tristan Vaccon.
- Kein Ebindja, 2025, 3 months.
- Alexandre Paulin, 2024, 2 months, co-advised with Francisco Silva.
- Anais Rat, 2017, 2 months, co-advised with Benedetto Piccoli.

PhD students

- Nail Baloul (supervised at 45%), started in October 2024 (co-advised with Amaury Hayat and Pierre Lissy).

Postdoctoral researchers

- Laure Anne Poissonnier, started in June 2025 for a duration of 1 year.
- Kala Agbo, started in October 2025 for a duration of 1 year.

1.2.3 Funding received

- Appel à projets scientifiques exploratoires 2024, Université de Limoges entitled "Modeling the Impact of Individual and Collective Cognition on Ant Foraging". Duration : 1 year and half (2024-2025) Funding received : 12,500 €.
- AOI 2025, Université de Limoges, entitled "Reinforcement learning for polynomial system solving". Duration : 1 year (2025-2026). Funding received : 4,500 €.
- ANR JCJC, entitled "Connecting Deep learning with Dynamic models for Traffic flow Management". Duration : 4 year (2024-2028). Funding received 247,657 €.

Part I

Monitoring of Traffic flow model

Chapter 2

Traffic flow models, Autonomous Vehicles and Data Reconstruction

2.1 Impact of Autonomous Vehicles on Microscopic and Macroscopic Models

The advent of vehicle automation has the capability to substantially transform the management of transportation systems. As disruptive technologies such as autonomous vehicles come closer to reality, the potential for improved traffic control using Autonomous Vehicles (shortly AVs) as Lagrangian actuators in the traffic flow has been highlighted experimentally [91]. In [91], the authors set up an experiment on a single-lane ring road with more than 20 vehicles where traffic waves emerge consistently. Then, they demonstrate experimentally that an autonomous vehicle is able to dampen stop-and-go waves [92, 93, 95] that can arise even in the absence of geometric or lane changing triggers. These experimental findings suggest a paradigm shift in traffic management: it is possible to have a positive impact (total fuel consumption, travel time) from a limited number of probes using maximum flow controllers. To have a better understanding of traffic flow behavior and to design efficient controllers that stabilize it, the development and analysis of accurate models are essential. The modeling of vehicular traffic flow has historically evolved along two complementary paradigms: microscopic models and macroscopic models.

Microscopic models describe traffic flow at the individual vehicle level. Each vehicle is modeled as a particle whose dynamics are governed by a system of ODEs. Among the most studied microscopic models are the Bando (or Optimal Velocity) - Follow The Leader Model [9, 50], for any $i \in \{1, \cdots, N\}$,

$$\begin{aligned}
&\dot{x}_i(t) = v_i(t), \\
&\dot{v}_i(t) = a\tfrac{v_{i+1}(t)-v_i(t)}{(x_{i+1}(t)-x_i(t))^2} + b\left[V(x_{i+1}(t)-x_i(t)) - v_i(t)\right],
\end{aligned} \tag{2.1.1}$$

where $x_i(t)$ and $v_i(t)$ are respectively the position and velocity of the i-th vehicle. This model combines an optimal velocity part derived in [9] which represents the incentive of a driver to reach its "own" optimal velocity depending of the space between his vehicle and the vehicle in front, and a Follow The Leader (shortly FTL) part proposed in [50] which represents the incentive of the driver to mimic the vehicle in front. To model the impact of an AV on a single-lane ring road with more than 20 vehicles, as considered in the experimental study of [91], the system (2.1.1) is closed by assuming that the $(N+1)$-vehicle is the autonomous vehicle, which acts as the leader and also coincides with the first vehicle.

$$\begin{aligned}
&\dot{x}_{N+1}(t) = v_{N+1}, \\
&\dot{v}_{N+1}(t) = u(t), \\
&v_{N+1} = v_1, \\
&x_{N+1} = x_1
\end{aligned} \tag{2.1.2}$$

This model has been shown to accurately reproduce stop and go waves for a ring-road in [36, 41], both theoretically and numerically. In traffic flow applications, a natural question is : can we find a feedback controller that steers the system to a steady-state in speed, with all cars moving at same speed $\bar{v} = V(d)$ where $d \leq L/N$ and for any $i \in \{1, \cdots, N\}$, $d = x_{i+1} - x_i$?
For any arbitrary large ring road L and for any arbitrary large number of cars N, the authors in [58] prove that the system (2.1.1) with the feedback controller $u(t) = k(\bar{v} - v_{N+1})$ and $k < 0$ is locally exponentially stable around any steady state $\bar{v}$. The design of the controller u relies on the structure of the ring road, particularly its length L.

While microscopic models provide detailed insights into individual behaviors, they become computationally costly as the number of vehicles increases. This motivates the use of macroscopic models, which describe the evolution of aggregate quantities such as vehicle density $\rho(t, x)$ and flow $f(\rho)$. These models are formulated as Partial Differential Equations (PDEs) and are inspired by fluid dynamics. The classical macroscopic model is the Lighthill-Whitham-Richards (LWR) model, introduced independently by Lighthill and Whitham (1955) and Richards (1956), which uses the conservation law:

$$\partial_t \rho(t, x) + \partial_x f(\rho(t, x)) = 0,\ (t, x) \in \mathbb{R}_+^* \times \mathbb{R} \tag{2.1.3}$$

with $f(\rho) = \rho v(\rho)$, where $v(\rho)$ is a decreasing function of ρ to capture traffic congestion. This first-order model is capable of describing shock waves and the formation of traffic jams. Both theoretically and numerically, this family of equations is rather peculiar among all PDEs since one can show that for many smooth initial data ρ_0, the solution develops discontinuities in finite time, see Figure 2.1. As a consequence, the global (in time) existence of classical solutions fails. Considering weak solutions is quite natural, i.e for $(t, x) \in (0, +\infty) \times \mathbb{R}$, i.e for all $\varphi \in C_c^1(\mathbb{R}^2, \mathbb{R})$,

$$\int_{\mathbb{R}_+} \int_{\mathbb{R}} (\rho \partial_t \varphi + f(\rho) \partial_x \varphi) dx dt + \int_{\mathbb{R}} \rho_0(x) \varphi(0, x) dx = 0,$$

but uniqueness is lost and one finds some of those weak solutions to be wildly physically irrelevant to underlying physical situations, see Figure 2.2. Selection criteria for "admissible" weak solutions inspired by physics often bear the name of entropy solutions (see Kruzhkov [65]), i.e $\forall k \in \mathbb{R}$, $\forall \varphi \in C_c^1(\mathbb{R}^2, \mathbb{R}_+)$,

$$\int_{\mathbb{R}_+} \int_{\mathbb{R}} (|\rho - k| \partial_t \varphi + \operatorname{sgn}(\rho - k)(f(\rho) - f(k)) \partial_x \varphi) dx dt + \int_{\mathbb{R}} |\rho_0 - k| \varphi(0, x) dx \geq 0.$$

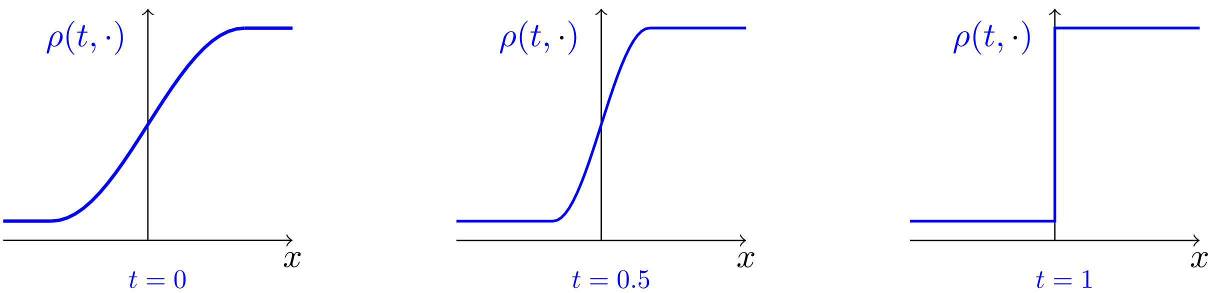

Figure 2.1 – Creation of a discontinuity (called shock) in finite time when f is a concave function

However, to model the impact of AVs on the traffic flow, another weak solution is selected using a coupled PDE-ODE and a point limitation of the flux created by autonomous vehicles [39], see Figure 2.3.

$$\partial_t \rho(t, x) + \partial_x (f(\rho(t, x))) = 0, \qquad (t, x) \in \mathbb{R}_+ \times \mathbb{R}, \tag{2.1.4a}$$

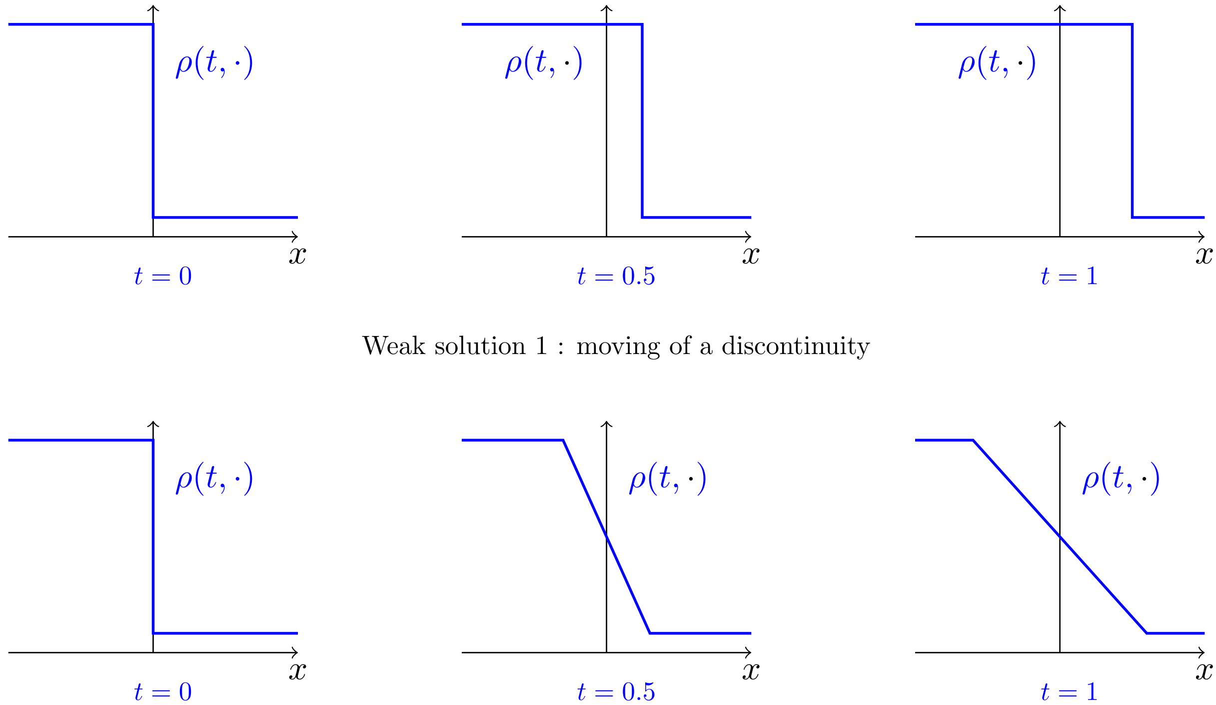

Weak solution 1 : moving of a discontinuity

Weak (entropy) solution 2 : dissipation of a discontinuity

Figure 2.2 – Non-uniqueness of weak solutions for conservation laws when f is a concave function

$$\rho(0,x) = \rho_0(x), \qquad x \in \mathbb{R}, \tag{2.1.4b}$$
$$f(\rho(t,y(t))) - \dot{y}(t)\rho(t,y(t)) \leq F_\alpha(\dot{y}) := \alpha \max_{\rho \in [0,\rho_{\max}]} (f(\rho) - \dot{y}\rho), \qquad t \in \mathbb{R}_+, \tag{2.1.4c}$$
$$\dot{y}(t) = \min(V_b, v(\rho(t,y(t)+))), \qquad t \in \mathbb{R}_+, \tag{2.1.4d}$$
$$y(0) = y_0. \tag{2.1.4e}$$

The ODE (2.1.4d) with (2.1.4e) describes the trajectory of the AV starting at $(t,x) = (0,y_0)$: the AV moves at its maximum speed $V_b \in (0, V_{\max})$ as long as the downstream traffic moves faster, otherwise it has to adapt its velocity accordingly to the traffic density in front. The AV is regarded as a slow moving vehicle, see Figure 2.3. It acts on the evolution of vehicular traffic through the moving constraint (2.1.4c). The left side of (2.1.4c) represents the flux of cars at the position of the AV in the AV reference frame. The quantity $F_\alpha(\dot{y}) := \alpha \max_{\rho \in [0,\rho \max]}(f(\rho) - \dot{y}\rho)$ in the right side of (2.1.4c) stands for the reduced maximum flow due to the presence of the AV.

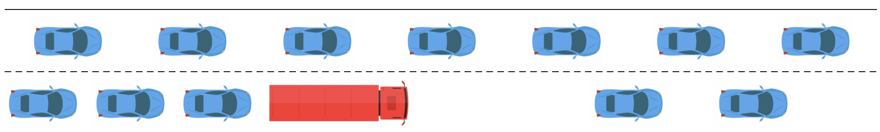

Figure 2.3 – Impact of an AV, regarded as a slow moving vehicle, on the traffic flow

To prove existence of solutions for (2.1.4), a standard method is to construct approximate solutions (ρ^n, y^n) of (2.1.4) using wave-front tracking algorithms proposed by Dafermos [37]. Due to the presence of the AV, a "non-classical" wave-front can be generated that violates the Lax entropy condition. Thus, a careful analysis has to be done to prove convergence of the approximate solutions. In [39], the authors proved the existence of (ρ, y) that satisfies (2.1.4a), (2.1.4b) and (2.1.4c). In [72, 73], we managed to prove existence and uniqueness of (2.1.4), see more details in Section 3.1.

However, the LWR model has limitations, especially in capturing the heterogeneity of driver behavior and second-order phenomena such as stop-and-go waves. To address this, second-order models have been developed, the most prominent being the Aw-Rascle-Zhang (ARZ) model [7, 96] and its generalization the Generalized Aw-Rascle-Zhang (GARZ) model [44]. The ARZ second-order model consists of two hyperbolic equations formulated to enforce the conservation of mass and momentum. A notable feature of this model is its ability to incorporate diverse velocity-density relationships corresponding to different driver behaviors. However, a key limitation arises from the fact that these heterogeneous driver profiles lead to vastly different densities at which traffic flow stagnates. To address this issue, the Generalized Aw-Rascle-Zhang (GARZ) model introduces a more flexible framework. It establishes a general functional relationship between traffic density and the velocity on an empty road. Unlike the classical ARZ model, the GARZ formulation allows all drivers to have a unique maximum density at which they stop. The GARZ model takes the form of

$$
\begin{aligned}
&\partial_t \rho(t,x) + \partial_x \left(\rho(t,x)\, V(\rho(t,x), w(t,x))\right) = 0, && (t,x) \in \mathbb{R}_+ \times \mathbb{R}, && \text{(2.1.5a)}\\
&\partial_t (\rho(t,x) w(t,x)) + \partial_x \left(\rho(t,x) w(t,x)\, V(\rho(t,x), w(t,x))\right) = 0, && (t,x) \in \mathbb{R}_+ \times \mathbb{R}, && \text{(2.1.5b)}\\
&\rho(0,x) = \rho_0(x), && x \in \mathbb{R}, && \text{(2.1.5c)}\\
&w(0,x) = w_0(x), && x \in \mathbb{R}, && \text{(2.1.5d)}
\end{aligned}
$$

where $w \in [w_{\min}, w_{\max}]$ is a particular feature of each driver and $V(\rho, w)$ is the speed of cars. To model the impact of AVs on the traffic flow modeled by Generalized Aw-Rascle-Zhang (GARZ) model, in [57] we add the following constraints to (2.1.5)

$$
\begin{aligned}
&\rho\left(t, y(t)\right) \left(V(\rho(t,y(t)), w(t,y(t))) - \dot{y}(t)\right) \leq F_\alpha(\dot{y}(t)), && t \in \mathbb{R}_+, && \text{(2.1.6a)}\\
&\dot{y}(t) = \min\left(V_b, V(\rho(t,y(t)+), w(t,y(t)+))\right) && t \in \mathbb{R}_+, && \text{(2.1.6b)}\\
&\dot{y}(0) = y_0 && && \text{(2.1.6c)}
\end{aligned}
$$

where $F_\alpha(\dot{y}) = \alpha \max_{\rho \in [0, \rho_{\max}]} \rho(V(\rho, w_{\min}) - \dot{y})$ and $V_b < w_{\min}$. It means that any driver can be slowed down by the AV. The ODE (2.1.6b) influences the PDE (2.1.5a) through the moving constraint on the flux (2.1.6a). The definition of solutions requires special entropy condition that selects non-classical shocks and allows for vacuum waves and a careful analysis has to be made to understand the interaction between non-classical shocks generated by AV and first and second family waves associated to (2.1.5). In [57], we prove existence of solutions to (2.1.5) and (2.1.6), see more details in Section 3.1.

2.2 Macroscopic state reconstruction from microscopic observation

In Section 2.1, we have considered macroscopic models that capture the influence of autonomous vehicles on traffic flow. Our main objective is to design feedback controllers that regulate the velocity of AVs to positively influence overall traffic dynamics. These controllers are functions of macroscopic quantities, in particular the traffic density ρ. However, in practical scenarios, the available data typically consist of microscopic information, such as individual vehicle positions obtained from GPS and the data collected are limited. Therefore, to enable effective and robust traffic control, it is essential to perform accurate state reconstruction of the macroscopic variables from the available microscopic observations.

In [10, 11], the authors considered the problem of traffic density reconstruction using measurements from a small number of probe vehicles. These vehicles, governed by an ODE analogous to (2.2.1) and traffic density modeled by a PDE as (1.1.1), are supposed to be partially unknown and subjected to noisy measurements. They used machine learning techniques that provide a flexible framework for extracting patterns from data and building predictive models to reconstruct the state. More precisely, they implement a Physics-Informed Neural Network (PINN), a class of neural networks trained not only on data but also by enforcing the LWR model through PDE-derived Lagrangian terms in their optimization problem. However, the reconstruction techniques in [10, 11] suffer from a lack of theoretical convergence guarantees, i.e to prove that the reconstructed density converges to a weak-entropy solution of (1.1.1). Moreover, they need a large amount of measurements; the position of cars at any time and the local density around each car at any time. In [63], the authors also adopted a Physical Informed Neural Network (PINN) strategy but they used instead density and flow measurements from synthetic data computed at fixed spatial locations. They illustrated that accuracy of their traffic state estimation improves when the number of locations increases. In [90], the authors designed a Physics-Informed Deep Learning (PIDL) method that integrates machine learning to learn the Fundamental Diagram (FD) mapping from traffic density to flow or velocity. In [59], the authors conducted the Mobile Century field experiment where they studied the feasibility of using GPS-enabled mobile phones as a cost-effective traffic monitoring system. The system collected continuous trajectory data, with position and velocity updates recorded every three seconds. This extensive data collection ensured sufficient information for traffic monitoring. Their results suggested that a $2-3\%$ penetration of GPS-equipped phones in the driver population could provide accurate measurements of traffic flow velocity.

In contrast, in [8], we require less information than [10, 11, 59, 63, 90] as it only assumes the knowledge of initial and final positions of the probe vehicles. More precisely, we propose an efficient method for reconstructing traffic density with low penetration rate of probe vehicles. Specifically, we rely on measuring only the initial and final positions of a small number of cars which are generated using microscopic dynamical systems. We then implement a machine learning algorithm from scratch to reconstruct the approximate traffic density. Then, we get theoretical guarantees for traffic state reconstruction using the passage to the limit from microscopic to macroscopic models, see more details in Section 3.2.

This analysis naturally relies on the relationship between microscopic and macroscopic descriptions, which is rigorously established through many-particle limits. In particular, the convergence of the microscopic FTL model (2.2.1) to the LWR model (1.1.1) has been proven in [42, 62]. More precisely, the FTL microscopic model consists of dynamical system

$$\begin{cases} \dot{x}_N^N(t) = v_{\max}, & t > 0, \\ \dot{x}_i^N(t) = v\left(\frac{L}{N\left(x_{i+1}^N(t) - x_i^N(t)\right)}\right), & t > 0, \\ x_i^N(0) = \bar{x}_i, & i = 0, \dots, N, \end{cases} \tag{2.2.1}$$

where $x_i^N(\cdot)$ is the position of each vehicle, L is the cumulative length of the vehicles and v is the aveerage speed of drivers. In [42], the authors established well-posedness of system (2.2.1) under the condition that the initial positions satisfy $\bar{x}_0 < \bar{x}_1 < \cdots < \bar{x}_{N-1} < \bar{x}_N$. Moreover, they prove that the empirical measure $\rho^N(t) = \frac{L}{N}\sum_{i=0}^{N-1}\delta_{x_i^N(t)}$ (respectively the discretised density $\hat{\rho}^N(t,x) = \sum_{i=0}^{N-1}\frac{L}{N\left(x_{i+1}^N(t)-x_i^N(t)\right)}\chi_{[x_i(t),x_{i+1}(t)[}$), obtained from the Follow-The-Leader system, converges in the 1-Wasserstein topology (respectively in L^1_{loc}) to the unique weak-entropy solution of the LWR model (1.1.1). The convergence of the empirical measure is obtained using Wasserstein distance and a generalization of the Aubin-Lions Lemma.

We will now present the articles [48, 57, 72, 73] that deals with existence of solutions of PDE-ODE modeling the impact of AVs on road traffic, see Section 3.1 and the articles [8, 75, 76] that explains how we can improve state reconstruction using only sparse data.

Chapter 3

Main Contributions

3.1 Existence of Solutions for coupled PDE-ODE Models

To prove existence of solutions for (2.1.4), we will construct an approximate solution (ρ^n, y^n) of (2.1.4) using a wave-front tracking algorithm proposed by Dafermos [37]. As explained in Section 2.1, we must account for new "non-classical" shocks generated by the AV. We first explain what is a standard Riemann problem for a strictly concave flux function $f \in C^2([0, \rho_{\max}])$ and then explain how the wave-front tracking algorithm can be adapted to incorporate this new non-classical shock.

We consider the LWR model with Riemann type initial data

$$\rho_0(x) = \begin{cases} \rho_L & \text{if} \quad x < 0, \\ \rho_R & \text{if} \quad x > 0. \end{cases}$$

If $\rho_L < \rho_R$ then a shock is generated at $(0,0)$ with Rankine-Hugoniot speed and if $\rho_L > \rho_R$ then a rarefaction wave is generated, see Figure 3.1. The wave-front tracking method is described as follows. The initial density

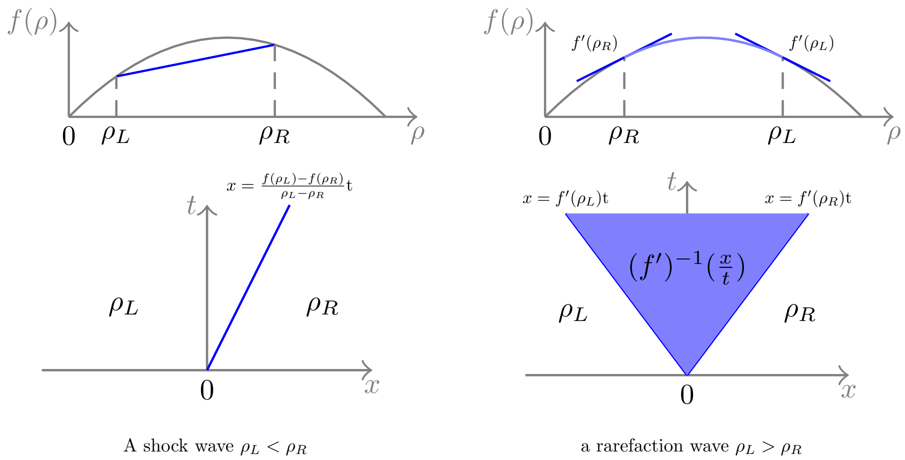

Figure 3.1 – Standard Riemann solution with a C^2 strictly concave flux function

ρ_0 is approximated by piecewise constant functions ρ_0^n and we solve a Riemann problem at each jump (or discontinuity). When a rarefaction wave is generated ($\rho_L < \rho_R$), we split it into centered rarefaction fan (a sequence of non-classical shocks) travelling with speed given by Rankine-Hugoniot condition. Then, we piece solutions together and we construct a solution ρ^n until two waves meet at time t_1. We define y^n to be the solution of

$$\begin{cases} \dot{y}(t) = \min(V_d, v(\rho^n(t, y(t)+))), & t \in [0, t_1), \\ y(0) = y_0, \end{cases} \tag{3.1.1}$$

where $\rho^n(t,\cdot)$ is the wave-front tracking approximate solution at time t as described above with initial data ρ_0^n, see also [49, Section 2.6]. From the standard Riemann solver $\mathcal{R}$ for the LWR model, we construct the constrained Riemann solver $\mathcal{R}^\alpha : [0, \rho_{\max}]^2 \mapsto \mathbf{L}^1_{\text{loc}}(\mathbb{R}; [0, \rho_{\max}])$ for (2.1.4) as follows.

Case 1. If $f(\mathcal{R}(\rho_L, \rho_R)(V_d)) > F_\alpha(V_d) + V_d \mathcal{R}(\rho_L, \rho_R)(V_d)$, then

$$\mathcal{R}^\alpha(\rho_L, \rho_R)(x/t) = \begin{cases} \mathcal{R}(\rho_L, \hat{\rho}_\alpha(V_d))(x/t) & \text{if} \quad x < V_d t, \\ \mathcal{R}(\check{\rho}_\alpha(V_d), \rho_R)(x/t) & \text{if} \quad x \geq V_d t, \end{cases} \quad \text{and} \quad y(t) = V_d t.$$

Case 2. If $V_d \mathcal{R}(\rho_L, \rho_R)(V_d) \leq f(\mathcal{R}(\rho_L, \rho_R)(V_d)) \leq F_\alpha(V_d) + V_d \mathcal{R}(\rho_L, \rho_R)(V_d)$, then

$$\mathcal{R}^\alpha(\rho_L, \rho_R) = \mathcal{R}(\rho_L, \rho_R) \quad \text{and} \quad y(t) = V_d t.$$

Case 3. If $f(\mathcal{R}(\rho_L, \rho_R)(V_d)) < V_d \mathcal{R}(\rho_L, \rho_R)(V_d)$, then

$$\mathcal{R}^\alpha(\rho_L, \rho_R) = \mathcal{R}(\rho_L, \rho_R) \quad \text{and} \quad y(t) = v(\rho_R) t.$$

where $\check{\rho}_\alpha(V_d)$ and $\hat{\rho}_\alpha(V_d)$ are the two solutions of $f(\rho) = F_\alpha(V_d)$ with $\check{\rho}_\alpha(V_d) < \hat{\rho}_\alpha(V_d)$. An illustration is given in Figure 3.2. We now solve the constrained Riemann problem at the position of the autonomous

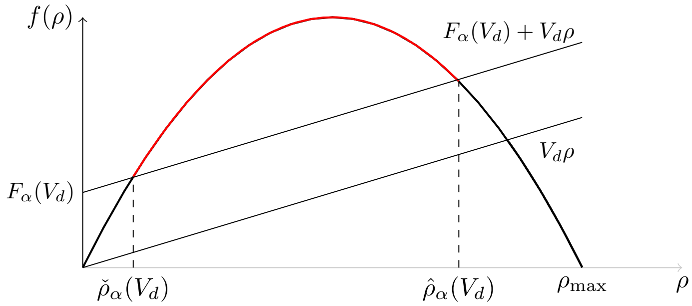

Figure 3.2 – Illustration o the constrained Riemann solver when $f(\rho) = \rho(1-\rho)$ for any $\rho \in [0, \rho_{\max}]$.

vehicle, leading to three possible outcomes. Case 1 illustrates the generation of a non classical-shock $(\hat{\rho}_\alpha(V_d), \check{\rho}_\alpha(V_d))$, Case 2 corresponds to the AV traveling at speed V_d without influencing the surrounding traffic flow and Case 3 shows an AV that adapts its speed to the traffic flow ahead and follows it, see Figure 3.3. This leads to the construction of an approximate solution (ρ^n, y^n) of (2.1.4). The main difficulty is the presence of possible non-classical shocks generated when the AV slows down and the traffic flow around is high enough. In that case, the shock waves does not satisfies the Lax entropy condition, that is $f'(\rho_R) < s < f'(\rho_L)$ where s stands for the speed of the shock wave, connecting a left state ρ_L to a right state ρ_R. Thus, the standard theory for conservations laws cannot be applied directly and we should describe all possible interactions we can have between shocks, rarefaction shocks and non-classical shocks. To prove the convergence of (ρ^n, y^n) to (ρ, y), we follow the same arguments as in [39]. For a.e $t \in \mathbb{R}_+$, we define the Total Variation functional

$$\Gamma(t) = \Gamma(\rho^n(t,\cdot)) = TV(\rho^n(t,\cdot)) + \gamma(t), \tag{3.1.2}$$

where γ is given by

$$\gamma(t) = \begin{cases} -2|\hat{\rho}_\alpha(V_d) - \check{\rho}_\alpha(V_d)| & \text{if} \quad \rho^n(t, y^n(t)-) = \hat{\rho}_\alpha(V_d) \text{ and } \rho^n(t, y^n(t)+) = \check{\rho}_\alpha(V_d), \\ 0 & \text{otherwise.} \end{cases}$$

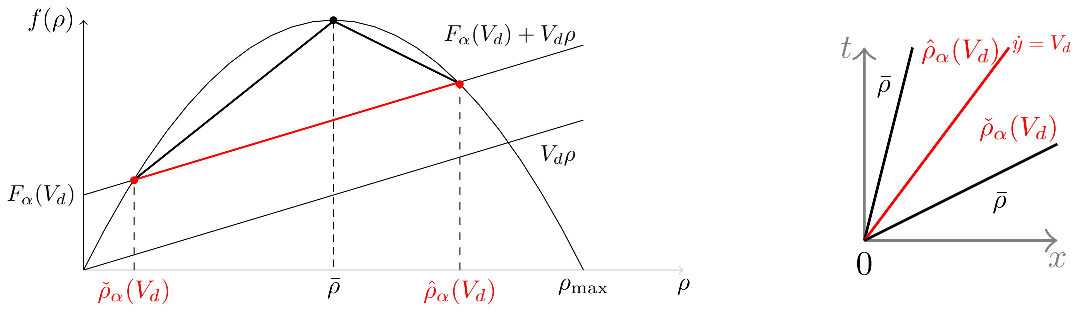

Example of solution corresponding to case 1. of the Constraint Riemann problem for $\rho_L = \rho_R = \bar\rho$ and $\check\rho_\alpha(V_d) < \bar\rho < \hat\rho_\alpha(V_d)$

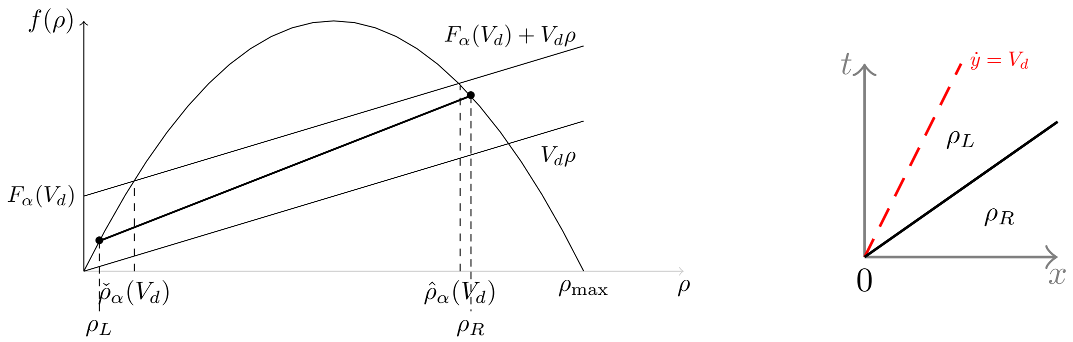

Example of solution corresponding to case 2. of the Constraint Riemann problem for $0 < \rho_L < \check\rho_\alpha(V_d)$ and $\check\rho_\alpha(V_d) < \rho_R < \rho^*$ with ρ^* verifying that $\rho V_d = f(\rho)$.

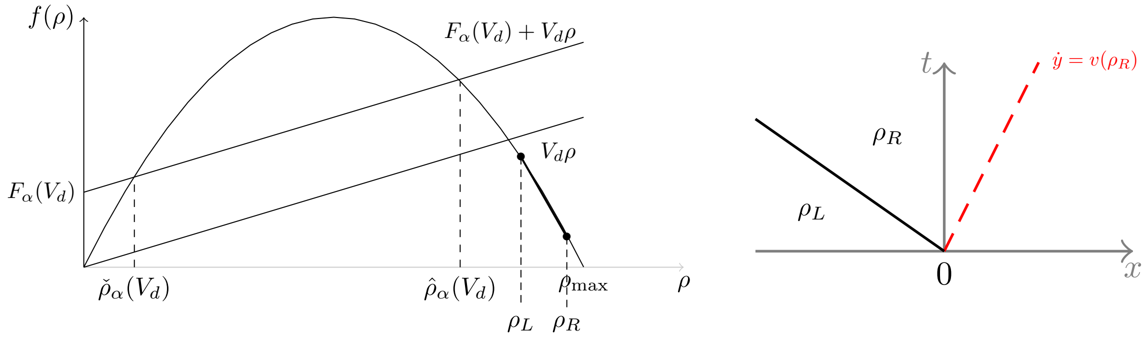

Example of solution corresponding to case 3. of the Constraint Riemann problem for $\rho^* < \rho_L < \rho_R$ with ρ^* verifying that $V_d\rho = f(\rho)$.

Figure 3.3 – The constrained Riemann solver when $f(\rho) = \rho(1-\rho)$ for any $\rho \in [0, \rho_{\max}]$.

The term γ is added to control the behavior of $TV(\rho^n)$ when a wave interacts with the autonomous vehicle creating or canceling a non classical shock. In [39, 73], we get the following Lemma

Lemma 3.1.1. *For every $n \in \mathbb{N}$, at any interaction, the functional $\Gamma(t)$ either decreases by at least $\rho_{\max}2^{-n-1}$ or remains constant and the number of waves does not increase.*

From (3.1.1) and using Helly's Theorem (see [18, Theorem 2.4]), we have, up to a subsequence, the following convergences

$$\begin{aligned}&\rho^n \to \rho, \quad \text{in } L^1_{\text{loc}}(\mathbb{R}_+ \times \mathbb{R}; [0, \rho_{\max}]),\\ &y^n(\cdot) \to y(\cdot), \quad \text{in } L^\infty([0,T]; \mathbb{R}) \text{ for all } \ T > 0,\\ &\dot{y}^n(\cdot) \to \dot{y}(\cdot), \quad \text{in } L^1([0,T]; \mathbb{R}) \text{ for all } \ T > 0,\end{aligned}$$

for some $\rho \in C^0(\mathbb{R}_+; L^1 \cap BV(\mathbb{R}; [0, \rho_{\max}]))$ and $y \in W^{1,1}([0,T]; \mathbb{R}) \cap C^0([0,T]; \mathbb{R})$ with Lipschitz constant V_d. Since (ρ^n, y^n) satisfies (2.1.4a) (2.1.4b), (2.1.4c) and (2.1.4e), it follows directly that (ρ, y) also satisfies the same ones. It remains to prove that (ρ, y) satisfies (2.1.4d). If we were in the setting of weak-entropy solutions, from [19, Lemma 15], we would have

$$\lim_{n \to \infty} \rho^n(t, y^n(t)+) = \rho(t, y(t)+), \tag{3.1.3}$$

and (ρ, y) satisfying (2.1.4d) would be a direct consequence of the construction of the approximate solution (ρ^n, y^n). Unfortunately, the equality (3.1.3) may fail due to the presence of non-classical shocks, see an example in [73, Section 2.4]. Thus, by obtaining careful estimates of the approximate solution of (ρ^n, y^n) at $(t, y(t))$, see [73, Section 3.3], we get the following theorem

Theorem 3.1.1 ([73])**.** *Let $\rho_0 \in BV(\mathbb{R}, [0, \rho_{\max}])$, then the Cauchy problem (2.1.4) admits a solution in the sense of [73, Definition 1.1].*

In [72], we prove uniqueness and continuous dependence of solutions with respect to initial data of bounded variation when the solution is constructed using wave-front tacking method.

Theorem 3.1.2 ([72])**.** *The solution $(\rho, y) \in C^0(\mathbb{R}^+; L^1 \cap BV(\mathbb{R}, [0,1])) \times W^{1,1}(\mathbb{R}^+, \mathbb{R})$ in the sense of [72, Definition 2.2] for the Cauchy problem (2.1.4) depends in a Lipschitz continuous way from the initial datum. More precisely, let $T > 0$ and (ρ^1, y^1) and (ρ^2, y^2) two solutions of (2.1.4) constructed using wave-front tacking algorithms with corresponding initial data (ρ^1_0, y^1_0) and (ρ^2_0, y^2_0), then there exists $C > 0$ such that*

$$\|\rho^2(t) - \rho^1(t)\|_{L^1(\mathbb{R})} + |y^2(t) - y^1(t)| \leq C(\|\rho^2_0 - \rho^1_0\|_{L^1(\mathbb{R})} + |y^2_0 - y^1_0|),$$

for every $t \in [0,T]$. Above, the constant C depends on V_d, $TV(\rho_0)$ and α.

The proof is based on a new backward in time method established to capture the values of the norm of generalized tangent vectors at every time.

In [48], we extend the existence of solutions for (2.1.4) replacing V_d in (2.1.4d) by a time-dependent control function $t \to u(t)$, see more details in Section 6.1. The main difference with (2.1.4) where the autonomous vehicle travels at a constant speed V_d lies in the creation of non-classical shocks along the vehicle's trajectory, even in the absence of interactions with other waves and when the AV's speed changes. Additionally, rarefaction waves may be generated at positive time $t > 0$. As a consequence, it becomes essential to incorporate these new wave interactions into the analysis. This is achieved by extending the definition of the Total Variation functional, specifically by including the term $TV(u; [t, \infty])$ to account for the variation generated by these phenomena over the future time interval. This corresponds to an open-loop control strategy, where the control input has bounded variation in time. This formulation serves as a foundational step toward establishing more advanced control results, including feedback control strategies.

In [57], we also extend the existence of solutions for initial data with bounded variation to the second-order GARZ model (2.1.5)–(2.1.6), under the assumption that V_d is constant. To achieve this, we introduce a new definition of weak solutions that explicitly incorporates the selection of non-classical shocks and permits the presence of vacuum waves. Similar to [73], approximate solutions are constructed using a wave-front tracking method, and their limits provide solutions to the Cauchy problem for the PDE–ODE system (2.1.5)–(2.1.6). To achieve this, we introduce a TV-type functional that compensates for interactions between the slow vehicle trajectory and both 1-waves and 2-waves, and we provide careful estimates of the approximate solution constructed via the wave-front tracking algorithm around the slow vehicle's position.

3.2 Improved State Reconstruction with Sparse Data

Initial data Identification Problem for scalar conservation laws

In this section, we observe u^T, a solution of the one-dimensional Burgers equation (3.2.1) at a final time T subjected to possible disturbances. Our goal is to fully characterize the set of initial data that generate weak-entropy solutions of (3.2.1) which are as close as possible to u^T at time T in $L^2(\mathbb{R})$-norm. More precisely, in [76], we consider the following one-dimensional Burgers equation

$$\begin{cases} \partial_t u(t,x) + \partial_x f(u(t,x)) = 0, & (t,x) \in \mathbb{R}^+ \times \mathbb{R}, \\ u(0,x) = u_0(x), \end{cases} \tag{3.2.1}$$

where u is the state, u_0 is the initial state and the flux function f is defined by $f(u) = \frac{u^2}{2}$. Kruzkov's theory provides existence and uniqueness of solutions of Burgers equation with initial datum $u_0 \in L^\infty(\mathbb{R})$. This solution is called a weak-entropy solution, denoted by $(t,x) \to S_t^+(u_0)(x)$. For a given target function u^T, we introduce the backward entropy solution $(t,x) \to S_t^-(u^T)(x)$ as follows : for every $t \in [0,T]$, for a.e $x \in \mathbb{R}$

$$S_t^-(u^T)(x) = S_t^+(x \to u^T(-x))(-x).$$

We introduce the following optimal control problem

$$\inf_{u_0 \in \mathcal{U}_{\mathrm{ad}}^0} J_0(u_0) := \|u^T(\cdot) - u(T,\cdot)\|_{L^2(\mathbb{R})}, \tag{$\mathcal{O}_T$}$$

where u^T is a given target function and the class of admissible initial data $\mathcal{U}_{\mathrm{ad}}^0$ is defined by

$$\mathcal{U}_{\mathrm{ad}}^0 = \{u_0 \in L^\infty(\mathbb{R}) \,/\, \|u_0\|_{L^\infty(\mathbb{R})} < C \text{ et } \operatorname{supp}(u_0) \subset K_0\}. \tag{3.2.2}$$

where $C > 0$ is a constant large enough. This study is motivated by the minimization of the sonic boom effects generated by supersonic aircrafts which are modeled by an augmented Burgers equation [3, 29].

To solve the optimization problem ($\mathcal{O}_T$), some difficulties arise from a theoretical and numerical point of view.

— Since the entropy solution u of (3.2.1) may contain shocks even if the initial datum is a smooth function, this generates important added difficulties that have been the object of intensive study in the past, see [16, 17, 20, 21] and the references therein. In [16, 17, 20, 21], the derivative of the cost function J_0 in ($\mathcal{O}_T$) is regarded in a weak sense by requiring strong conditions on the set of initial data. This leads to require that entropy solutions of (3.2.1) have a finite number of non-interacting jumps.

— When J_0 is weakly differentiable, gradient descent methods have been implemented in [2, 26, 27] to solve numerically the optimization problem ($\mathcal{O}_T$). In the cases where it was applied successfully, only one possible initial datum emerges, namely the backward entropy solution. This is mainly due to the numerical viscosity that numerical schemes introduce to gain stability. To find some multiple minimizers, the authors in [54] use a filtering step in the backward adjoint solution.

In [76], we give a full characterization of the set of minimizers for the optimization problem ($\mathcal{O}_T$)

Theorem 3.2.1 ([76]). *Let $T > 0$ and $u^T \in L^\infty(\mathbb{R})$ such that $supp(u^T) \subset K^T$. The optimal control problem ($\mathcal{O}_T$) admits multiple optimal solutions. Moreover, the initial datum $u_0 \in L^\infty(\mathbb{R})$ is an optimal solution of ($\mathcal{O}_T$) if and only if $u_0 \in L^\infty(\mathbb{R})$ satisfies $S_T^+(u_0) = S_T^+(S_T^-(u^T))$.*

The full characterization of $\{u_0 \in L^\infty(\mathbb{R})/S_T^+(u_0) = S_T^+(S_T^-(u^T))\}$ is given in [32, 43, 75]. We have also implemented a wave-front tracking algorithm to construct the set of minimizers of the optimal problem ($\mathcal{O}_T$). For instance, we consider the target function u^T defined by

$$u^T(x) = \begin{cases} 2 & \text{if } x \in (-0.2, 1.1) \bigcup (2, 3.1) \bigcup (4.1, 5.3) \bigcup (6.1, 7.2), \\ -1 & \text{otherwise.} \end{cases}$$

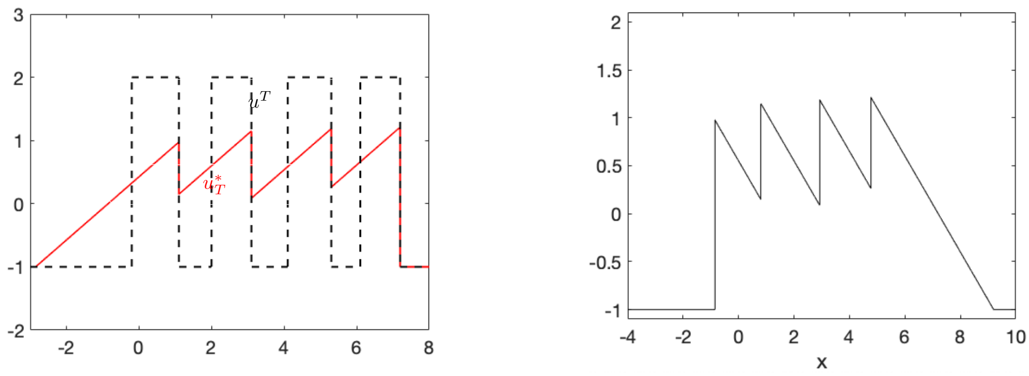

Figure 3.4 – Left. Plotting of the target function u^T and the backward-forward function $u_T^* := S_T^+(S_T^-(u^T))$ with $T = 2$. Right. Plotting of the backward entropy solution $S_T^-(u^T)$, a minimizer of the optimal problem $(\mathcal{O}_T)$.

We construct numerically four different minimizers $u_0^{rand,n}$ of $(\mathcal{O}_T)$, plotted in Figure 3.5. Note that $S_T^+(u_0^{rand,n}) = S_T^+(S_T^-(u^T))$.

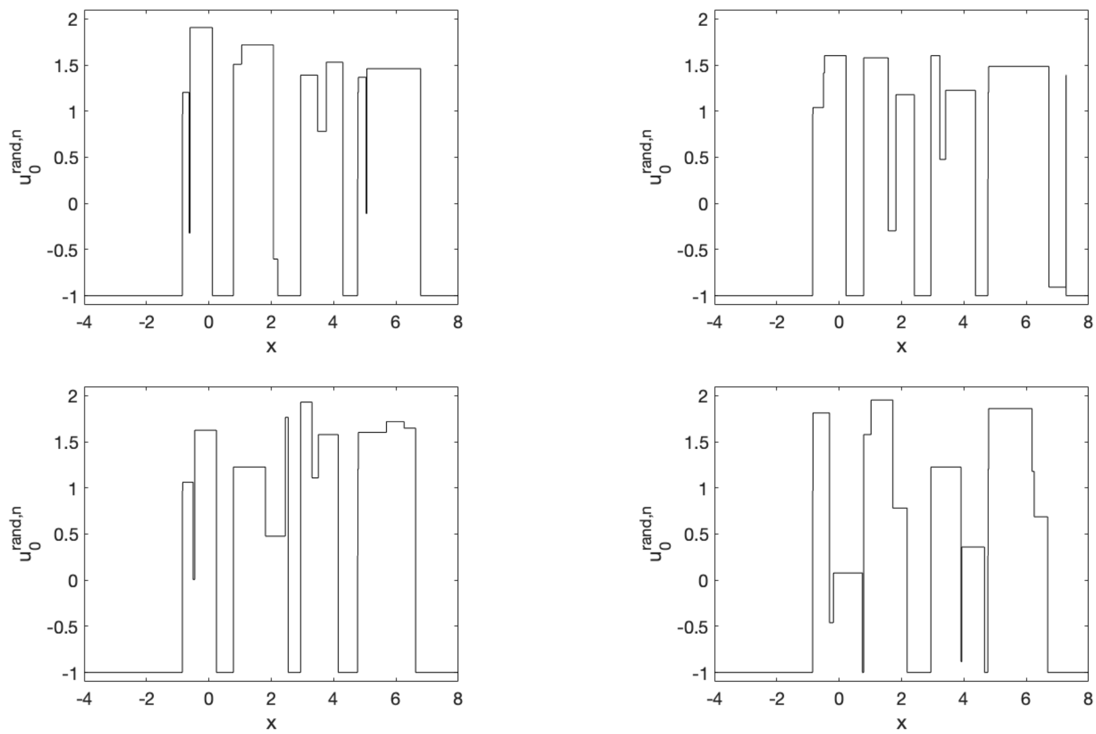

Figure 3.5 – Plotting of four different minimizers $u_0^{\mathrm{rand,n}}$ of $(\mathcal{O}_T)$ with u^T defined in Figure 3.4 and $T = 2$.

State reconstruction from limited collected data

In contrast to many existing approaches as in [76], we do not assume access to prescribed initial or final density profiles. This lack of information poses a significant challenge, since density plays a central role in accurately modeling and predicting traffic flow. To address this limitation, we must instead rely on more realistic sources of information, namely the initial and final positions of limited number of probe vehicles, to reconstruct the full traffic density. We address this optimization problem using an approach that differs from machine leaning techniques combined with physics-informed methods. The main idea is to avoid directly including the PDE in the learning process, since such approaches generally lack theoretical convergence guarantees. Instead, we rely on the well-established convergence, under suitable conditions, of the microscopic Follow-the-Leader (FTL) model (2.2.1) to the macroscopic LWR model (1.1.1). This convergence will allow us to ensure mass conservation without the need to explicitly enforce PDE constraints, allowing flexibility in the reconstructed solution while preserving physical consistency. Although directly enforcing the PDE constraints would not be computationally difficult, it would introduce a strong dependence on data. In particular, it would require time-dependent density measurements at specific spatial locations, which are not available in our setting, as our methodology assumes no density measurements.

To do this, we will modify the structure of the machine learning pipeline (see Figure 3.6) to get advantages of the two standard methods for traffic state reconstruction : a labeled model-based method [40, 89] using microscopic and macroscopic models and a data driven method [13, 60] using measurement data to derive system properties or predict the near future. Then we get theoretical guarantees for traffic state reconstruction in the following sense. If the data set is only derived from data augmentation (data created artificially using dynamical systems), we will prove that the traffic state reconstructed using neural networks tends to a solution of a macroscopic system as the number of neurons and layers tends to infinity, i.e. the accuracy score in Figure 3.6 tends to zero.

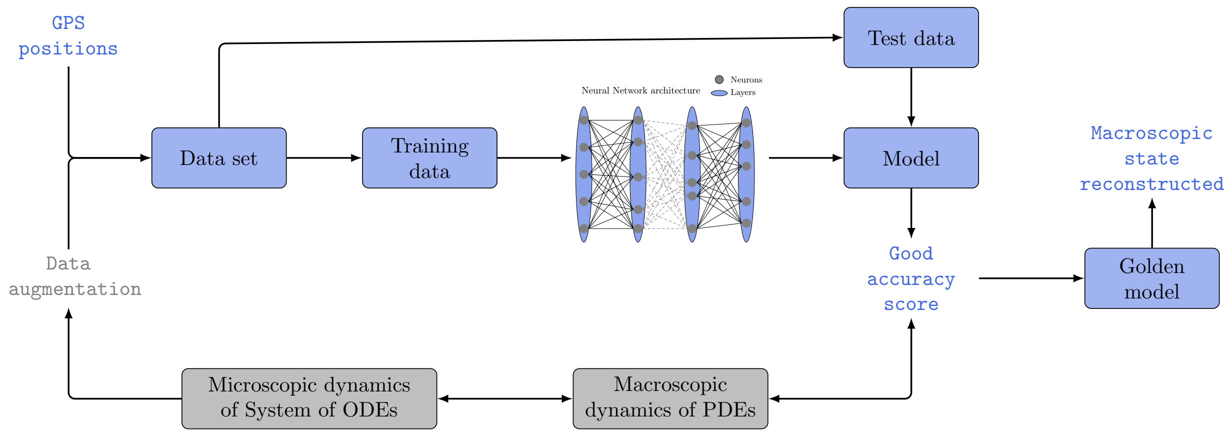

Figure 3.6 – Machine learning pipeline with theoretical guarantees

In [8], the data set is only derived from data augmentation. Specifically, it is constructed by simulating N vehicle trajectories using the Follow-the-Leader (FTL) model (2.2.1), denoted as $(x_i(\cdot))_{i\in\{1,\cdots,N\}}$ over the time interval $[0,T]$. From these, a smaller subset of $n+1$ trajectories is selected, with $n+1<N$. For each of the selected trajectories, only the initial and final positions are saved. The resulting input/output data structure is defined by reindexing these selected pairs as $[(x_i(0))_{i\in\{0,\cdots,n\}},(x_i(T))_{i\in\{0,\cdots,n\}}] := [\bar{x},\bar{y}]$. The dynamic of the trajectory of the $n+1$ vehicles can be rewritten as the following ODE system

$$\begin{cases} \dot{x}_n(t) = v_{\max}, & t\in(0,T], \\ \dot{x}_i(t) = v\left(\frac{\alpha_i^N L}{N(x_{i+1}(t)-x_i(t))}\right), & t\in(0,T],\ i=0,\dots,n-1, \\ x_i(0)=\bar{x}_i, & i=0,\dots,n, \end{cases} \tag{3.2.3}$$

where, for any $i\in\{0,\cdots,n-1\}$, the unknown parameter $\alpha_i^N\in\mathbb{R}$ stands for the number of vehicles in the segment $[x_i(\cdot),x_{i+1}(\cdot))$ between consecutive probe vehicles i and $i+1$. Moreover, we impose the following condition $\sum_{i=0}^{n-1}\alpha_i^N = N$. In line with standard machine learning practice, the dataset is partitioned into a training set $[\bar{x}_{\text{Train}}, \bar{y}_{\text{Train}}]$ and a test set $[\bar{x}_{\text{Test}}, \bar{y}_{\text{Test}}]$. We introduce the following optimization problem to reconstruct α^N from the training data set

$$\underset{\alpha^N}{\text{minimize}} \quad \frac{1}{2}\left\|x(T)-\bar{y}_{\text{Train}}\right\|^2 \tag{3.2.4a}$$

$$\text{s.t.} \quad \dot{x}(t) = V\left(W_{\alpha^N}x(t)+b_{\alpha^N}(t)\right), \quad t\in[0,T], \tag{3.2.4b}$$

$$x(0) = \bar{x}_{\text{Train}}, \tag{3.2.4c}$$

where W_{α^N} is a bi-diagonal matrix chosen to ensure that (3.2.4b) and (3.2.4c) is the same ODE than (3.2.3). In [8], we have designed a network architecture using a residual network (ResNet) approach and the first-order discretization of the ODE (3.2.4a) to find a minimiser α_*^N of the optimization problem (3.2.4). The learning procedure is described in Figure 3.7 where each residual block in our ResNet corresponds to a single time step in the simulation.

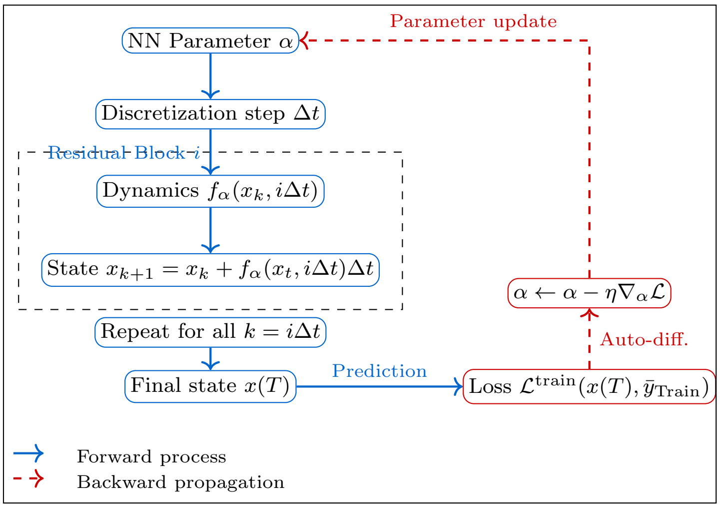

Figure 3.7 – Learning procedure where f_α is obtained from the first-order discretization of the ODE (3.2.4a) and $\mathcal{L}^{\text{train}}(x(T),\bar{y}_{\text{Train}}) = \frac{1}{2}\left\|x(T)-\bar{y}_{\text{Train}}\right\|^2$.

After the training phase, we recover the discrete vehicle densities ρ^N from α_*^N as follows. We have, for any $x\in\mathbb{R}$,

$$\rho^N(t,x) = \sum_{i=0}^{n-1}\rho_i^N(t)\chi_{[x_i(t),x_{i+1}(t))}(x), \quad t\in[0,T], \tag{3.2.5}$$

where χ_A is the characteristic function of the set A and for $i=0,\dots,n-1$,

$$\rho_i^N(t) = \frac{\left(\alpha_*^N\right)_i L}{N(x_{i+1}(t)-x_i(t))}, \quad t\in[0,T]. \tag{3.2.6}$$

Then, we use the test data to validate α_*^N using the following test function $\mathcal{L}^{\text{test}}(x^*(T),\bar{y}_{\text{Test}}) = \frac{1}{n_{\text{test}}}\sum_{j=0}^{n_{\text{test}}}|x_j^*(T)-\bar{y}_j|^2$ where $n_{\text{test}}+1$ is the number of test data and x_j^* solves the ODE

$$\begin{cases} \dot{x}_j(t) = v\left(\rho^N(t,x_j(t)^+)\right), & t\in(0,T], \\ x_j(0) = \left(\bar{x}_{\text{Test}}^N\right)_j & j=0,\dots,n_{\text{test}}. \end{cases} \tag{3.2.7}$$

When the data set is only generated by dynamical systems, we prove that that approximate density $\rho^N(0,\cdot)$ in (3.2.5) constructed by our machine learning model converges to the initial condition $\bar{\rho}$ in the LWR model

(1.1.1) when the number of vehicles approaches infinity. To achieve this, we make the important observation that by construction the initial traffic density must satisfy for $i = 0, \dots, n-1$

$$\bar{x}_{i+1} = \sup \left\{ x \in \mathbb{R} : \int_{\bar{x}_i}^{x} \bar{\rho}(y) dy \leq \frac{\alpha_i^N L}{N} \right\}. \tag{3.2.8}$$

Indeed, although we do not have access to the truth initial car density $\bar{\rho}$, we do know that initial positions $\bar{x}_i$ of our probe vehicles verify (3.2.8) which states that the number of unobserved vehicles between $[x_i, x_{i+1})$ is given by α_i^N. The following result inspired from [42, Proposition 4] ensures that the discretization aligns consistently with the true initial density when N tends to infinity.

Proposition 3.2.1. *Let $\bar{\rho}$ satisfy (3.2.8) and assume that*

$$\max_{i=0,\dots,n-1} \alpha_i^N = o(N). \tag{3.2.9}$$

Then, the sequence $(\rho^N(0,\cdot))_{N\in\mathbb{N}}$ converges to $\bar{\rho}$ in the sense of the $\mathrm{W}_{L,1}$-Wasserstein distance in (3.2.10).

The Wasserstein distance is defined in [42] by

$$\mathrm{W}_{L,1}(f,g) = \|f((-\infty,\cdot]) - g((-\infty,\cdot)\|_{L^1(\mathbb{R},\mathbb{R})}. \tag{3.2.10}$$

We refer readers to [42, Section 2.3] which provides a rigorous introduction to this concept.

Numerical simulations. We consider a traffic scenario where the maximum speed of traffic is $V_{\max} = 120$ km/h and the maximum traffic density is $\rho_{\max} = 200$ cars/km. A time period of 0.1 corresponds to a real-world duration of 6 minutes. One captures a traffic pattern characterized by alternating regions of congestion and free flow. Let $\rho(0,x) = 0.6\rho_{\max} + 0.3\rho_{\max}\sin(2\pi k x)$ be the initial density of the overall fleet. We have 10% of the total fleet serving as probe vehicles for training data and an additional 2.5% of the total fleet are selected for testing purposes. Figure 3.8 A. and Figure 3.8 B. illustrate the errors obtained by both training and testing phases of our learning procedure with different values of N and T. Precisely, during the testing phase where $N = 2000$ and $T = 0.1$, Mean Squared Error (MSE) was calculated to be 0.0483, while Relative Error (RE) was 0.0053. When the number of vehicles was increased to $N = 4000$ and the time duration to $T = 0.2$, both MSE and RE decreased to 0.0076 and 0.0020 respectively. This demonstrates the robustness of our methods even when applied to high dimensional data. Additionally, the method allows us to reconstruct density for all times. Figure 3.8 D. compares the reconstructed discrete density with the solution to LWR model (2.1.3), which is computed using a Godunov scheme. Figure 3.8 D. represents the final reconstructed density and the final density obtained by solving PDE (2.1.3) for different values of N and T. Thus, by using only 10% of the total fleet as probe vehicles, we can accurately reconstruct the traffic density.

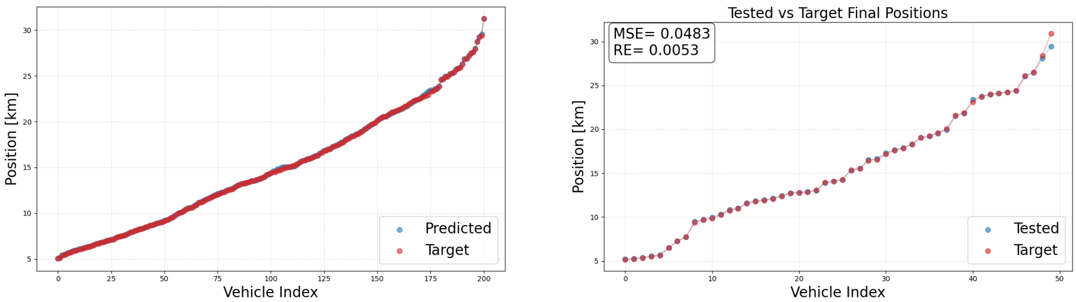

NN learning using 5,000 epochs

Testing using predicted density

A. Comparison between predictions and data with $N = 2000$

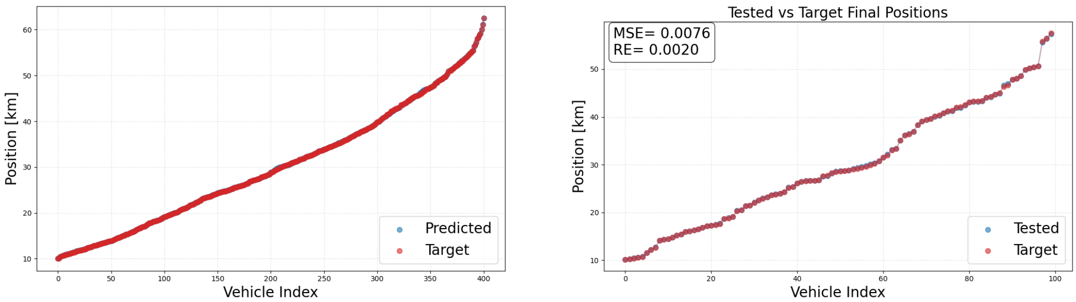

NN learning using 5,000 epochs

Testing using predicted density

B. Comparison between predictions and data with $N = 4000$

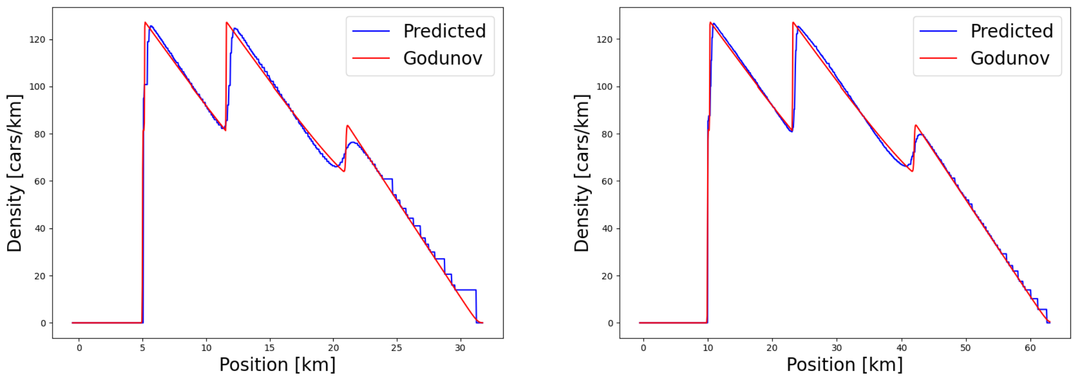

$N = 2000,\ T = 0.1$

$N = 4000,\ T = 0.2$

C. Reconstructed final traffic density

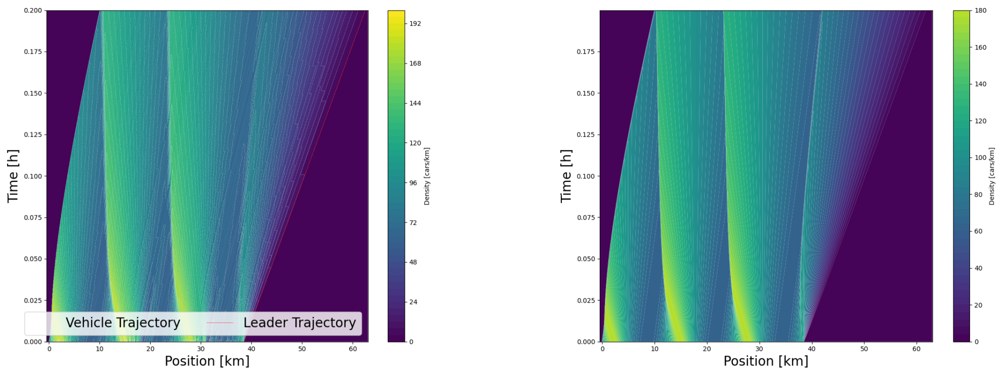

Reconstructed density

Godunov density

D. Comparison between the predicted density and Godunov scheme density with $N = 4000$ and $T = 0.2$

Figure 3.8 – Reconstruction of density using limited start and final positions of cars generated by FTL model (2.2.1)

Chapter 4

Perspectives for traffic flow network modeling

4.1 Traffic flow network modeling

Another important extension of macroscopic traffic models is their application to road networks. In real-world scenarios, traffic evolves not only along highways but also through intersections, junctions, and merges. Modeling traffic flow on such networks requires specifying conservation laws on each road segment (edge) and coupling conditions at the junctions (nodes). These coupling conditions must ensure mass conservation and often involve priority rules, capacity constraints, or distribution coefficients. The formulation of entropy-consistent coupling conditions at network nodes is a non-trivial challenge and an active area of research, especially when shock waves interact at intersections.

We will follow the presentation of a road network given in [30, Chapter 4]. A network is a couple $(\mathcal{I}, \mathcal{J})$ where the following conditions hold.

Cond 1. $\mathcal{I}$ is a finite collection of edges, which are intervals in $\mathbb{R}$,

$$I_i = [a_i, b_i] \subseteq \mathbb{R}, \qquad i = 1, \dots, N;$$

Cond 2. $\mathcal{J}$ is a finite collection of junctions and each junction J is union of two non empty subsets $\mathrm{Inc}(J)$ and $\mathrm{Out}(J)$ of $\{1, \dots, N\}$.

Cond 3. For every $J \neq J' \in \mathcal{J}$ we have

$$\mathrm{Inc}(J) \cap \mathrm{Inc}(J') = \emptyset \quad \text{and} \quad \mathrm{Out}(J) \cap \mathrm{Out}(J') = \emptyset.$$

Cond 4. If $i \notin \bigcup_{J \in \mathcal{J}} \mathrm{Inc}(J)$ then $b_i = +\infty$ and if $i \notin \bigcup_{J \in \mathcal{J}} \mathrm{Out}(J)$ then $a_i = -\infty$. Moreover, the two cases are mutually exclusive.

Cond 1 and **Cond 2** essentially asks the network to be a graph. According to the previous definition, each junction can be identified with a $n - m$ tuple $(i_1, \cdots, i_n, i_{n+1}, \cdots, i_{m+n})$ where the first n-tuple indicates the set of incoming edges and the second m-tuple indicates the set of outgoing edges. **Cond 3** implies that each edge can be incoming for at most one junction and outgoing for at most one junction. Moreover, **Cond 4** implies that some edges may extend to infinity but are connected to at least one junction, see Figure 4.1. On each edge (road), we consider the Lighthill-Whitham-Richards model for traffic

$$\partial_t \rho(t, x) + \partial_x f^i(\rho(t, x)) = 0, \; (t, x) \in \mathbb{R}_+^* \times I_i \tag{4.1.1}$$

where for any $(t, x) \in \mathbb{R}_+^* \times I_i$, $\rho(t, x) \in [0, \rho_{\max}]$ is the density of cars, v_i is the average speed on the road I_i and $f^i(\rho) = \rho v^i(\rho)$ is the flux. We additionally assume that $\rho_{\max} = 1$, the flux f^i is a strictly concave C^2

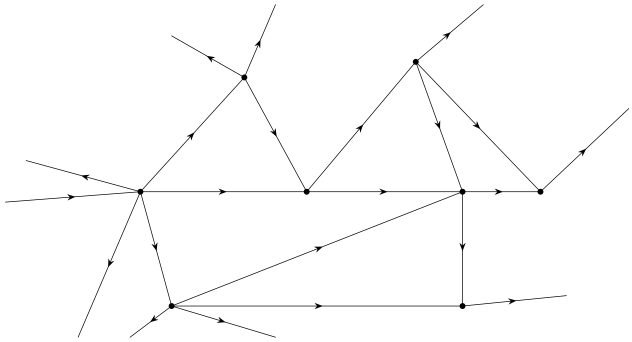

Figure 4.1 – A road network

function and $f^i(0) = f^i(1)$. Thus, f^i has a unique point of maximum $\sigma^i \in]0,1[$.

Construction of a Riemann solver at J. We now want to define and solve Riemann problems at junctions. Let $J \in \mathcal{J}$ be a junction and assume that $\mathrm{Inc}(J) = \{1, \cdots, n\}$ and $\mathrm{Out}(J) = \{n+1, \cdots, n+m\}$, see Figure 4.2. We look for centered solutions on each edge, which are the building blocks to construct solutions

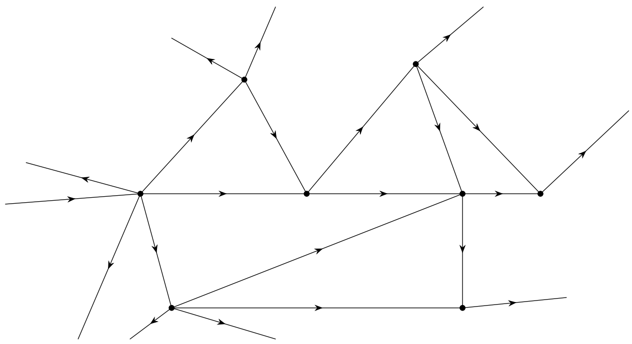

Figure 4.2 – A junction J in a network with n entering road and m exiting road

to the Cauchy problem via a wave-front tracking algorithm. Thus on each edge, we expect a solution to be formed by rarefactions or shocks. A Riemann solver is a map assigning a solution to each Riemann initial data. Since we consider only centered solutions, it is sufficient to assign on each edge a constant boundary value. A Riemann Solver for the $n : m$ junction J is a function $RS_J : \mathbb{R}^{n+m} \to \mathbb{R}^{n+m}$ that associates to every Riemann data $\rho_0 = (\rho_0^1, \cdots, \rho_0^{n+m})$ at J a vector $\hat{\rho} = (\hat{\rho}_1, \cdots, \hat{\rho}_{n+m})$ so that the following holds. On each edge I_i, $i \in \{1, \cdots, n+m\}$, the solution is given by the solution to the initial-boundary value problem with initial data ρ_0^i and boundary data $\hat{\rho}_i$. Moreover, we assume a consistency condition $RS_J(RS_J(\rho_0)) = RS_J(\rho_0)$. The initial-boundary value problem on each edge may produce a solution which does not attain the boundary value pointwise. So, to ensure conservation of ρ, we must ask for solutions to the initial boundary value problems to have negative characteristic velocities on incoming edges and positive characteristic velocities on outgoing ones. This is equivalent to ask that the Riemann problem on a real line with initial data $(\rho_0^i, \hat{\rho}_i)$, $i = 1, \cdots, n$ produces only waves with negative velocities and the Riemann problem on a real line with initial data $(\hat{\rho}_i, \rho_0^i)$, $i = n+1, \cdots, n+m$ produces only waves with positive velocities. More precisely, let RS^i_{road} be a Riemann solver on the road I_i connected to the junction J. We construct a Riemann solver at the function J, denoted by $RS_J : \mathbb{R}^{n,m} \to \mathbb{R}^{n,m}$ that is compatible with RS_{road} as follows.

— For any $i \in \{1 \cdots, n\}$, $RS^i_{\text{road}}(\rho^i_0, \hat{\rho}_i)$ should generate either no waves and $\rho^i_0 = \hat{\rho}_i$ or a negative wave to have $\rho_i(t, 0-) = \hat{\rho}_i$ for $t > 0$.

— For any $i \in \{n+1 \cdots, n+m\}$, $RS^i_{\text{road}}(\rho^i_0, \hat{\rho}_i)$ should generate either no waves and $\rho^i_0 = \hat{\rho}_i$ or a positive wave to have $\rho_i(t, 0+) = \hat{\rho}_i$ for $t > 0$.

If RS^i_{road} is the entropy Riemann solver, denoted by $RS^{\text{entropy},i}_{\text{road}}$, we can characterize the set of all possible $(\hat{\rho}_i)_{i\in\{1,\cdots,n\}}$ as follows. For any $i \in \{1, \cdots, n\}$ (entering road I_i), we have

$$\hat{\rho}_i \in \begin{cases} \{z \in \mathbb{R} : (f^i)'(z) < 0 \text{ and } f^i(z) < f^i(\rho^i_0)\} \cup \{\rho^i_0\} & \text{if } (f^i)'(\rho^i_0) > 0, \\ \{z \in \mathbb{R} : (f^i)'(z) \leq 0\} & \text{if } (f^i)'(\rho^i_0)) \leq 0. \end{cases} \tag{4.1.2}$$

and for $i \in \{n, \cdots, n+m\}$ (exiting road I_i), we have

$$\hat{\rho}_i \in \begin{cases} \{z \in \mathbb{R} : (f^i)'(z) > 0 \text{ and } f^i(z) < f^i(\rho^i_0)\} \cup \{\rho^i_0\} & \text{if } (f^i)'(\rho^i_0) < 0, \\ \{z \in \mathbb{R} : (f^i)'(z) \geq 0\} & \text{if } (f^i)'(\rho^i_0)) \geq 0. \end{cases} \tag{4.1.3}$$

As a consequence, for any $i \in \{1, \cdots, n\}$, for any $j \in \{n+1, \cdots, n+m\}$

$$\hat{\gamma}_i := f^i(\hat{\rho}_i) \in \Omega_i := [0, D^i(\rho^i_0)] \text{ and } \hat{\gamma}_j := f^j(\hat{\rho}_j) \in \Omega_j := [0, S^j(\rho^j_0)] \tag{4.1.4}$$

where D^i and S^j are respectively the demand and the supply function introduced by J.P Lebacque and Khoshyaran [66–68],

$$D^i(\rho) = \begin{cases} f^i(\rho) & \text{if } \rho \in [0, \sigma^i], \\ f^i(\sigma) & \text{if } \rho \in]\sigma^i, 1], \end{cases} \quad \text{and} \quad S^j(\rho) = \begin{cases} f^j(\sigma) & \text{if } \rho \in [0, \sigma^j], \\ f^j(\rho) & \text{if } \rho \in]\sigma^j, 1], \end{cases} \tag{4.1.5}$$

Note that from (4.1.2), (4.1.3) and from the knowledge of γ_i, there exists a unique $\hat{\rho}_i$ such that $\hat{\gamma}_i := f^i(\hat{\rho}_i)$. Moreover, since the number of cars entering the junction J are the same as the number of cars exiting the junction, we have

$$\sum_{i=1}^{n} \hat{\gamma}_i = \sum_{i=n+1}^{m} \hat{\gamma}_i. \tag{4.1.6}$$

To construct a boundary Riemann solver at the function J, we need to give additional constraints to (4.1.4) and (4.1.6) to select a unique $(\hat{\gamma}_1, \cdots, \hat{\gamma}_{n+m})$.

In [30], the authors select a unique $(\hat{\gamma}_1, \cdots, \hat{\gamma}_{n+m})$ solving the following maximization problem

$$\sup_{(\gamma_1,\cdots\gamma_n)\in\Omega} \sum_{i=1}^{n} \gamma_i,$$

where

$$\Omega = \left\{(\gamma_1, \cdots \gamma_n) \in \Omega_1 \times \cdots \times \Omega_n \,/\, A(\gamma_1, \cdots \gamma_n)^T \in \Omega_{n+1} \times \cdots \Omega_{n+m}\right\}. \tag{4.1.7}$$

The set $(\Omega_i)_{i=1,\cdots n+m}$ are defined in (4.1.4) and A is a traffic distribution matrix that describes the distribution of the traffic among outgoing roads. The matrix

$$A = \begin{pmatrix} \alpha_{n+1,1} & \cdots & \alpha_{n+1,n} \\ \vdots & \vdots & \vdots \\ \alpha_{n+m,1} & \cdots & \alpha_{n+m,n} \end{pmatrix}$$

satisfies for any $i \in \{1, \cdots, n\}$, $\sum_{j=n+1}^{n+m} \alpha_{j,i} = 1$ and a "restricted" technical condition (see condition (C) in [30]). In particular, Condition (C) requires that $m \geq n$. In [30], the authors proved that the optimization problem admits a unique maximizer $(\hat{\gamma}_1, \cdots, \hat{\gamma}_n)$ and $(\hat{\gamma}_{n+1}, \cdots, \hat{\gamma}_{n+m}) := A(\gamma_1, \cdots \gamma_n)^T \in$

$\Omega_{n+1} \times \cdots \times \Omega_{n+m}$. When there are $n \geq 2$ incoming roads and $m = 1$ outgoing road, condition (C) on A in [30] do not hold. Thus, the authors in [30] added a priority lane constraint $q\gamma_2 = (1-q)\gamma_1$ to find a unique $(\hat{\gamma}_1, \cdots, \hat{\gamma}_{n+m})$.

We can also select a unique $(\hat{\gamma}_1, \cdots, \hat{\gamma}_{n+m})$ from real-world junctions when considering $n:1$ junctions and $1:m$ junction, see Figure 4.4. The choices of using $n:1$ junctions and $1:m$ junctions will be explained later in Section 4.2.1, motivated by the use of flux interchanges. For clarity, we restrict the presentation to the case $2:1$ and $1:2$. The cases $n:1$ an $1:m$ are easy to adapt from $2:1$ and $1:2$

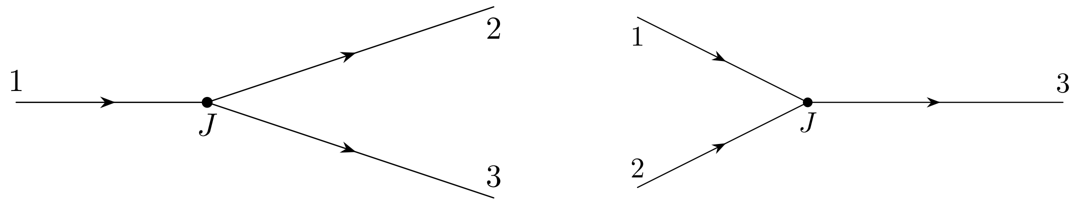

Figure 4.3 – Illustration of 1:2 Junction and 2:1 junction

Junction $2:1$**.** We need to give additional constraints to (4.1.4) and (4.1.6) in order to select a unique $(\hat{\gamma}_1, \hat{\gamma}_2, \hat{\gamma}_3)$. From (4.1.4), we have $\hat{\gamma}_1 + \hat{\gamma}_2 = \hat{\gamma}_3$.

— Junctions without spillover and with capacity-weighted allocation :

$$\hat{\gamma}_1 = \min\left(D(\rho_0^1), q(S(\rho_0^3))\right),$$
$$\hat{\gamma}_2 = \min\left(D(\rho_0^2), (1-q)(S(\rho_0^3))\right),$$

where $q \in [0.1]$ is a capacity-weighted parameter.

— Junctions with spillover and capacity-weighted allocation :

$$\hat{\gamma}_1 = \min\left(D(\rho_0^1), \max\left(S(\rho_0^3) - D(\rho_0^2), q(S(\rho_0^3))\right)\right),$$
$$\hat{\gamma}_2 = \min\left(D(\rho_0^2), \max\left(S(\rho_0^3) - D(\rho_0^1), (1-q)(S(\rho_0^3))\right)\right),$$

where $q \in [0.1]$ is a capacity-weighted parameter. This case corresponds to the flux maximization described in [30, Section 5.2.2].

— Junctions with mix-spillover (crossing allowed from road 2 to road 1) and capacity-weighted allocation

$$\hat{\gamma}_1 = \min\left(D(\rho_0^1), q(S(\rho_0^3))\right),$$
$$\hat{\gamma}_2 = \min\left(D(\rho_0^2), \max\left(S(\rho_0^3) - D(\rho_0^1), (1-q)(S(\rho_0^3))\right)\right),$$

where $q \in [0.1]$ is a capacity-weighted parameter.

— Junctions with spillover and lane priority allocation, we have

$$\hat{\gamma}_1 = \min\left(D(\rho_0^1), S(\rho_0^3)\right),$$
$$\hat{\gamma}_2 = \min\left(D(\rho_0^2), S(\rho_0^3) - \hat{\gamma}_1\right).$$

In a more general case, for a junction of type $n:1$, we can choose any $(\gamma_1, \cdots, \gamma_n, \gamma_{n+1})$ that satifies, for any $i \in \{1, \cdots, n\}$,

$$\gamma_i = \min(D(\rho_0^i), \alpha_i(S(\rho_0^{n+1}))) \text{ and } \gamma_e = \sum_{i=1}^{n} \gamma_i = \sum_{i=1}^{n} \min(D(\rho_0^i), \alpha_i(S(\rho_0^{n+1}))) \leq S(\rho_0^{n+1}), \tag{4.1.8}$$

where $\alpha_i : [0, f^i_{\max}] \to \mathbb{R}_+$ is a non-decreasing continuous function that encodes ingoing rules at the junction J.

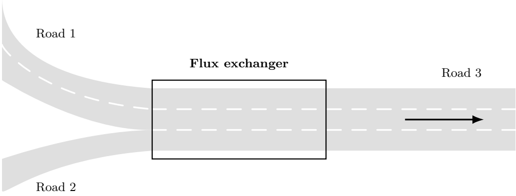

Junctions with spillover : overtaking is allowed

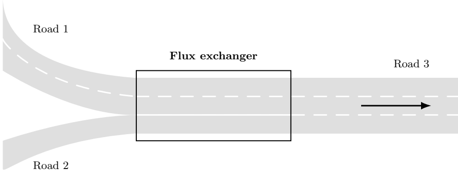

Junctions without spillover : overtaking is prohibited

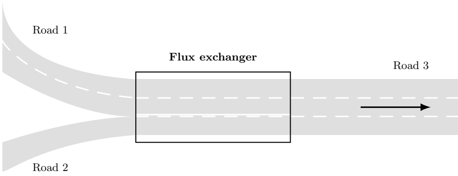

Junctions with mix-spillover : crossing from road 2 to road 1 is allowed

Figure 4.4 – Different real-world junctions $J_{2:1}$

Junction $1:2$**.** From (4.1.4), we have $\hat{\gamma}_1 = \hat{\gamma}_2 + \hat{\gamma}_3$.

— The FIFO rules [49], i.e if an outgoing road is blocked, no flow through the junction is allowed :

$$\begin{aligned}
\hat{\gamma}_1 &= \min\left(D(\rho_0^1), \tfrac{S(\rho_0^2)}{\beta}, \tfrac{S(\rho_0^3)}{(1-\beta)}\right), \\
\hat{\gamma}_2 &= \beta\hat{\gamma}_1, \\
\hat{\gamma}_3 &= (1-\beta)\hat{\gamma}_1.
\end{aligned}$$

— Junction J without spillover [61, 67] :

$$\begin{aligned}
\hat{\gamma}_2 &= \min\left(\beta D(\rho_0^1), S(\rho_0^2)\right), \\
\hat{\gamma}_3 &= \min\left((1-\beta)D(\rho_0^1), S(\rho_0^3)\right),
\end{aligned} \tag{4.1.9}$$

with $\beta \in [0,1]$.

— Junction with spillover:

$$\begin{aligned}
\hat{\gamma}_2 &= \min\left(\max(\beta D(\rho_0^1), D(\rho_0^1) - S(\rho_0^3)), S(\rho_0^2)\right) \\
\hat{\gamma}_3 &= \min\left(\max((1-\beta)D(\rho_0^1), D(\rho_0^1) - S(\rho_0^2)), S(\rho_0^3)\right)
\end{aligned} \tag{4.1.10}$$

with $\beta \in [0,1]$. The term $D(\rho_0^1) - S(\rho_0^i)$ could be replaced by $D(\rho_0^1) - \gamma_i S(\rho_0^i)$ where $\gamma_i \in [0,1]$ is the percent of drivers that want to choose road i even if it is blocked.

In a more general case, for a junction of type $1:m$, we can choose any $(\gamma_1, \gamma_2, \cdots, \gamma_{1+m})$ that satisfies, for any $i \in \{2, \cdots, 1+m\}$,

$$\gamma_i = \min(\beta_i(D(\rho_0^1)), S(\rho_0^i)) \text{ and } \gamma_1 = \sum_{i=2}^{1+m} \gamma_i \leq \sum_{i=2}^{1+m} \min(\beta_i(D(\rho_0^1)), S(\rho_0^i)) \leq D(\rho_0^1) \tag{4.1.11}$$

where $\beta_i : [0, f^i_{\max}] \to \mathbb{R}_+$ is a non-decreasing continuous function that encodes outgoing rules at the junction J.

$\mathcal{G}$-entropy solutions for Cauchy network problem. We have so far described the structure of junctions with n ingoing roads and m outgoing roads for any $n, m \in \mathbb{N}^*$ using Riemann solvers for the ingoing/outgoing roads and within the junction. The structure is inspired by real-word junctions that incorporate capacity-weighted and priority lanes allocation (with or without spillover). Using wave-front tracking algorithms, we construct approximate solution $(\rho^1_p, \cdots, \rho^{n+m}_p)$ of the following first order macroscopic traffic flow models for networks, see [4, 5, 79]. We now give a mathematical setting to have existence of solutions for a Cauchy Problem using the notion of $\mathcal{G}$-entropy solutions, see in [79].

Let $J = 0$ a $n : m$ junction. We say that $\rho = (\rho^i)_{i=1,\cdots n+m}$ is a $\mathcal{G}$-entropy solution if

$$\begin{cases} \partial_t \rho^i(t,x) + \partial_x f^i(\rho^i(t,x)) = 0, & (t,x) \in \mathbb{R}^+ \times I_i, \\ \rho^i(0,x) = \rho^i_0(x), & x \in I_i, \\ \rho(t,0) \in \mathcal{G}, & t \in \mathbb{R}^+, \end{cases} \tag{4.1.12}$$

where the junction conditions satisfied by the trace of $\rho = (\rho^1, \cdots, \rho^{n+m})$ on $\{x = 0\}$, are encoded by a given set $\mathcal{G} \in [0,1]^{n+m}$. More precisely, for any $i \in \{1, \cdots, n+m\}$, for any number $k \in [0,1]$ and any positive function $\phi \in C^1_c(\mathbb{R} \times (a_i, b_i))$, we have

$$\begin{aligned} &\int_0^{+\infty} \int_{a_i}^{b_i} |\rho^i(t,x) - k|\, \partial_t \phi(t,x) + \operatorname{sgn}(\rho^i(t,x) - k) \left(f^i(\rho^i(t,x)) - f^i(k)\right) \partial_x \phi(t,x)\, dx\, dt \\ &\quad + \int_0^L |\rho^i_0(x) - k|\, \phi(0,x)\, dx \geq 0, \end{aligned} \tag{4.1.13}$$

and the set $\mathcal{G} \in [0,1]^{n+m}$ is a germ defined by stationary solutions for associated Riemann problems on the junction.

Definition 4.1.1 ($\mathcal{G}$-Riemann problem [79])**.** Let $\rho_0 = (\rho^i_0)_{i=1,\cdots,n+m} \in [0,1]^{n+m}$, we say that $\rho = (\rho^i)_{i=1,\cdots,n+m}$ is a $\mathcal{G}$-entropy solution to the $\mathcal{G}$-Riemann problem with initial data ρ_0, if ρ^i satisfies (4.1.13) and for all i, we have

$$\begin{cases} \rho^i(t,x) = \rho^i(1, \frac{x}{t}), & (t,x) \in \mathbb{R}^+ \times I_i, \\ \rho^i(0,x) = \rho^i_0(x), & x \in I_i, \\ \rho(t,0) = p \in \mathcal{G}, & t \in \mathbb{R}^+, \end{cases} \tag{4.1.14}$$

for some $p = (p^1, \cdots, p^{n+m}) \in \mathcal{G}$. The solution is denoted by $\rho = \rho^{\mathcal{G}}_{\rho_0,p}$.

Definition 4.1.2 (Generalized Riemann germ [79])**.** A set $\mathcal{G}$ is called a generalized Riemann germ if for any initial data $\rho_0 \in [0,1]^{n+m}$, there exists a unique $\mathcal{G}$-entropy solution $\rho^{\mathcal{G}}_{\rho_0,p}$ to the $\mathcal{G}$-Riemann problem (4.1.14) with some trace $p \in \mathcal{G}$ at $x = 0$.

Let $\mathcal{G} \subset [0,1]^{n+m}$ be a generalized Riemann germ. We will consider a particular subclass of $\mathcal{G}$, so-called Kruzkov germs (or D-germ).

Definition 4.1.3 (Kruzkov germs [79])**.** We say that $\mathcal{G}$ is a Kruzkov germ if it satisfies, for any $(p, \bar{p}) \in \mathcal{G}^2$,

$$D^f(p, \bar{p}) := \sum_{i=1}^{n} q_i(p^i, \bar{p}^i) - \sum_{i=n+1}^{m} q_i(p^i, \bar{p}^i) \geq 0, \tag{4.1.15}$$

where q_i is the entropy flux defined by, for any $i \in \{1, \cdots, n+m\}$, $q_i(p^i, \bar{p}^i) = \operatorname{sign}(p^i - \bar{p}^i)(f^i(p^i) - f^i(\bar{p}^i))$.

We now five an example of a Kruzkov germ on 1:2 junctions introduced in [25, Section 2.1].

Example. In [25, Section 2.1], the authors introduce a general family of germs on 1:2 junctions defined as follows. The family is described by a set of parameters

$$\Lambda = \{\bar{\lambda}^0, \bar{\lambda}^1, \bar{\lambda}^2, \hat{\lambda}^1, \hat{\lambda}^2\},$$

satisfying the following conditions

$$\begin{cases} \bar{\lambda}^i \in [0, f^i_{\max}], & i = 0,1,2, \\ \bar{\lambda}^0 = \bar{\lambda}^1 + \bar{\lambda}^2, & \\ \text{the map } \hat{\lambda}^i : [0, f^0_{\max}] \to [0, f^i_{\max}] \text{ is nondecreasing and continuous,} & i = 1,2, \\ \hat{\lambda}^i(0) = 0, \quad \hat{\lambda}^i(\bar{\lambda}^0) = \bar{\lambda}^i, & i = 1,2, \\ \hat{\lambda}^1(\lambda) + \hat{\lambda}^2(\lambda) = \min(\lambda, \bar{\lambda}^0). & \end{cases} \tag{4.1.16}$$

The function $(\hat{\lambda}^i)_{i=1,2}$ stands for the distribution traffic on the $1:2$ junction, i.e $\hat{\lambda}^i(\cdot)$ describes how the traffic is distributed in percentages to the road i from the ingoing road 0. The germ G_Λ is defined from Λ as follows :

$$G_\Lambda := \left\{ P = (p^0, p^1, p^2) \in [0,1]^3 \;\middle|\; \begin{array}{l} 0 \le f^i(p^i) \le \bar{\lambda}^i, \;\; i = 0,1,2, \\ f^0(p^0) = f^1(p^1) + f^2(p^2), \\ D^i(p^i) \ge \hat{\lambda}^i\big(D^0(p^0)\big), \;\; i = 1,2 \end{array} \right\}. \tag{4.1.17}$$

Let $i = 1,2$, the condition $D^i(p^i) \ge \hat{\lambda}^i\big(D^0(p_0)\big)$ means the number of vehicles per time going to road i from the road 0 is at least $\hat{\lambda}_i\big(D^0(p^0)\big)$ when the road k is empty or fluid. In [25, Lemma 2.14], the authors prove that G_Λ is a Kruzkov germ. For the sake of completeness, we will give a direct and intuitive proof that could be easily adapted to the case 2:2 junction.

Proof. Let $(p, \bar{p}) \in G^2_\Lambda$. Without loss of generality, we assume that $\bar{p}^0 < p^0$. From (4.1.6) and Definition 4.1.3, we have

$$\begin{aligned} D^f(p, \bar{p}) &= q^0(p^0, \bar{p}^0) - \textstyle\sum_{i=1}^2 q^i(p^i, \bar{p}^i), \\ &= \operatorname{sign}(p^0 - \bar{p}^0)(f^0(p^0) - f^0(\bar{p}^0)) - \textstyle\sum_{i=1}^2 q_i(p^i, \bar{p}^i), \\ &= \big[1 - \operatorname{sign}(p^1 - \bar{p}^1)\big]\,(f^1(p^1) - f^1(\bar{p}^1)) + \big[1 - \operatorname{sign}(p^2 - \bar{p}^2)\big]\,(f^2(p^2) - f^2(\bar{p}^2)), \\ &= 2\textstyle\sum_{k \in J}(f(p^k) - f(\bar{p}^k)), \end{aligned}$$

where $q^k(p^k, \bar{p}^k) := \operatorname{sign}(p^k - \bar{p}^k)(f^k(p^k) - f^k(\bar{p}^k))$ and $J = \{k \in \{1,2\} \,/ p^k < \bar{p}^k\}$. Let $k \in J$, we have three different cases : $p^k < \bar{p}^k < \sigma^k$, $p^k < \sigma^k < \bar{p}^k$ and $\sigma^k < p^k < \bar{p}^k$. Thus, we have

$$D^f(p, \bar{p}) = 2 \sum_{\substack{k \in J \\ p^k < \bar{p}^k < \sigma^k}} (f^k(p^k) - f^k(\bar{p}^k)) + 2 \sum_{\substack{k \in J \\ p^k < \sigma^k < \bar{p}^k}} (f^k(p^k) - f^k(\bar{p}^k)) + 2 \sum_{\substack{k \in J \\ \sigma^k < p^k < \bar{p}^k}} (f^k(p^k) - f^k(\bar{p}^k)). \tag{4.1.18}$$

We assume that $\sigma^0 \le p^0$. From (4.1.17) and the definition of the demand function, we have for any $k = 1,2$, $\sigma^k \le p^k$. Moreover, for any $k \in J$, we have $\sigma^k < p^k < \bar{p}^k$. By definition of f^k, we deduce that for any $k \in J$, $f^k(p^k) - f^k(\bar{p}^k) \ge 0$. From (4.1.18), $D^f(p, \bar{p}) \ge 0$. We now consider the case where $\bar{p}^0 < p^0 < \sigma^0$. In that case, we have $f^0(\bar{p}^0) \le f^0(p^0)$.

— If $\operatorname{card}(J) = 2$, from (4.1.17) and (4.1.18), we have $D^f(p, \bar{p}) = 2(f^1(p^1) - f^1(\bar{p}^1)) + 2(f^2(p^2) - f^2(\bar{p}^2)) = f^0(p^0) - f^0(\bar{p}^0) \ge 0$.

— If $\operatorname{card}(J) = 1$, without loss of generality, we assume that $1 \in J$ and we have $\bar{p}^2 \le p^2$. If $\bar{p}^2 \ge \sigma^2$, we have $f^2(p^2) \le f^2(\bar{p}^2)$ and using $f^0(\bar{p}^0) \le f^0(p^0)$ together with (4.1.17) and (4.1.18), $D^f(p, \bar{p}) = f^1(p^1) - f^1(\bar{p}^1) \ge f^2(\bar{p}^2) - f^2(p^2) \ge 0$.

  — If $\bar{p}^2 < \sigma^2$ and $p^1 < \sigma^1$, from (4.1.17), we have $f^2(\bar{p}^2) \ge \hat{\lambda}^2\big(D^0(\bar{p}^0)\big)$ and $f^1(p^1) \ge \hat{\lambda}^1\big(D^0(p^0)\big)$. We argue by contradiction that $f^1(\bar{p}^1) \le \hat{\lambda}^1\big(D^0(\bar{p}^0)\big)$; assuming that $f^1(\bar{p}^1) > \hat{\lambda}^1\big(D^0(\bar{p}^0)\big)$. From $f^2(\bar{p}^2) \ge \hat{\lambda}^2\big(D^0(\bar{p}^0)\big)$, (4.1.16) and (4.1.17), we have

$$\lambda^0 \ge f^0(\bar{p}^0) = f^1(\bar{p}^1) + f^2(\bar{p}^2) > \hat{\lambda}^1\big(D^0(\bar{p}^0)\big) + \hat{\lambda}^2\big(D^0(\bar{p}^0)\big) = \min(D^0(\bar{p}^0), \bar{\lambda}^0),$$

that leads to a contradiction using that $D^0(\bar{p}^0) = f^0(\bar{p}^0)$. Thus, we have

$$f^1(\bar{p}^1) \leq \hat{\lambda}^1\big(D^0(\bar{p}^0)\big) \leq \hat{\lambda}^1\big(D^0(p^0)\big) \leq D^1(p^1) = f^1(p^1).$$

As a consequence, from (4.1.18), $D^f(p,\bar{p}) = f^1(p^1) - f^1(\bar{p}^1) \geq 0$.

— If $\bar{p}^2 < \sigma^2$ and $\sigma^1 < p^1 < \bar{p}^1$, we have $f^1(p^1) \geq f^1(\bar{p}^1)$ and from (4.1.18), $D^f(p,\bar{p}) = f^1(p^1) - f^1(\bar{p}^1) \geq 0$.

— If $\mathrm{card}(J) = 0$, from (4.1.18), we have $D^f(p,\bar{p}) = 0$.

$\square$

Let $\rho_0^k \in BV(I_k;[0,1])$ for all $k = 0,1,2$, from [79, Theorem 2.34], there exists a unique $\mathcal{G}$-entropy solution ρ of (4.1.12) with initial data ρ^0. Moreover, we have $\rho \in Lip([0,\infty);\prod_{k=0}^{2} L^1(I_k))$. Moreover, the L^1-contraction property holds for (4.1.12), i.e if ρ_0 and $\bar{\rho}_0$ are two initial data and ρ and $\bar{\rho}$ are respectively their associated $\mathcal{G}$-entropy solutions, then we have for all time $t > 0$,

$$\int_{\{t\}\times I} |\rho - \bar{\rho}|(t,\cdot)dx \leq \int_J |\rho_0 - \bar{\rho}_0|dx,$$

where $I = \{0\} \cup_{k=0}^{2} I_k$.

4.2 Open questions and perspectives

4.2.1 Road network with a flux interchange

To avoid condition (C) on the distributive matrix A (see Section 4.1), we will use a flux interchange. More precisely, scalar macroscopic models cannot distinguish which specific vehicles entering a junction from different incoming roads correspond to which vehicles exiting on the outgoing roads. Thus, the junction $n : m$ is decomposed into an $n : 1$ junction followed by a $1 : m$ junction. Roughly speaking, the flux of the n incoming roads passes into a flux interchange, which distributes it across the m exiting roads, see Figure 4.5. We assume that the flux of cars thought the interchange is a strictly concave C^2 function f^e and

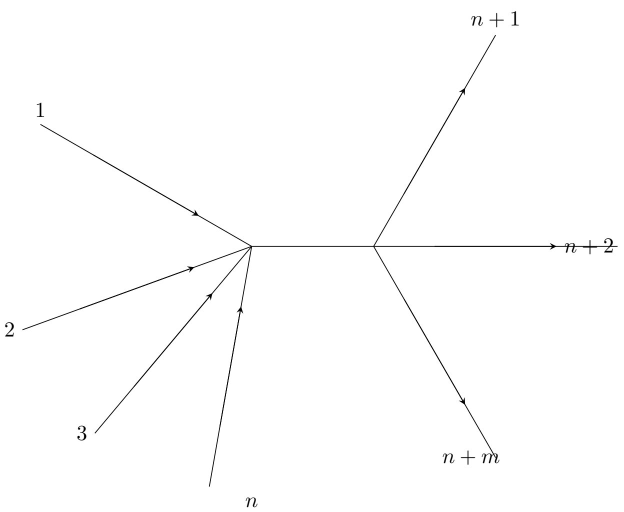

Figure 4.5 – The flux of the n incoming roads passes into a flux interchange, which distributes it across the m exiting roads.

$f^e(0) = f^e(1)$. The density of cars ρ_e in the interchange depends on the flux entering and exiting the flux interchange. Let $\rho_0^e \in [0,1]$, we construct the Riemann solution $RS_J(\rho_0^1, \cdots, \rho_0^{n+m})$ at the junction J with n entry roads and m exit roads in two steps. First we construct the Riemann solver $RS_{J_{n:1}}(\rho_0^1, \cdots, \rho_0^n, \rho_0^e)$ at the $n:1$ junction $J_{n:1}$ and the Riemann solver $RS_{J_{1:m}}(\rho_0^e, \rho_0^{n+1}, \cdots, \rho_0^{n+m})$ at the $1:m$ junction $J_{1:m}$ as in Section 4.1. Finally, we choose a density ρ_0^e such that (4.1.6) holds, i.e the number of cars entering the flux interchange is the same as the ones exiting it.

Existence of the flux interchange density ρ_e for $n : m$ junction. Let us define $\varphi : \rho_0^e \to \sum_{i=1}^n \hat{\gamma}_i(\rho_0^e) - \sum_{i=n+1}^{n+m} \hat{\gamma}_i(\rho_0^e)$. From (4.1.8), (4.1.11) and since, for any $i \in \{1, \cdots, n+m\}$, $S^i(1) = 0$ and $D^i(0) = 0$, we have, for any $i \in \{1, \cdots, n\}$, $\hat{\gamma}_i(1) = 0$ and for any $i \in \{n+1, \cdots, n+m\}$, $\hat{\gamma}_i(0) = 0$. Thus, $\varphi(0) \geq 0$ and $\varphi(1) \leq 0$. Since $\alpha_i : [0, f^i_{\max}] \to \mathbb{R}_+$, $\beta_i : [0, f^i_{\max}] \to \mathbb{R}_+$ and the demand function $D^i(\cdot)$ are non-decreasing continuous functions and the supply function $S^i(\cdot)$ is a non-increasing continuous function, we deduce that $\rho_0^e \to \sum_{i=1}^n \hat{\gamma}_i(\rho_0^e)$ is a non-increasing continuous function and $\rho_0^e \to \sum_{i=1+n}^{n+m} \hat{\gamma}_i(\rho_0^e)$ is a non-decreasing continuous function. As a consequence, φ is a non-increasing continuous function. Thus, there exists at least one $\rho_0^e \in [0,1]$ such that $\varphi(\rho_0^e) = 0$. Moreover, if there exists an interval $[a,b]$ such that for any $\rho \in [a,b]$, $\varphi(\rho) = 0$, then the value of $\hat{\gamma}_i$ is constant over $[a,b]$. Thus, we can choose any $\rho_0^e \in [a,b]$. From (4.1.5), we note that $S^e(\rho_0^e)$ and $D^e(\rho_0^e)$ depends on the flux f^e through the interchange.

We now give an example of Kruzkov germ on 2:2 junction using the flux interchange. Using Section 4.1, we introduce a general family of germs on 2:2 junctions similarly to (4.1.16) and (4.1.17) as follows (see Figure 4.6). The family is described by a set of parameters

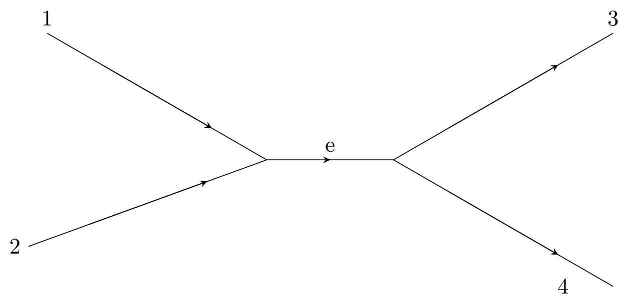

Figure 4.6 – The flux of the 2 incoming roads passes into a flux interchange, which distributes it across the 2 exiting roads.

$$\Lambda = \{\bar{\lambda}^1, \bar{\lambda}^2, \bar{\lambda}^3, \bar{\lambda}^4, \bar{\lambda}^e, \hat{\lambda}^1, \hat{\lambda}^2, \hat{\lambda}^3, \hat{\lambda}^4\}$$

satisfying the following conditions

$$\begin{cases} \bar{\lambda}^k \in [0, f^k_{\max}], & k \in \{1,2,e,3,4\} \\ \bar{\lambda}^1 + \bar{\lambda}^2 = \lambda^e = \bar{\lambda}^3 + \bar{\lambda}^4, & \\ \text{the map } \hat{\lambda}^k : [0, f^e_{\max}] \to [0, f^k_{\max}] \text{ is nondecreasing and continuous,} & k \in \{1,2,3,4\}, \\ \hat{\lambda}^k(0) = 0, \quad \hat{\lambda}^k(\bar{\lambda}^e) = \bar{\lambda}^k, & k \in \{1,2,3,4\}, \\ \hat{\lambda}^1(\lambda) + \hat{\lambda}^2(\lambda) = \min(\lambda, \bar{\lambda}^e) = \hat{\lambda}^3(\lambda) + \hat{\lambda}^4(\lambda). & \end{cases} \tag{4.2.1}$$

The germ G_Λ is defined from Λ as follows :

$$G_\Lambda := \left\{ P = (p^1, p^2, p^e, p^3, p^4) \in [0,1]^5 \;\middle|\; \begin{array}{l} 0 \leq f^k(p^k) \leq \bar{\lambda}^k, \; k = \{1,2,e,3,4\} \\ f^1(p^1) + f^2(p^2) = f^e(p^e) = f^3(p^3) + f^4(p^4) \\ S^k(p^k) \geq \hat{\lambda}^k\big(S^e(p^e)\big), \; k = 1,2 \\ D^k(p^k) \geq \hat{\lambda}^k\big(D^e(p^e)\big), \; k = 3,4 \end{array} \right\}. \tag{4.2.2}$$

Let $k = 1, 2$, the inequality $S^k(p^k) \geq \lambda^k\big(S^e(p^e)\big)$ means that, when the k^{th} ingoing road is congested ($\sigma^k < \rho^k$), the number of vehicles per time going from the road k to e road is at least $\lambda^k\big(S^e(p^e)\big)$. The condition $D^k(p^k) \geq \hat{\lambda}_k\big(D^0(p_0)\big)$ means that, when the road k is empty or fluid ($\rho^k < \sigma^k$), the number of vehicles per time going to road k from the road e is at least $\hat{\lambda}^k\big(D^e(p_e)\big)$. Adapting the proof showing that G_Λ defined in (4.1.17) for $1:2$ junctions is a Kruzkov germ, we have G_Λ defined in (4.2.2) for $2:2$ junctions is a Kruzkov germ, i.e for any $(p,\bar{p}) \in G^2_\Lambda$, $D^f(p,\bar{p}) \geq 0$. From [79, Theorem 2.34], we deduce that there exists a unique $\mathcal{G}$-entropy solution ρ of (4.1.12) with $\mathcal{G} := G_\Lambda$ defined in (4.2.2).

4.2.2 Open problem 1 : find physically realistic germ families and prove existence of solutions

The general family of germs on $1:2$ junctions (4.1.17), defined in [25, Section 2.1], has certain limitations as described below.

The general family of germs on $1:3$ junctions $G^{1:3}_\Lambda$ defined by

$$G^{1:3}_\Lambda := \left\{ P = (p^0,p^1,p^2,p^3) \in [0,1]^4 \;\middle|\; \begin{array}{l} 0 \leq f^k(p^k) \leq \bar{\lambda}^k, \; k = 0,1,2,3 \\ f(p^0) = f^1(p^1) + f^2(p^2) + f^3(p^3) \\ D^k(p^k) \geq \hat{\lambda}^k\big(D^0(p^0)\big), \; k = 1,2,3 \end{array} \right\}, \tag{4.2.3}$$

is not an Krukzkov germ. More precisely, we consider the flux $f : \rho \to 100\rho(1-\rho)$ for any road, i.e $f^0 = f^1 = f^2 = f^3 := f$, the distribution traffic conditions are, for any $\lambda \in [0,25]$, $\hat{\lambda}^1 = \frac{1}{4}\lambda$, $\hat{\lambda}^2(\lambda) = \frac{1}{4}\lambda$ and $\hat{\lambda}^3(\lambda) = \frac{1}{2}\lambda$ and $(\bar{\lambda}^0, \bar{\lambda}^1, \bar{\lambda}^2, \bar{\lambda}^3) = (25, 6.25, 6.25, 12.5)$. Let $(p,\bar{p}) \in [0,1]^8$ defined by $f(p^0) = 22$ and $p^0 < 0.5$, $f(p^1) = 5.5$ and $p^1 < 0.5$, $f(p^2) = 4$ and $p^2 > 0.5$, $f(p^3) = 12,5$ and $p^3 > 0.5$ and $f(\bar{p}^0) = 20$ and $\bar{p}^0 < 0.5$, $f(\bar{p}^1) = 6,25$ and $\bar{p}^1 < 0.5$, $f(\bar{p}^2) = 3.75$ and $\bar{p}^2 > 0.5$, $f(\bar{p}^3) = 10$ and $\bar{p}^3 < 0.5$. We see that $(p,\bar{p}) \in G^{1:3}_\Lambda$, in particular we have

$$\begin{array}{l} 5.5 = f(p^1) \geq \hat{\lambda}^1(D(p^0)) = 5.5, \\ 6.25 = f(\bar{p}^1) \geq \hat{\lambda}^1(D(\bar{p}^0)) = 5, \\ 10 = f(\bar{p}^3) \geq \hat{\lambda}^3(D(\bar{p}^0)) = 10. \end{array}$$

Since $\bar{p}^0 < p^0$, we have

$$\begin{array}{rl} D^f(p,\bar{p}) & = q(p^0,\bar{p}^0) - \sum_{i=1}^3 q(p^i,\bar{p}^i), \\ & = \mathrm{sign}(p^0 - \bar{p}^0)(f(p^0) - f(\bar{p}^0)) - \sum_{i=1}^3 q(p^i,\bar{p}^i), \\ & = 2\sum_{k\in J}(f(p^k) - f(\bar{p}^k)), \end{array} \tag{4.2.4}$$

where $q(p^k,\bar{p}^k) := \mathrm{sign}(p^k - \bar{p}^k)(f(p^k) - f(\bar{p}^k))$ and $J = \{k \in \{1,2,3\} \,/ p_k < \bar{p}_k\}$. From the definition of $(p,\bar{p})$, we have $\bar{p}^0 < p^0 < 0.5$, $p^1 < \bar{p}^1 < 0.5$, $0.5 < p^2 < \bar{p}^2$ and $\bar{p}^3 < 0.5 < p^3$. From (4.2.4), we deduce that

$$\begin{array}{rl} D^f(p,\bar{p}) & = 2(f(p^1) - f(\bar{p}^1)) + 2(f(p^2) - f(\bar{p}^2), \\ & = 2(5.5 - 6.25) + 2(4 - 3.75) < 0. \end{array}$$

The general family of germs on $1:2$ junctions (4.1.17) has limited spillover effects. More precisely, we consider the flux $f : \rho \to 100\rho(1-\rho)$ for any road, i.e $f^0 = f^1 = f^2 := f$, the distribution traffic conditions are, for any $\lambda \in [0,25]$, $\hat{\lambda}^1(\lambda) = \frac{1}{5}\lambda$, $\hat{\lambda}^2(\lambda) = \frac{4}{5}\lambda$ and $(\bar{\lambda}^0, \bar{\lambda}^1, \bar{\lambda}^2, \bar{\lambda}^3) = (25, 5, 20)$. Let $p = (p^0,p^1,p^2) \in [0,1]^3$ such that $p^0 \geq 0.5$ and $p^2 = 1$, it means that the outgoing road 2 is fully congested. To have $p \in G^{1:3}_\Lambda$ defined in (4.1.17), we need to impose that $f(p^1) \leq \bar{\lambda}^1 = \hat{\lambda}^1(25) = 5$ and $f(p^0) = f(p^1)$. Thus, we cannot redirect all the vehicles from the road 2 to the road 1. But it could be done using the description of $1:2$ junctions in Section 4.1. More precisely, we consider the initial data $(\rho^0_0, \rho^1_0, \rho^2_0)$ such that $f(\rho^0_0) = 20$ and $\rho^0_0 > 0.5$, $\rho^1_0 = 0$ and $\rho^2_0 = 1$. From (4.1.10),

$$\begin{array}{l} f(p^1) = \min\big(\max(\beta D(\rho^0_0), D(\rho^0_0) - S(\rho^2_0)), S(\rho^1_0)\big) = \min(\max(5,25),25) = 25, \\ f(p^2) = \min\big(\max((1-\beta)D(\rho^0_0), D(\rho^0_0) - S(\rho^1_0)), S(\rho^2_0)\big) = \min(\max(20,0),0) = 0, \\ f(p^0) = f(p^1) + f(p^2) = 25. \end{array}$$

Thus, since the road 2 is fully congested, all vehicles are redirected to the road 1.

This leads to the following interesting open questions :

1. Is it possible to define a general germ $\mathcal{G}$ that captures realistic intersection behaviors, including spillover effects (e.g. road markings), priority rules, traffic signals, and flow/speed-reducing features (e.g. tollgates, speed bump) ?
2. For any type of junction (traffic light, stop sign, roundabout, on-ramp, off-ramp, etc.), can one identify a sub-germ $\mathcal{G}^J$ of $\mathcal{G}$ that accurately models its behavior?
3. Can we prove existence of $\mathcal{G}$-entropy solutions/ $\mathcal{G}^J$-entropy solutions for Cauchy network problem ?
4. Can we replace LWR equation on each branch by a second-order models as GARZ (2.1.5)?

To find a realistic family of germs on $n : m$ junctions, rules can be introduced to specify entry priorities into the flux exchanger or/and to redistribute traffic from a congested road $n+j$ to the remaining outgoing roads $(n+i)_{i\neq j}$. Can we find additional rules that make the Germ G_Λ a Kruzkov germ and use existence and uniqueness theory for Kruzkov germs from [79]. We can also prove existence of solutions using two other different strategies

— We can try to estimate the number of waves and interactions, and the total variation of the flux along an approximate wave front tracking solution as in [49, Section 5.3] for $2 : 2$ junctions. At first glance, it should be the most suitable approach since the framework developed in [79] does not extend to second-order models.

— We can try to use a system of ODEs that models the evolution of traffic flow at the microscopic level on the network.

The following section addresses this latter point and will enable the construction of realistic germs derived from microscopic junctions such as roundabouts and entry or exit lanes.

4.2.3 Open problem 2 : microscopic to macroscopic networks

In [42, 62], the authors prove that the microscopic model FTL (2.2.1) converge to the LWR model (1.1.1). In [35], the authors extend the micro–macro correspondence to traffic flow on networks by introducing a microscopic follow-the-leader model in which each vehicle follows a prescribed path through the network. They prove that the microscopic dynamics converge to the LWR-based multi-path model [22, 23]. However, this convergence result is only partial since the correspondence in the limit between the microscopic and the macroscopic model is proven population by population, i.e. fixing a path p and assuming the other paths/solutions are fixed/given. A global convergence result for all interacting paths simultaneously would require a well-posed macroscopic limit system, which remains an open problem.

Furthermore, the microscopic formulation is based on FIFO (first-in, first-out) dynamics (a.e if the first car on the incoming road wants to go to the congested road, it will stop. After that, all the following cars will stop too, even if they want to turn to the other outgoing road). It also permits mild vehicle overlaps near junctions (a.e if two cars reach a junction simultaneously from different roads and intend to take different exits, they do not interact and experience no slowdown). This phenomenon significantly reduces the model's physical realism. In [25], the author rigorously derive macroscopic junction conditions for traffic flow models governed by scalar conservation laws through a homogenization process. The study focuses on $1 : 2$ and $2 : 1$ junctions, where at the mesoscopic scale, vehicle dynamics are controlled by periodic traffic lights or flux limiters. The paper introduces a general family of Kruzkov germs G_Λ defined in (4.1.17) for 1:2 junctions and they prove the convergence (homogenization) of the mesoscopic model toward a macroscopic conservation law network with the Kruzkov germs G_Λ. In [24], the authors derive a macroscopic conservation law for a network with $2 : 1$ junctions from a discrete follow-the-leader model, where the junction priority is controlled by a time-periodic traffic light. The solution is understood in the sense of (4.1.12) where the generalized germ is defined as

$$G_\Lambda := \left\{ P = (p^0, p^1, p^2) \in [0, \rho_{\max}]^3 \;\middle|\; \begin{array}{l} 0 \le f^k(p^k) \le \theta^k \max f^k,\ k = 0, 1, 2, \\ f^0(p^0) = f^1(p^1) + f^2(p^2), \\ S^k(p^k) \ge \theta^k S^2(p^2),\ k = 0, 1, \end{array} \right\}, \tag{4.2.5}$$

where $f^1 = f^2 = f^3 := f$ and $\theta^1 := \theta$, $\theta^2 = 1 - \theta$ and $\theta^3 = 1$, with $\theta \in (0, 1)$. These works are limited to 1:2 and 2:1 junctions, extension to larger networks remains open. Finally, as already mentioned in Section 4.2.2, the Kruzkov germs G_Λ defined (4.1.17) has limited spillover effect and they fail to incorporate rerouting dynamics.

This leads to the following interesting open questions.

1. For each type of junctions J (stop, roundabout, on-ramp, off-ramp, with spillover, without spillover), can we construct a system of ODEs that converge to the $\mathcal{G}^J$-entropy solutions for Cauchy network problem with $n : m$ junctions?
2. Can we prove microscopic to macroscopic results when we replace LWR on each road by the second-order model GARZ?

The main difficulty to extend the results in [42, 62] to macroscopic network lies in redefining the notion of the vehicle "ahead," since the index $i + 1$ is no longer necessarily the car directly in front of vehicle. Moreover, the non-overlapping condition (the discrete maximum principle) may fail when two vehicles coming from different incoming roads reach the junction simultaneously. At the microscopic level, the authors in [35] select specific vehicle paths within the network, while those in [24, 25] impose time-dependent traffic light rules to prescribe active paths over given intervals. This allows the dynamics to be described by a follow-the-leader behavior along each path, making it possible to apply the convergence results established in [42, 62]. To address the two open questions, the condition $\rho^k(t, 0) = p^k \in \mathcal{G}$ will be regarded as a reduction of the speed at the microscopic scale and we will derive LWR equations with boundary conditions from a Follow-the-leader type ODEs.

A preliminary results consists on finding a system of ODE that converges to the flux-constrained PDE

$$\partial_t \rho(t, x) + \partial_x (f(\rho(t, x))) = 0, \qquad (t, x) \in \mathbb{R}_+ \times \mathbb{R}, \tag{4.2.6a}$$

$$\rho(0, x) = \rho_0(x), \qquad x \in \mathbb{R}, \tag{4.2.6b}$$

$$f(\rho(t, 0))) \le \alpha \max_{\rho \in [0, \rho_{\max}]} f(\rho), \qquad t \in \mathbb{R}_+, \tag{4.2.6c}$$

This model describes the impact of tollgates on traffic flow and can be viewed as a particular case of (2.1.4), corresponding to a stationary autonomous vehicle (i.e, $\dot{y} = 0$).
Assuming that $\rho_0 \in BV(\mathbb{R})$ with $\|\rho_0\|_{L^1(\mathbb{R})} = 1$, $\rho_0 \ge 0$ and there exists a compact set $K \subset \mathbb{R}$ such that $\mathrm{Supp}(\rho_0) \subset K := [k_{\min}, k_{\max}]$. We introduce the sequence $(\bar{x}_i^n)_{i=0,\cdots,n}$ such that, for every $i \in \{1, \cdots, n\}$,

$$\bar{x}_i^n = \sup_{x \in \mathbb{R}} \left\{ x \in \mathbb{R} : \int_{\bar{x}_{i-1}^n}^{x} \rho_0(x) dx < l_n := \frac{1}{n} \right\}.$$

Above, $x_0^n := \sup\{x_0 \in \mathbb{R} / \rho_0(x) \le 0, \forall x \in (-\infty, x_0]\}$. We introduce the following system of ODE

$$\begin{cases} \dot{x}_i^n(t) = v\left(\frac{l_n}{x_{i+1}^n - x_i^n}\right) \phi_\epsilon(x_i^n(t)),\ i \in \{0, \cdots, n-1\}, \\ \dot{x}_n^n(t) = v_{\max} \phi_\epsilon(x_n^n(t)), \\ x_i^n(0) = \bar{x}_i^n,\ i \in \{0, \cdots, n\}, \end{cases} \tag{4.2.7}$$

with $\phi_\epsilon \in W^{2,\infty}(\mathbb{R})$ is a cut-off function defined by

$$\phi_\epsilon(x) = \begin{cases} 1, & \text{if } x \in (-\infty, -2\epsilon) \cup (2\epsilon, \infty), \\ \alpha \in (0, 1), & \text{if } x \in (-\epsilon, \epsilon). \end{cases} \tag{4.2.8}$$

We introduce the discretized density associated to (4.2.7) defined by

$$\rho_\epsilon^n(t,x) = \sum_{i=0}^{n-1} \frac{l_n}{x_{i+1}^n(t) - x_i^n(t)} \mathbb{1}_{[x_i^n(t), x_i^n(t))}(x), \tag{4.2.9}$$

with $l_n = \frac{1}{n}$ and for every $i \in \{0, \cdots, n\}$, $x_i(\cdot)$ is solution of (4.2.7). Since $\phi_\epsilon \in W^{2,\infty}(\mathbb{R})$, Kruzkov's theory [65] applies and provide existence and uniqueness of a weak entropy solution of

$$\begin{cases} \partial_t \rho(t,x) + \partial_x(\phi_\epsilon(x) f(\rho(t,x))) = 0, \\ \rho(0,x) = \rho_0(x). \end{cases} \tag{4.2.10}$$

From [46], the discretized density ρ_ϵ^n defined in (4.2.9) converge as $n \to \infty$ to ρ_ϵ the entropy solution of (4.2.10). From [31, Theorem 3.6], ρ_ϵ converges in L^1_{loc} to a function ρ as $\epsilon \to 0$ which is the unique weak entropy solution of (4.2.6). Thus, we have

$$\lim_{\epsilon \to 0} \lim_{n \to \infty} \rho_\epsilon^n = \rho, \quad \text{in } L^1_{\text{loc}}(\mathbb{R}_+ \times \mathbb{R}),$$

with ρ the unique entropy solution of (4.2.6). Informally, we have constructed a system of ODEs that converge to $\mathcal{G}^J$-entropy solutions for Cauchy network problem with $1:1$ junctions where J is a flux restriction area (tollgates, speed bump), see more details in Section 7.1. Physically speaking, our strategy is as follows. We consider n vehicles moving on a traffic network consisting of one incoming and one outgoing road, with the junction located at $x = 0$. Within the interval (ϵ, ϵ), the vehicle speed is reduced by a factor α. We then take the limit as the number of vehicles tends to infinity while conserving the total mass, and finally shrink the speed-limited region to a point by letting $\epsilon \to \infty$. Note that this approach naturally gives rise to two open sub-questions.

1. Can we construct a system of ODEs that converge to the coupled PDE-ODE (2.1.4), that models the impact of autonomous vehicles on traffic flow?
2. If we modify (4.2.7) by

$$\begin{cases} \dot{x}_i^n(t) = \min(v(\frac{l_n}{x_{i+1}^n - _i^n}), \phi_\epsilon(x_i^n(t))),\ i \in \{0, \cdots, n-1\} \\ \dot{x}_n^n(t) = v_{\max} \phi_\epsilon(x_n^n(t)) \\ x_i^n(0) = \bar{x}_i^n\ i \in \{0, \cdots, n\}. \end{cases} \tag{4.2.11}$$

   To which PDEs that system of ODEs converge?

In [45], the authors prove rigorous convergence from FTL type models to weak solutions of the ARZ system in the many particle limit in presence of vacuum. A formal derivation of this limit can be found in [6]. To deal with micro-to-macro traffic network governed by the GARZ on each branch, we should first extend the results from [45] to obtain a rigorous convergence from FTL type models with to weak solutions of the ARZ system with space dependent flux ϕ_ϵ. When ϵ tends to 0, we should get the model (2.1.5) and (2.1.6), for which the existence of solutions has been proven in [57].

Part II

Management of Traffic flow

Chapter 5

Control and stabilization of conservation laws

The objective of this chapter is to design boundary or distributed controllers that steer a weak solution of conservation law toward a desired state. In the context of vehicular traffic, one standard approach is to control the inflow or outflow at the boundaries or to influence the system using internal control as speed limits, ramp metering, or autonomous vehicles in order to positively influence traffic flow.

When we have candidate controllers, there are many mathematical techniques to solve stabilization problems for regular solutions of PDE [12, 33] as control Lyapunov functions, backstepping or linearization techniques. Unfortunately, solutions of (1.1.1) may develop discontinuities in finite time (see Figure 2.1) which makes standard stabilization methods inapplicable. Moreover, the interpretation of the boundary condition is delicate, as the Dirichlet condition may fail to hold pointwise a.e. in time. Hence, it is necessary to specify the precise sense in which entropy boundary conditions are understood (see [38]). The LWR equation (1.1.1) over $[0, L]$ with boundary Dirichlet conditions at $x = 0$ and at $x = L$ is defined as, for a.e $t \geq 0$,

$$\rho(t, 0^+) \in \mathrm{Adm}_l(u_l(t)) \text{ and } \rho(t, L^-) \in \mathrm{Adm}_r(u_r(t)),$$

where $\mathrm{Adm}_l(\cdot)$ and $\mathrm{Adm}_r(\cdot)$ are defined by

$$\mathrm{Adm}_l(u) := \begin{cases} \{z \in \mathbb{R} \,/\, f'(z) \leq 0\}, & \text{if } f'(u) \leq 0, \\ \{z \in \mathbb{R} \,/\, f'(z) < 0 \text{ and } f(z) \leq f(u)\} \cup \{u\}, & \text{if } f'(u) > 0, \end{cases} \tag{5.0.1}$$

and

$$\mathrm{Adm}_r(u) := \begin{cases} \{z \in \mathbb{R} \,/\, f'(z) \geq 0\}, & \text{if } f'(u) \geq 0, \\ \{z \in \mathbb{R} \,/\, f'(z) > 0 \text{ and } f(z) \leq f(u)\} \cup \{u\}, & \text{if } f'(u) < 0. \end{cases} \tag{5.0.2}$$

The function u_l and u_r above are the boundary controllers acting respectively at $x = 0$ and at $x = L$. For instance, if the road is blocked over $[0, +\infty)$ ($\rho_0 = 1$ and $u_r = 1$), the weak-entropy solution (1.1.1) with boundary conditions (5.0.1) and (5.0.2) is $\rho(t, x) = 1$ for any $(t, x) \in \mathbb{R}_+ \times [0, L]$ whatever the controller $u_l(\cdot)$ chosen. As a consequence, the controller may be inactive. Moreover, due to the finite propagation, the controller acts on solutions of conservation laws with delay. The presence of discontinuities, switching, and delay phenomena makes obtaining stabilization results challenging. Thus, very few articles [15, 34, 82, 83, 94] study them in the framework of weak-entropy solutions. In [15] the authors consider solutions with a finite number of shocks to find the derivative of a Lyapunov function candidate. In [94], the authors assume that the solutions is only determined by the boundaries, i.e the controllers are active all the time and they use the Hamilton-Jacobi formulation. In [83], a saturated proportional controller is provided to stabilize asymptotically the weak-entropy solution of LWR around a stationary shocks using the notion of generalized characteristics.

We now present the article [74], which shows that controlling the speed of autonomous vehicles can have a positive impact on traffic flow by reducing total fuel consumption. In [71] (see Section 6.2), we extend the work of [83] to stabilize (1.1.1) for $\mathcal{G}$-solutions using more robust feedback controllers, namely controllers that exhibit improved performance in the presence of unknown disturbances, such as sliding mode controllers (SMC).

Chapter 6

Main Contributions

6.1 Positive impact of Autonomous Vehicles on traffic flow

At the macroscopic level, the recent articles [28, 74, 84] have numerically attempted to control the trajectory of autonomous vehicles to have a positive impact (fuel consumption reduction, traffic jam dissipation) on the traffic flow using as model the coupled PDE-ODE (2.1.4), see [72, 73]. In [84], the authors use a model predictive control (MPC) approach to achieve a reduction in fuel consumption in congested traffic. In [28], the authors dissipate a traffic jam via the use of controlled autonomous vehicles. The evolution of traffic flow is modeled by a cell transmission model (CTM) that is consistent with the discretization of PDE traffic model (1.1.1) using Godunov scheme. They show numerically that a single autonomous vehicle can reduce the overall average travel time in traffic by applying an explicit speed-feedback controller.

In [74], the impact of $N \in \mathbb{N}^*$ autonomous vehicles (AVs) on traffic flow is modeled by

$$\begin{aligned}
&\partial_t \rho(t,x) + \partial_x(f(\rho(t,x))) = 0, && (t,x) \in \mathbb{R}_+ \times \mathbb{R}, && \text{(6.1.1a)}\\
&\rho(0,x) = \rho_0(x), && x \in \mathbb{R}, && \text{(6.1.1b)}\\
&f(\rho(t,y_i(t))) - \dot{y}_i(t)\rho(t,y_i(t)) \le F_\alpha(\dot{y}_i(t)), && t \in \mathbb{R}_+,\ i = 1,\cdots,N && \text{(6.1.1c)}\\
&\dot{y}_i(t) = \min\{V_i(t), v(\rho(t,y_i(t)+))\}, && t \in \mathbb{R}_+,\ i = 1,\cdots,N && \text{(6.1.1d)}\\
&y_i(0) = y_i^0, && i = 1,\cdots,N. && \text{(6.1.1e)}
\end{aligned}$$

The function $t \to V_i(t)$ is the control function that assigns the speed to the i^{th} AV. The equality (6.1.1d) means that the i^{th} AV drives at its maximum desired speed V_i except when the traffic in front is too dense. In that case, the autonomous vehicle has to reduce its velocity accordingly. For any $i \in \{1, \cdots, N\}$, the flux constraint in (6.1.1c) describes the influence of the i^{th} AV on the evolution of traffic. The function F_α, $\alpha \in (0,1)$ stands for the maximal road capacity reduction due to the presence of the i^{th} autonomous vehicle, that acts as a moving bottleneck which imposes unilateral constraint at the AV position.

Existence of solutions when $N = 1$. When the maximum speed of the AV is constant in time, the existence and the stability of solutions for (6.1.1) with $N = 1$ has been proven in [39, 72, 73] (see Section 3.1). When the maximum speed of the AV depends on time, the existence of solutions for (6.1.1) has been proven in [48]. More precisely, the proof follows the same structure as those presented in Section 3.1. We construct approximate solutions using wave-front tracking and then pass to the limit by means of compactness estimates and Helly's compactness theorem. The main difference with respect to [73] lies in the fact that discontinuous waves may be generated at times $t > 0$ when the AV's speed is adjusted (see Figure 6.1). As a consequence, we need to introduce an additional term in the Total Variation functional defined in (3.1.2) in order to control the behavior of $TV(\rho^n)$ when a wave is generated by the jump in the AV's speed.

$$\Gamma(t) = \Gamma(\rho^n(t,\cdot), V^n) := TV(\rho^n(t,\cdot)) + 2R + \gamma(t) + \frac{6}{\beta} TV(V^n(\cdot); [t, +\infty[), \tag{6.1.2}$$

where γ is given by

$$\gamma(t) := \begin{cases} -2\left(\hat{\rho}(V^n(t)) - \check{\rho}(V^n(t))\right) & \text{if } \rho^n(t, y^n(t)_-) = \hat{\rho}(V^n(t)),\ \rho^n(t, y^n(t)_+) = \check{\rho}(V^n(t)), \\ 0 & \text{otherwise.} \end{cases}$$

where V^n is a sequence of piecewise constant functions that converges to V in L^1 as $n \to \infty$ and $TV(V^n) \leq TV(V)$ for any $n \in N$. Thanks to Proposition 3.1 and Corollary 3.1 in [48], we have

$$TV\left(\rho^n(t, \cdot)\right) \leq \Gamma(t) \leq \Gamma(0) \leq TV(\rho_0) + 2R + TV(V).$$

Thus, using Ascoli Theorem, we deduce that, up to a subsequence, (ρ^n, y^n) converges to a solution of (6.1.1) when $N = 1$ as $n \to \infty$.

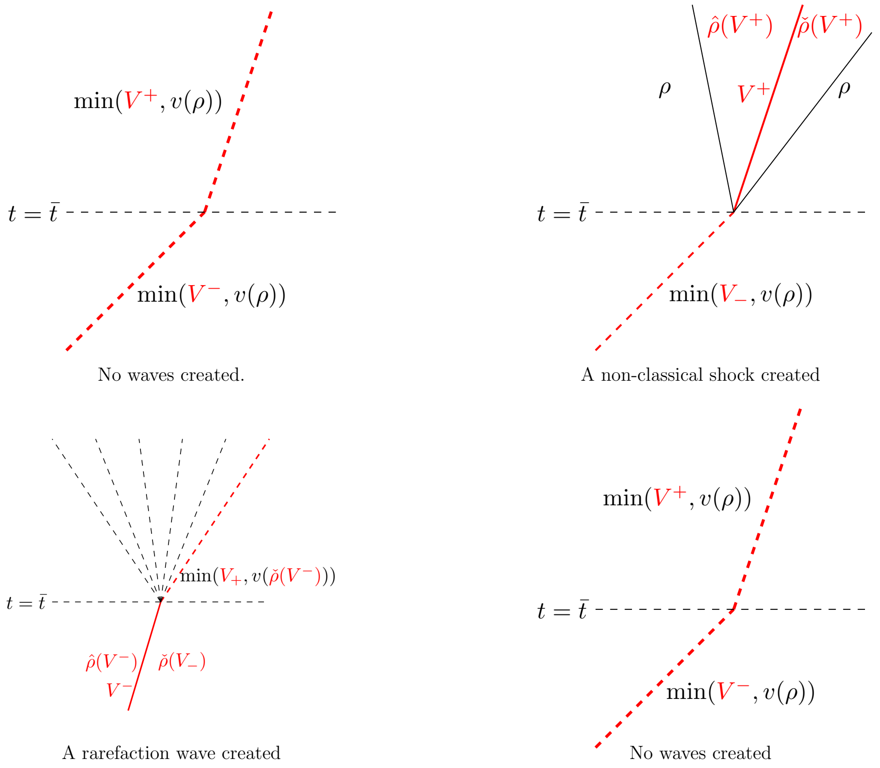

Figure 6.1 – Speed jump from V_- to V_+

Existence of solutions when $N > 1$. To get existence of solutions for the coupled PDE-ODEs (6.1.1), we impose additional conditions on $(V_i)_{i\in\{1,\cdots,N\}}$, i.e an autonomous vehicle must never catch up to the AV ahead of it. Mathematically speaking, it means two non-classical shocks cannot interact.

Assumption. Let $\epsilon > 0$ and introduce the class of admissible maximal speed $\mathcal{V}_N^\epsilon \subset BV\left(\mathbb{R}^+; [0, V_{\max}]\right)^N$. The sequence $(V_i)_{i\in\{1,\cdots,N\}} \in \mathcal{V}_N^\epsilon$ if, for every $t \geq 0$ and for every $i \in \{1, \cdots, N-1\}$,

$$y_i(t) - \epsilon < y_{i+1}(t),$$

with y_i is solution of (6.1.1d). Note that the set $\mathcal{V}_N^\epsilon$ depends on the initial density ρ_0 and the initial position of the N autonomous vehicles $(y_i^0)_{i\in\{0,\cdots,N\}}$. Under assumption on $\mathcal{V}^\epsilon$, the proof of existence of solutions for $N = 1$ given in [48] can be adapted without difficulty.

Theorem 6.1.1 ([74]). *Let $\epsilon > 0$, $N \in \mathbb{N}\backslash\{0\}$ and let us assume that $\rho_0 \in BV(\mathbb{R}, [0, \rho_{\max}])$, $(y_i^0)_{i=1,\cdots,N} \in \mathbb{R}^N$ and $(V_i)_{i\in\{1,\cdots,N\}} \in \mathcal{V}_N^\epsilon$. Then, the Cauchy problem (6.1.1) admits a solution in the sense of Definition 3.1 in [48].*

The objective of the optimization is to drive the AVs in such a way that they minimizes the fuel consumption of the entire traffic flow, i.e. the total fuel consumption of all vehicles. Therefore, the control functions are the maximum speed of AVs, denoted by $V_1, \cdots, V_N$. This leads to the optimal control problem described in [74], stated as follows. Let $\epsilon > 0$, $T_f > 0$, $C > 0$ and $x_1, x_2 \in \mathbb{R}$ such that $x_1 < x_2$. Fix $\rho_0 \in \left(L^1 \cap BV\right)(\mathbb{R}; [0, \rho_{\max}])$ and for every $i \in \{1, \cdots, N\}$, $y_i^0 \in \mathbb{R}$. Find the minimizer $V^{\text{opt}} = (V_1^{\text{opt}}, \cdots, V_N^{\text{opt}}) \in \mathcal{V}_N^\epsilon$ that solves the following optimization problem

$$\inf_{\substack{(V_i)_{i=1,\cdots,N} \in \mathcal{V}_N^\epsilon \\ \|V_i\|_{BV} \leq C}} \mathbf{TFC}(V) := \int_0^{T_f} \int_{x_1}^{x_2} \rho(t,x) K(v(\rho(t,x))) dt dx, \tag{6.1.3}$$

where $(\rho, y_1, \cdots, y_N)$ is the solution of (6.1.1) associated to $(\rho_0, y_1^0, \cdots, y_N^0)$. Above, K is the fuel rate in liters per hour (ℓ/h) as a function of the speed v in kilometers per hour (km/h), obtained in [85] using the fuel consumption rates of four different commercially available vehicles. The functional **TFC** represents the Total Fuel Consumption computed on a highway section of length $x_2 - x_1$ km during T_f hours. In [74, Theorem 3.3], the existence of at least one optimal solution is proved using minimizing sequences and properties of the approximate density ρ^n and AV positions $(y_1^n, \cdots, y_N^n)$ constructed using wave-front tracking algorithms.

Numerical Simulations. We now present numerical examples to demonstrate how AVs can be used as moving bottlenecks to control the flow of traffic and optimize the fuel consumption of not only the individual AVs, but also the entire traffic flow. The optimal trajectory of each AV consists of a finite series of speeds to drive at for a corresponding time interval. This is based on the predicted traffic state and position of each AV as solved using the coupled ODE-PDE system. The optimization problem (6.1.3) is solved using the genetic algorithm as implemented in the Matlab Global Optimization Toolbox (`ga()`) while the solution $(\rho, y_1, \cdots, y_N)$ of (6.1.1) is solved using the wave-front tracking algorithm. The choice of genetic algorithm is motivated by the fact that the cost function **TFC** is not differentiable with respect to $V \in BV\left(\mathbb{R}^+; [0, V_{\max}]\right)^N$ (see [74, Lemma 3.4]) and by the desire to investigate whether AVs can have a positive impact by creating controlled bottlenecks.

Scenario 1 : Optimal constant speeds of multiple AVs over one hour. For any piecewise constant initial data ρ_0, we numerically solve the optimal control problem (6.1.3) considering three different cases.

1. When each AV drives at maximum speed $V_{\max}$ over the duration of the numerical experiment and the AVs don't influence the traffic flow.
2. When only one AV is used, i.e. $N = 1$ in (6.1.3), we choose $y_1^0 = 25$ and we denote the approximate optimal solution of (6.1.3) as $V_1^{\text{opt}}(\rho_0)$.
3. When two AVs are used, i.e., $N = 2$ in (6.1.3), we choose $[y_1^0, y_2^0] = [25, 35]$ and we denote the approximate optimal solution of (6.1.3) as $(V_1^{\text{opt}}(\rho_0), V_2^{\text{opt}}(\rho_0))$.

The values of $\mathbf{TFC}(V_{\max})$, $\mathbf{TFC}(V_1^{\text{opt}}(\rho_0))$, and $\mathbf{TFC}(V_1^{\text{opt}}(\rho_0), V_2^{\text{opt}}(\rho_0))$ are plotted with respect to the initial data ρ_0 in Figure 6.2. As shown in the figure, three distinct optimal driving strategies arise:

1. When the initial density ρ_0 is low ($\rho_0 \in (0, 87)$ for one AV and $\rho_0 \in (0, 199)$ for two AVs), the use of a moving bottleneck is needed to optimize (reduce) the total fuel consumption.
2. When the initial density ρ_0 is moderate ($\rho_0 \in (87, 326)$ for one AV and $\rho_0 \in (199, 326)$ for two AVs), the optimal speed of the moving bottleneck is 0 km/h, and thus a fixed bottleneck produces the optimal fuel consumption results when optimizing (6.1.3).
3. When the initial density ρ_0 is high ($\rho_0 \in (326, 400)$ for one and two AVs), the density is too great and the AV is unable to control the traffic flow. Mathematically speaking, the constraint (6.1.1c) is inactive.

Note that when more AVs are deployed on the road to actively control the flow of traffic and optimize the fuel consumption of the entire fleet, the range of initial densities where a moving bottleneck is needed to optimize the fuel consumption increases.

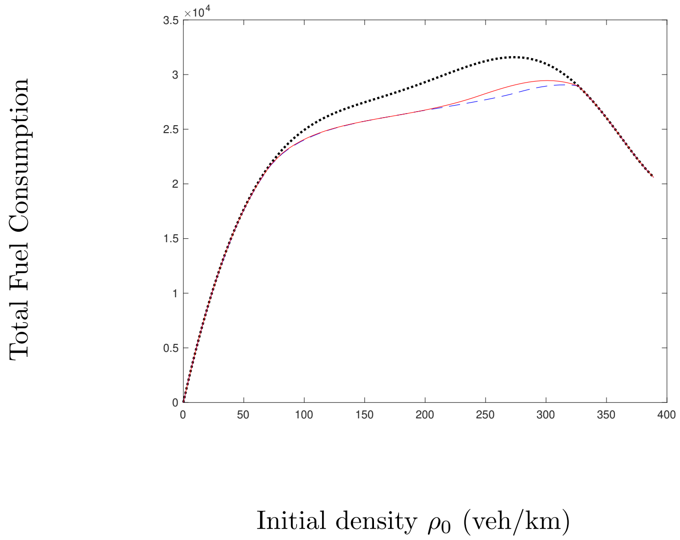

Figure 6.2 – Plotting of $\mathbf{TFC}(V_{\max})(\cdots)$, $\mathbf{TFC}(V_1^{\text{opt}}(\rho_0))(-)$ and $\mathbf{TFC}(V_1^{\text{opt}}(\rho_0), V_2^{\text{opt}}(\rho_0))(--)$ with respect to the initial data ρ_0.

Scenario 2 : Multiple optimal speeds of multiple AVs over one hour. In this scenario, the initial traffic state is

$$\rho_0(x) = \begin{cases} 0, & \text{if } x < -35, \\ 121, & \text{if } 35 < x < 0, \\ 80, & \text{if } 0 < x < 50, \\ 371, & \text{if } 50. \end{cases}$$

Moreover, each AV changes its speed six times in the one-hour numerical experiment. As seen in Figure 6.3, if the AV drives at the maximum possible velocity at all times, the AV encounters the leading edge of the shock wave after roughly 0.2 hours. This results in a total fuel consumption of 17740 ℓ of fuel. However, when the AV is acting as a moving bottleneck to control the traffic and reduce the fuel consumption, it is able to achieve a lower density gap between the wave and the AV. By using the control strategy optimized with the genetic algorithm, the total fuel consumption for the same traffic flow is reduced to 17613 ℓ, a reduction of 0.72%. When two AV are acting as a moving bottleneck to control the traffic and reduce the fuel consumption, the total fuel consumption for the same traffic flow is reduced to 17487 ℓ, a reduction of 1.43%.

In conclusion, the use of AVs as moving bottlenecks to control traffic flow may have a positive impact on traffic flow, in particular to reduce total fuel consumption in the presence of a traffic wave. However, these controllers suffers from a lack of theoretical guarantee, automation and robustness. Moreover, in [28, 74, 84] the feedback controller require the full knowledge of the density of cars over $\mathbb{R}_+ \times \mathbb{R}$. In the next section, we show how to overcome these difficulties in the specific case of tollgates. More precisely, we construct robust feedback controllers that regulate traffic flow around a stationary solution and they only rely on the measurement of the total number of vehicles on the road.

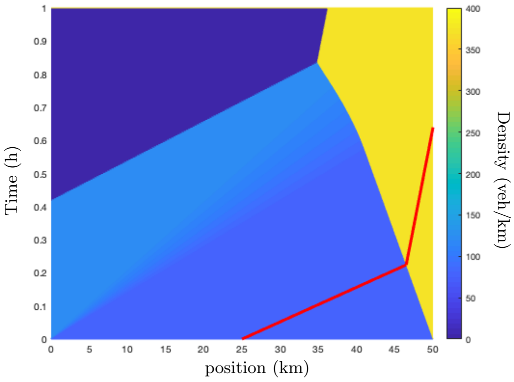

AV with $V = V_{\max}$. TFT=17740 l. of fuel

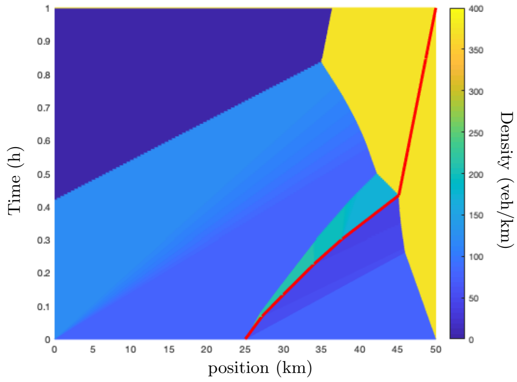

One optimal AV. TFT=17613 l. of fuel

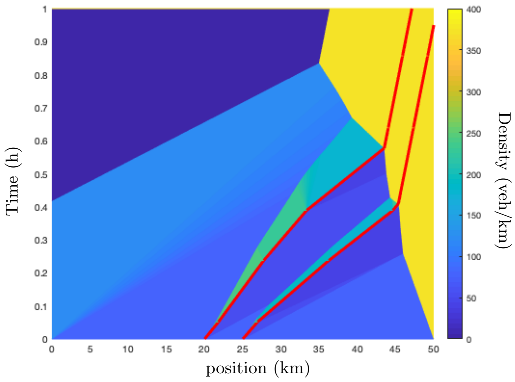

Two optimal AVs. TFT=17487 l. of fuel

Figure 6.3 – Traffic density evolution showing wave-fronts under the optimal driving strategy with AVs plotted in red.

6.2 Stabilization of traffic flow using toll gates

In [71], we address a problem of stabilization of a scalar conservation laws with fixed flux pointwise constraints defined as

$$\begin{cases} \rho_t(t,x) + \partial_x f(\rho(t,x)) = 0, & t \in \mathbb{R}_+, x \in \mathbb{R}, \\ \rho(0,x) = \rho_0(x), & x \in \mathbb{R}, \\ f(\rho(t,0)) \le F_1(t,\rho), & t \in \mathbb{R}_+, \\ f(\rho(t,L)) \le F_2(t,\rho), & t \in \mathbb{R}_+. \end{cases} \tag{6.2.1}$$

The PDE (6.2.1) models two toll gates along highway or road lights (see [31]), see Figure 6.4.

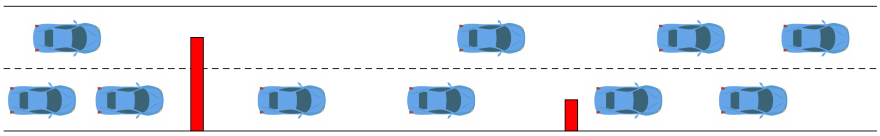

Figure 6.4 – Control the inflow and outflow of two toll gates along highway or road lights

Our goal is to find two feedback controllers F_1 and F_2 that stabilizes (6.2.1) over $(0, L)$ around the stationary solution w, defined by

$$w(x) = \begin{cases} w_L, & \text{if } 0 \le x < x_0, \\ w_R, & \text{if } x_0 < x \le L, \end{cases} \tag{6.2.2}$$

where $x_0 \in (0, L)$ and $w_L, w_R \in (0,1)$ satisfy $w_L < w_R$ and $f(w_L) = f(w_R) < f(\sigma)$ with $\sigma = \operatorname{argmax}_{\rho\in[0,1]} f(\rho)$.

Control design. Let $g : \mathbb{R} \to \mathbb{R}$ a continuous function satisfy

$$g(0) = 0 \text{ and } \forall x \in \mathbb{R}^*,\ xg(x) > 0. \tag{6.2.3}$$

The feedback controllers F_1 and F_2 have the following forms

$$F_1(t,u) = \max(\min(f(w_L) - g(m(t)), f(\sigma) - \varepsilon), 0) \text{ and } F_2(t,u) = f(w_R) \tag{6.2.4}$$

where $\varepsilon > 0$ is chosen such that $f(\sigma) - f(w_L) - \varepsilon > 0$ and

$$m(t) := \int_0^L (\rho(t,x) - w(x))dx. \tag{6.2.5}$$

From (6.2.5), we only need to measure the number of cars at time t over $[0, L]$, namely $\int_0^L (\rho(t,x)dx$ to regulate (6.2.1) around the target function w.

Cauchy problem. We now introduce the notion of solutions based on the admissibility germ defined in [4]. Let $\Pi = [0,\infty) \times \mathbb{R}$ and let $\phi : (\rho, k) \in \mathbb{R} \times \mathbb{R} \mapsto \operatorname{sgn}(\rho - k)(f(\rho) - f(k))$ denote the entropy flux associated with the Kruzhkov entropy $(\rho, k) \mapsto |\rho - k|$ (see [65]).

Definition 1 (Admissibility germ $\mathcal{G}(F)$,[4])**.** *Let $F \in [0, f(\overline{\rho})]$. The admissibility germ $\mathcal{G}(F)$ for the conservation law (3.2.1) is the subset of $[0,1]^2$ defined as the union $\mathcal{G}(F) = \mathcal{G}_1(F) \cup \mathcal{G}_2(F) \cup \mathcal{G}_3(F)$, where*

— $\mathcal{G}_1(F) := \{(c_l, c_r) \in [0,1]^2; c_l > c_r, f(c_l) = f(c_r) = F\}$,

— $\mathcal{G}_2(F) := \{(c, c) \in [0,1]^2; f(c) \le F\}$,

— $\mathcal{G}_3(F) := \{(c_l, c_r) \in [0,1]^2; c_l < c_r, f(c_l) = f(c_r) \le F\}$.

$\mathcal{G}_1(F)$ allows non-classical shocks to occur, $\mathcal{G}_2(F) := \{(c, c) \in [0,1]^2; f(c) \le F\}$ allows rarefaction waves to occur and $\mathcal{G}_3(F) := \{(c_l, c_r) \in [0,1]^2; c_l < c_r, f(c_l) = f(c_r) \le F\}$ allows entropy shock to occur.

Definition 2 ([4]). *Let $\rho_0 \in L^\infty(\mathbb{R},[0,1])$. We say that $\rho \in L^\infty(\Pi;[0,1])$ is a $\mathcal{G}$-entropy solution of (3.2.1) if*

1. *ρ is a Kruzhkov entropy solution for $x \in \mathbb{R}\backslash\{0,L\}$, i.e, for all nonnegative test functions $\varphi \in C_c^\infty(\Pi\backslash\{0,L\})$ and all $k \in [0,1]$,*

$$\int_0^{+\infty}\int_{\mathbb{R}}(|\rho(t,x)-k|\partial_t + \phi(\rho(t,x),k)\partial_x)\varphi(t,x)dxdt + \int_{\mathbb{R}}|\rho_0(x)-k|\varphi(0,x)dx \geq 0; \tag{6.2.6}$$

2. *in addition, for a.e $t>0$,*

$$((\gamma_0^l\rho)(t),(\gamma_0^r\rho)(t)) \in \mathcal{G}(F_1) \text{ and } ((\gamma_L^l\rho)(t),(\gamma_L^r\rho)(t)) \in \mathcal{G}(F_2). \tag{6.2.7}$$

where $\gamma_0^{l,r}$ and $\gamma_L^{l,r}$ denote the operators of left- and right-side strong traces on $\{x=0\}$ and $\{x=L\}$ and F_1 and F_2 are defined in (6.2.4).

Theorem 6.2.1 (Existence). *Let $\varepsilon>0$ satisfy $f(\sigma)-f(w_L)-\varepsilon>0$. For any $\rho_0 \in L^\infty(\mathbb{R};[0,1])$, there exists at least one $\mathcal{G}$-entropy solution ρ of (3.2.1) where F_1 and F_2 are defined in (6.2.4).*

Proof. Let $T>0$. The proof of existence of $\mathcal{G}$-solutions over $[0,T]$ is based on Schauder's fixed point theorem. The existence and the stability of $\mathcal{G}$-solutions for (6.2.1) when the feedback controllers F_1 and F_2 are replaced by open loop controllers $t \to Q_1(t)$ and $t \to Q_2(t)$ have been done in [4]. More precisely, let (ρ^1,ρ^2) be two $\mathcal{G}$-solutions of (6.2.1) associated respectively to (ρ_0^1,Q_1^1,Q_2^1) and (ρ_0^2,Q_1^2,Q_2^2), the authors in [4] prove that

$$\int_{\mathbb{R}}|\rho^1-\rho^2|(T,x)dx \leq 2\int_0^T|Q_1^1-Q_1^2|(t)dt + 2\int_0^T|Q_2^1-Q_2^2|(t)dt + \int_{\mathbb{R}}|\rho_0^1-\rho_0^2|(x)dx \tag{6.2.8}$$

Let us fix $T>0$. We introduce the operator $\mathcal{F}: W^{1,\infty}([0,T]) \to W^{1,\infty}([0,T])$ defined by

$$\forall t \in [0,T], \quad \mathcal{F}(z)(t) := \int_0^L(\rho(t,x)-w(x))\,dx,$$

where $\rho \in L^\infty([0,T]\times\mathbb{R};[0,1])$ is a $\mathcal{G}$-entropy solution of (6.2.1) replacing respectively F_1 and F_2 by

$$Q_1(t) = \max(\min(f(w_L)-g(z(t)), f(\sigma)-\varepsilon),0) \text{ and } Q_2(t) = f(w_R).$$

From Schauder's fixed point theorem [88], we prove that the operator $\mathcal{F}$ has at least one fixed point in $W^{1,\infty}([0,T])$. Thus, for any $T>0$, we get existence of $\mathcal{G}$-solutions for (6.2.1) over $[0,T]\times\mathbb{R}$. ☐

To prove the existence of $\mathcal{G}$-solutions for (6.2.1) over $\mathbb{R}_+\times\mathbb{R}$, we need to carefully analyze the behavior of $\mathcal{G}$-solutions over a long time horizon. We now state the stabilization results associated to (6.2.1).

Theorem 6.2.2 (Asymptotic stability). *Let $\varepsilon>0$ satisfy $f(\sigma)-f(w_L)-\varepsilon>0$. Let $v_0 \in L^\infty([0,L];[0,1])$, we consider the initia data ρ_0 defined by*

$$\rho_0(x;v_0) = \begin{cases} 1, & \text{if } x<0, \\ v_0(x), & \text{if } 0<0<L, \\ 0, & \text{if } L<x. \end{cases} \tag{6.2.9}$$

For any $v_0 \in L^\infty([0,L];[0,1])$, any $\mathcal{G}$-solution $\rho(t,\cdot)$ of (3.2.1) with initial datum u_0 converges to $w(\cdot)$ in $L^1(0,L)$ as $t\to\infty$.

Corollary 1 (Exponential stability). *Let $\varepsilon>0$ satisfy $f(\sigma)-f(w_L)-\varepsilon>0$ and $g: x\mapsto K_0x$ with $K_0>0$. For any $v_0 \in L^\infty([0,L];[0,1])$, any $\mathcal{G}$-solution $\rho(t,\cdot)$ of (3.2.1) with initial datum ρ_0 converges exponentially to $w(\cdot)$ in $L^1(0,L)$ as $t\to\infty$, i.e there exists $C>0$ such that for any $t\geq 0$,*

$$\|\rho(t,\cdot)-w(\cdot)\|_{L^1(0,L)} \leq Ce^{-K_0t}\left(\|\rho_0(\cdot)-w(\cdot)\|_{L^1(0,L)}+C\right).$$

Corollary 2 (Finite time stability). *Let $\varepsilon > 0$ satisfy $f(\sigma) - f(w_L) - \varepsilon > 0$ and g satisfied (6.2.3) and for any $\alpha \in \mathbb{R}^*$, $\int_0^\alpha \frac{dy}{g(y)} > -\infty$. For any $v_0 \in L^\infty([0,L];[0,1])$, the $\mathcal{G}$-solution $\rho(t,\cdot)$ of (3.2.1) with initial datum ρ_0 converges in finite time to $w(\cdot)$ in $L^1(0,L)$, i.e there exists a time $\bar{T} > 0$ such that for any $t \geq \bar{T}$, for a.e $x \in (0,L)$,*

$$\rho(t,x) = w(x).$$

Before proving the existence of $\mathcal{G}$-solutions over $\mathbb{R}_+ \times \mathbb{R}$ and Theorem 6.2.2, we will extend the notion of generalized backward characteristics for $\mathcal{G}$-entropy boundary conditions, see Proposition (6.2.3), [71, Proposition B.1] and an illustration in Figure 6.5. Note that, since non-classical shock can appear at $x = 0$ and $x = L$, we cannot directly apply the standard theory for weak-entropy solutions of conservation laws.

Proposition 6.2.3. *Let ρ be the unique $\mathcal{G}$-entropy solution of (3.2.1) and we assume that there exist $c, d > 0$ such that $c < d$ and for a.e $t \in [c,d]$*

$$e \leq f(\rho(t,0^+)) \leq E \text{ and } g \leq f(\rho(t,L^-)) \leq G \tag{6.2.10}$$

where e, E, g, G are given constants. We consider ξ a genuine characteristic on an interval $[a,b]$ such that

$$\forall t \in (a,b], \quad \xi(t) \in (0,L).$$

Then there exists a constant $v \in [0,1]$ such that, for any $t \in [a,b]$, $\dot{\xi}(t) = f'(v)$ and, for any $t \in (a,b)$, $\rho(t,\xi(t)) = v$. Moreover,

$$\xi(a) = 0 \text{ and } a > 0 \text{ implies } f'(v) > 0 \text{ and } \begin{cases} e \leq f(v) \leq E & \text{if } a \in (c,d), \\ 0 \leq f(v) \leq f(\sigma) - \varepsilon & \text{otherwise,} \end{cases} \tag{6.2.11}$$

$$a = 0 \text{ implies } \rho(a, \xi(a)+) \leq v \leq \rho(a, \xi(a)-), \tag{6.2.12}$$

$$\xi(a) = L \text{ and } a > 0 \text{ implies } f'(v) < 0 \text{ and } \begin{cases} g \leq f(v) \leq G & \text{if } a \in (c,d), \\ 0 \leq f(v) \leq f(w_R) & \text{otherwise.} \end{cases} \tag{6.2.13}$$

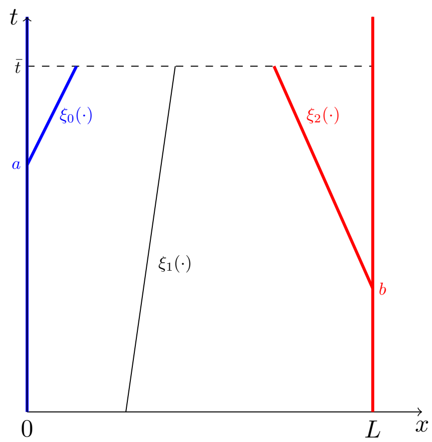

Figure 6.5 – Illustration of generalized backward characteristics reaching the boundaries at $x = 0$, $t = 0$ and $x = L$

Proposition 6.2.3 is the cornerstone for studying the behavior of the $\mathcal{G}$-solutions of (6.2.1). Roughly speaking, Proposition 6.2.3 allow us to find a time T_3 independent of the initial data ρ_0 and to construct a function $\beta(\cdot)$ such that any minimal generalized characteristic emanating from the left side (resp. right side) of $\beta(\cdot)$

reaches the boundary at $x = 0$ (resp. $x = L$), see Figure 6.6. Additionally with a careful analysis of the derivative of β, we also get for any $t \geq T_3$, $\beta(t) \in (0, L)$. Therefore, together with (6.2.9) and the germ condition (6.2.7), we can show that only non-classical shocks can be generated at $x = 0$ and $x = L$ after $t \geq T_3$. We deduce that for any $t \geq T_3$,

$$f(\rho(t, 0^+)) = F_1(t, \rho) \text{ and } f(\rho(t, L^-)) = F_2(t, \rho), \tag{6.2.14}$$

This implies that the controllers are active all the time. From the mass conservation, we deduce that for any $t \geq T_3$,

$$\dot{m}(t) = f(\rho(t, 0^+)) - f(\rho(t, L^-)) = F_1(t, \rho) - F_2(t, \rho) = -g(m(t)), \tag{6.2.15}$$

where $m(\cdot)$ is defined in (6.2.5).

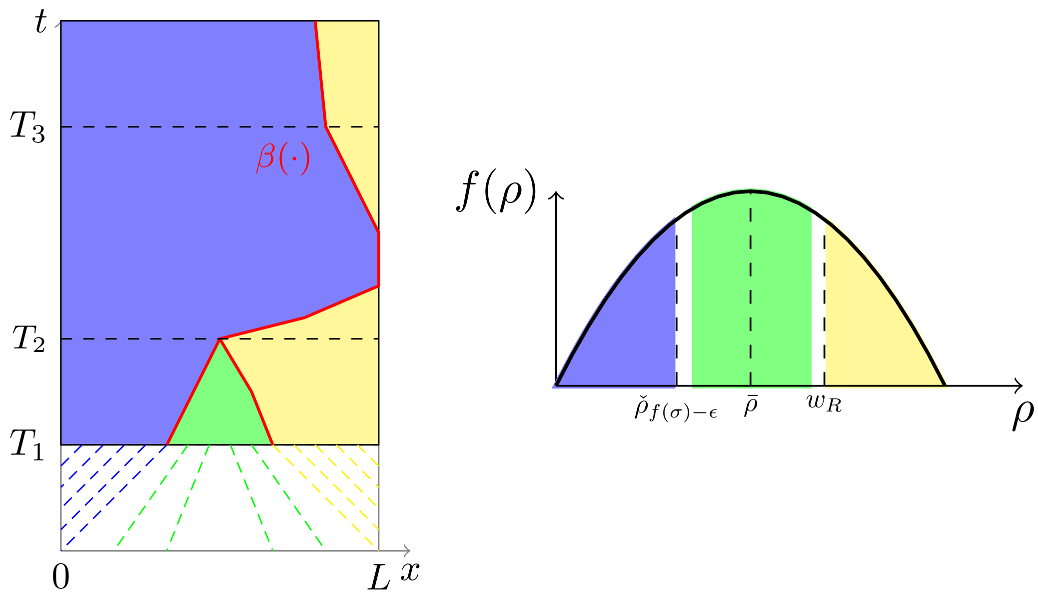

Figure 6.6 – Illustration of the proof of Theorem 6.2.2

Sketch of the proof of Theorem 6.2.1 (existence) . Let $\epsilon > 0$ and $T_4 := T_3 + \epsilon$. From Schauder's fixed point theorem, for any $\rho_0 \in L^\infty(\mathbb{R}; [0, 1])$, we have seen that, there exists at least one $\mathcal{G}$-entropy solution, denoted by ρ, of (3.2.1) over $[0, T_4]$ where F_1 and F_2 are defined in (6.2.4). We consider the following coupled PDE-ODE

$$\begin{cases} v_t(t,x) + \partial_x f(v(t,x)) = 0, & t \in (T_4, \infty), x \in \mathbb{R}, \\ v(T_4, x) = \rho(T_3, x), & x \in \mathbb{R}, \\ f(v(t,0)) \leq f(w_L) - g(\gamma(t)), & t \in (T_4, \infty), \\ f(v(t,L)) \leq f(w_R), & t \in (T_4, \infty), \\ \dot{\gamma}(t) = -g(\gamma(t)), & t \in (T_4, \infty), \\ \gamma(T_3) = \int_0^L (\rho(T_3, x) - w(x)) dx. \end{cases} \tag{6.2.16}$$

From [4, Theorem 2.11], the coupled PDE-ODE admits a unique $\mathcal{G}$-entropy solution, denoted by v, over $[T_4, \infty)$. By concatenating the two solutions ρ over $[0, T_4]$ and v over $[T_4, +\infty)$, we construct a $\mathcal{G}$-solutions of (6.2.1) over $\mathbb{R}_+ \times \mathbb{R}$.

Sketch of the proof of Theorem 6.2.2 (stabilization). From the candidate Lyapunov function $V : x \rightarrow \frac{x^2}{2}$, we see that the EDO (6.2.15) is asymptotically stable around the equilibrium point 0 (see [80]). Thus, together with the definition of the target function (6.2.2) and the construction of $\beta(\cdot)$, we deduce that $\lim_{t\to\infty} m(t) = 0$, $\lim_{t\to\infty} \beta(t) = x_0$ and $\lim_{t\to\infty} F_1(t,\rho) = f(w_L)$ and $\lim_{t\to\infty} F_2(t,\rho) = f(w_R)$. We deduce that any $\mathcal{G}$-solution $\rho(t,\cdot)$ of (3.2.1) with initial datum ρ_0 converges to $w(\cdot)$ in $L^1(0,L)$ as $t \to \infty$.

Numerical simulations. To construct an approximate solution of (3.2.1), we use a finite volume scheme described in [4]. In Figure 6.7, Figure 6.8, Figure 6.9, F_1 is a saturated proportional controller, i.e g in (6.2.4) is defined by, for any $x \in \mathbb{R}$, $g(x) = K_0 x$ where $K_0 > 0$ is the gain of the controller. Any $\mathcal{G}$-solution of the PDE (3.2.1) with the controller F_1 is asymptotically stable around the stationary solution $w(\cdot)$ (see Corollary 2). In Figure 6.10, Figure 6.11, Figure 6.12, F_1 is a saturated sliding mode controller, i.e $g : x \to K_0|x|^{\frac{1}{2}}\mathrm{sign}(x)$ where $K_0 > 0$ is the gain of the controller. Any $\mathcal{G}$-solution of the PDE (3.2.1) with the controller F_1 converges in finite time to the stationary solution $w(\cdot)$ (see Corollary 1).

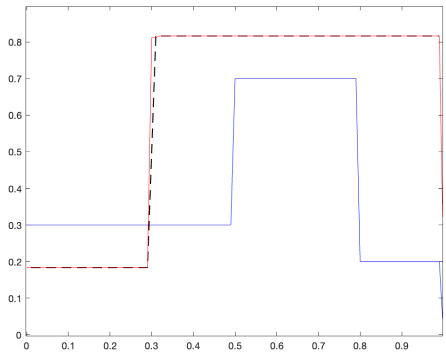

Figure 6.7 – Plottings of the initial data v_0 (—), the target function w (−−) and the $\mathcal{G}$-solution of (3.2.1) (—) over $(0,1)$ at time $t = 20$ with $L = 1$ and for any $x \in \mathbb{R}$, $g(x) = K_0 x$ with $K_0 = 0.4$.

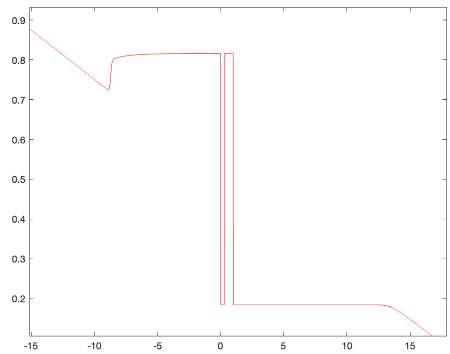

Figure 6.8 – Plotting of the $\mathcal{G}$-solution of (3.2.1) (—) over $(-15, 20)$ at time $t = 20$ with $L = 1$ and for any $x \in \mathbb{R}$, $g(x) = K_0 x$ with $K_0 = 0.4$.

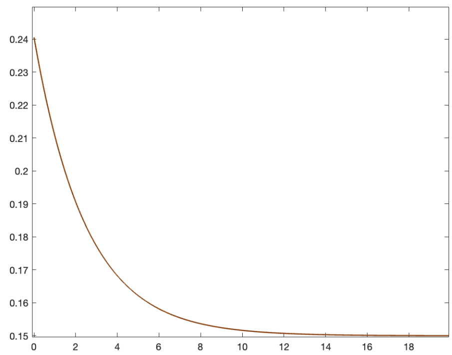

Figure 6.9 – Plotting of the saturated P-controller $F_1(\cdot)$ with respect to time t.

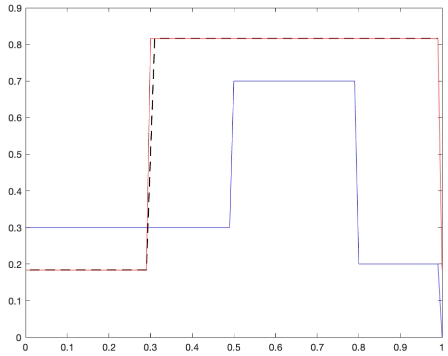

Figure 6.10 – Plottings of the initial data v_0 ($-$), the target function w ($--$) and the $\mathcal{G}$-solution of (3.2.1) ($-$) over $(0, 1)$ at time $t = 20$ with $L = 1$ and for any $x \in \mathbb{R}$, $g(x) = K_0|x|^{\frac{1}{2}}\text{sign}(x)$ with $K_0 = 0.4$.

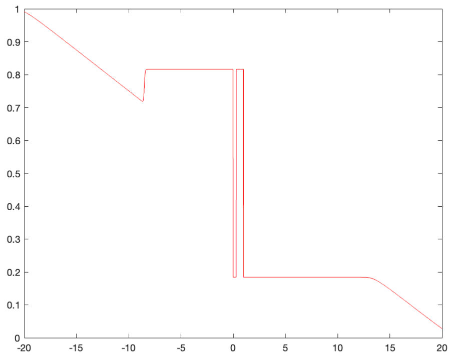

Figure 6.11 – Plotting of the $\mathcal{G}$-solution of (3.2.1) ($-$) over $(-15, 20)$ at time $t = 20$ with $L = 1$ and for any $x \in \mathbb{R}$, $g(x) = K_0|x|^{\frac{1}{2}}\text{sign}(x)$ with $K_0 = 0.4$.

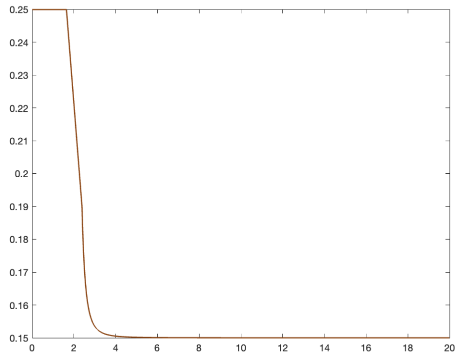

Figure 6.12 – Plotting of the saturated SMC-controller $F_1(\cdot)$ with respect to time t.

Chapter 7

Perspectives on Road Network Control

In this chapter, we consider the road network setting defined in Section 4.1 and Section 4.2.1. More precisely, on each road the evolution of the traffic flow is modeled by the LWR model defined in (4.1.12). At network junctions, we define appropriate coupling conditions to ensure conservation of vehicles, admissibility of flows, and consistency with traffic behavior. This is typically achieved through Riemann solvers for networks, which determine incoming and outgoing fluxes based on demand and supply constraints and priorities, see Section 4.1. The solutions will be understood in the sense of $\mathcal{G}$-solutions as defined in Section 4.1 and Section 4.2.2.

Our aim is to control traffic flow on road networks to improve overall system performance and to reduce congestion, pollution and accident, without relying on costly capacity expansion infrastructure projects. Several families of control mechanisms have emerged : flux restrictions at junctions (ramp metering [47, 51, 53, 64, 81, 86], traffic signals [55, 56]) or Controlled speed limits [47, 51, 78, 81]. In recent years, optimal control methods have been developed to design open-loop controllers aimed at optimizing various performance criteria, such as evacuating all vehicles from a given road segment [14, 47, 97], minimizing total travel time, or reducing overall fuel consumption [51, 86]. However, as explained in Section 6.1, the nonlinearity of the conservation law in (1.1.1) can make the cost function non-differentiable, which complicates the derivation of optimality conditions. This has led to the development of discrete adjoint techniques, in which the adjoint equations are derived directly from numerical flux schemes (time-space Godunov scheme [86], a spatial semi-discretized Lax-Friedrichs [14]).

7.1 Traffic Network Control Using Flux Limitations at Junctions

The solution of the PDE (6.2.1) modeling two toll gates along highway or road lights can be regarded as a $\mathcal{G}^{J^1,J^2}$-entropy solutions for Cauchy network problem with two $1:1$ junctions where J^1 and J^2 are two flux restriction area (tollgates, speed bump), see Figure 7.1.

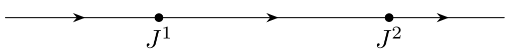

Figure 7.1 – A controlled network with two $1:1$ junctions J^1 and J^2

Let $n = m = 1$ and $f := f^0 = f^1$, the density $\rho = (\rho^0, \rho^1)$ is a $\mathcal{G}$-entropy solutions of PDE (6.2.1) if ρ

satisfies

$$\begin{cases} \partial_t \rho^k(t,x) + \partial_x f^k(\rho^k(t,x)) = 0, \quad (t,x) \in \mathbb{R}^+ \times I_k, \\ \rho^k(0,x) = \rho_0^k(x), \quad x \in I_k, \\ \rho(t,0) \in \mathcal{G}_{F^0(t)}, \quad t \in \mathbb{R}^+ \text{ and } \rho(t,L) \in \mathcal{G}_{F^1(t)}, \quad t \in \mathbb{R}^+, \end{cases} \tag{7.1.1}$$

where $I_1 =]-\infty, 0]$, $I_2 = [0, L]$, $I_3 = [L, +\infty[$ and the junction conditions satisfied by the trace of $\rho = (\rho^0, \rho^1)$ on $\{x = 0\}$ and on $\{x = L\}$, are encoded by a given set $\mathcal{G}_{F^i(t)} \in [0,1]^{n+m}$, $i \in \{0,1\}$:

$$\mathcal{G}_{F^i(t)} := \left\{ P = (p^0, p^1) \in [0,1]^2 \;\middle|\; \begin{array}{l} 0 \le f(p_j) \le F^i(t), \ j = 0,1, \\ f(p^0) = f(p^1), \end{array} \right\}. \tag{7.1.2}$$

Note that the germ (7.1.2) cannot be written as the germ G_Λ defined in (4.1.17) because the condition $D(p^k) \ge \hat{\lambda}_k\big(D(p^0)\big)$, $k = 1,2$ rules out non-classical shocks; when $n = m = 1$, $f := f^1 = f^2$, $\hat{\lambda}_1 : \lambda \to \min(\lambda, F^1)$, $p^1 < \sigma < p^0$ and $f(p^1) = f(p^0)$, we have $\lambda_k\big(D(p^0)\big) = f(\sigma) > f(p^1) = D(p^1)$. Moreover, the germ (7.1.2) is not a Kruzkov germ; when $p^1 < \bar{p}^0 < \sigma < \bar{p}^1 < p^0$ with $f(p^0) = f(p^1)$ and $f(\bar{p}^0) = f(\bar{p}^1)$, we have

$$D^f(p,\bar{p}) = \operatorname{sgn}(p^0 - \bar{p}^0)(f(p^0) - f(\bar{p}^0)) - \operatorname{sgn}(p^1 - \bar{p}^1)(f(p^1) - f(\bar{p}^1)) = f(p^0) - f(\bar{p}^0) < 0.$$

Note that the germ introduced in Definition 1 (see also [4]) does not coincide with the set defined in (7.1.2). More precisely, non-classical shocks $(\check{\rho}, \hat{\rho})$ satisfying $f(\check{\rho}) = f(\hat{\rho}) < F^i$ belong to the germ $\mathcal{G}_{F^i(t)}$ defined in (7.1.2) but they are all ruled out in the Definition 1; only those satisfying $f(\check{\rho}) = f(\hat{\rho}) = F^i$ are allowed. In (7.2.6), we introduce a germ that coincides with the one defined in Definition 1.

In Section 6.2 (see also [71]), we have proven existence of $\mathcal{G}$-solutions for the road network consisting of two $1:1$ junctions with two germs defined as in (7.2.6). We also construct two feedback controllers $F^1(\cdot)$ and $F^2(\cdot)$ that steers the solution on the road between the two junctions J_1 and J_2 to a given stationary solution without requiring any additional regularity assumptions. This leads to the following questions : can the stabilization results obtained for a road traffic network consisting of two $1:1$ junctions be extended to a general traffic network? In Section 6.1 (see also [74]), we have seen that autonomous vehicles, regarded as moving bottlenecks, could have a positive impact (total fuel consumption) on highway traffic dynamic. Can we extend the positive impact of AVs on traffic flow network?

7.2 Open questions and perspectives

Open problem 1 : stabilization on road networks using tollgates at junctions.

We want to get stabilization results for road traffic network as in (6.2.1) using maximum flux controllers at junctions. We consider the road network framework described in Section 4.1, where each junction J represents a real-world intersection (roundabout, traffic light, stop). Let $\rho_0 = (\rho_0^1, \cdots, \rho_0^{n+m})$ be a Riemann data at J. To take into account the maximum flux restriction F_i at the junction J, we will replace the Riemann solver RS^i_{road} on the road i that are connected to the junction J by the following constrained Riemann solver $RS^{\text{constr},i}_{\text{road}}$ defined by

$$RS^{\text{constr},i}_{\text{road}}(\rho_L, \rho_R)(x/t) = \begin{cases} \begin{cases} \mathcal{R}(\rho_L, \hat{\rho}_\alpha(F_i))(x/t), & \text{if} \quad x < 0, \\ \mathcal{R}(\check{\rho}_\alpha(F_i), \rho_R)(x/t), & \text{if} \quad x > 0, \end{cases} & \text{if } f^i(\mathcal{R}(\rho_L, \rho_R)(0)) > F_i, \\ \mathcal{R}(\rho_L, \rho_R), & \text{otherwise.} \end{cases}$$

where $\check{\rho}_\alpha(F_i) < \hat{\rho}_\alpha(F_i)$ are the two solutions of the equation $f^i(\rho) = F_i$. It means that we do not change the structure of the junction J but only restrict the junction J entering the flux from the road i. We can characterize the set of all possible $(\hat{\rho}_i)_{i \in \{1,\cdots,n\}}$ that are compatible with the constrained Riemann solver

$RS^{\text{constr},i}_{\text{road}}$. For any $i \in \{1, \cdots, n\}$ (entering road I_i), we have

$$\hat{\rho}_i \in \begin{cases} \{z \in \mathbb{R} : (f^i)'(z) < 0 \text{ and } f^i(z) < f^i(\rho_0^i)\} \cup \{\rho_0^i\}, & \text{if } (f^i)'(\rho_0^i) > 0 \text{ and } f^i(\rho_0^i) \le F_i, \\ \{z \in \mathbb{R} : (f^i)'(z) \le 0\}, & \text{if } (f^i)'(\rho_0^i)) \le 0 \text{ and } f^i(\rho_0^i) \le F_i, \\ \{z \in \mathbb{R} : (f^i)'(z) \le 0 \text{ and } f^i(z) \le F_i\}, & \text{if } f^i(\rho_0^i) > F_i, \end{cases} \tag{7.2.1}$$

and for $i \in \{n, \cdots, n+m\}$ (exiting road I_i), we have

$$\hat{\rho}_i \in \begin{cases} \{z \in \mathbb{R} : (f^i)'(z) > 0 \text{ and } f^i(z) < f^i(\rho_0^i)\} \cup \{\rho_0^i\}, & \text{if } (f^i)'(\rho_0^i) < 0 \text{ and } f^i(\rho_0^i) \le F_i, \\ \{z \in \mathbb{R} : (f^i)'(z) \ge 0\}, & \text{if } (f^i)'(\rho_0^i)) \ge 0 \text{ and } f^i(\rho_0^i) \le F_i, \\ \{z \in \mathbb{R} : (f^i)'(z) \ge 0 \text{ and } f^i(z) \le F_i\}, & \text{if } f^i(\rho_0^i) > F_i. \end{cases} \tag{7.2.2}$$

As a consequence, for any $i \in \{1, \cdots, n\}$, for any $j \in \{n+1, \cdots, n+m\}$

$$\hat{\gamma}_i := f^i(\hat{\rho}_i) \in [0, D^i_{F_i}(\rho_0^i)] \text{ and } \hat{\gamma}_j := f^j(\hat{\rho}_j) \in [0, S^j_{F_j}(\rho_0^j)] \tag{7.2.3}$$

where $D^i_{F_i}$ and $S^j_{F_j}$ are respectively the constraint Demand function and the constraint Supply function

$$D^i_{F_i}(\rho) = \min(D^i(\rho), F_i) \quad \text{ and } \quad S^j_{F_j}(\rho) = \min(S^j(\rho), F_j) \tag{7.2.4}$$

where D^i and S^j are defined in (4.1.5). Note that from (7.2.1), (7.2.2) and the knowledge of γ_i, there exists a unique $\hat{\rho}_i$ such that $\hat{\gamma}_i := f^i(\hat{\rho}_i)$. To construct a boundary Riemann solver at the function J, we need to give additional constraints to (7.2.3) and (4.1.6) to select a unique $(\hat{\gamma}_1, \cdots, \hat{\gamma}_{n+m})$. Since we do not change the structure of the junction J, the additional constraint is given directly from J and by replacing D^i and S^i by $D^i_{F_i}$ and $S^i_{F_i}$. Let us give two examples, one with a $1:1$ junction and another with $1:2$ junction.

Example 1. Let $\rho_0 = (\rho_0^1, \rho_0^2)$ be a Riemann data at J and J a $1:1$ junction associated to the germ

$$\mathcal{G}_{1:1} := \left\{ P = (p^0, p^1) \in [0,1]^2 \;\middle|\; \begin{array}{l} 0 \le f^i(p^i) \le \max_\rho D^i(\rho),\ i = 0, 1 \\ f^0(p^0) = f^1(p^1), \\ D^2(p^2) \ge D^1(p^1), \end{array} \right\}. \tag{7.2.5}$$

Note that in that case, we have $f^1(p^1) = f^2(p^2) = \min(D^1(\rho_0^1), S^2(\rho_0^2))$. Replacing D^i and S^i by $D^i_{F_i}$ and $S^i_{F_i}$ we get

$$\mathcal{G}^{F^1,F^2}_{1:1} := \left\{ P = (p^0, p^1) \in [0,1]^2 \;\middle|\; \begin{array}{l} 0 \le f^i(p^i) \le F^i,\ i = 0, 1 \\ f^0(p^0) = f^1(p^1), \\ \min(D^2(p^2), F_2) \ge \min(D^1(p^1), F_1), \end{array} \right\}. \tag{7.2.6}$$

and

$$f^1(p^1) = f^2(p^2) = \min(D^1(\rho_0^1), S^2(\rho_0^2), F_1, F_2).$$

Note that $\min(D^2(p^2), F_2) \ge \min(D^1(p^1), F_1)$ rules out all non-classical shocks (p^1, p^2) satisfying $f(p^1) = f(p^2) < F := \min(F_1, F_2)$ but we may have non-classical shock (p^1, p^2) such that $f(p^1) = f(p^2) = F$ with $p^2 < p^1$. The germ $\mathcal{G}^{F_1,F_2}_{1:1}$ in (7.2.6) coincides with the one defined in Definition 1. Moreover, it is a Kruzkov germ (see section [5, Section 4.9] and the notion of maximal L^1-dissipative admissibility germ). We also observe that our control strategy differs from that one used in [14]. In their approach, the control acts on the proportion of vehicles directed toward road 2, with

$$\hat{\gamma}^1 = \hat{\gamma}^2 = \min(D^1(\rho_0^1), (1 - F_2)S^2(\rho_0^2)).$$

In contrast, in our setting, when $F_1 = f^1_{\max}$ and $F_2 < f^1_{\max}$, the control is applied directly to the maximum flow entering road 2, i.e

$$\hat{\gamma}^1 = \hat{\gamma}^2 = \min(D^1(\rho_0^1), S^2(\rho_0^2), F_2).$$

Example 2. Let $\rho_0 = (\rho_0^1, \rho_0^2, \rho_0^3)$ be a Riemann data at J and J a $1:3$ junction without spillover. Replacing D^i and S^i by $D^i_{F_i}$ and $S^i_{F_i}$ in (4.1.9), we get

$$\begin{aligned}
\hat{\gamma}_2 &= \min\left(\beta D^1_{F_1}(\rho_0^1), S^2_{F_2}(\rho_0^2)\right) = \min\left(\beta D^1(\rho_0^1), S^2(\rho_0^2), \beta F_1, F_2\right), \\
\hat{\gamma}_3 &= \min\left((1-\beta) D^1_{F_1}(\rho_0^1), S^3_{F_3}(\rho_0^3)\right) = \min\left((1-\beta) D^1(\rho_0^1), S^3(\rho_0^3), (1-\beta) F_1, F_3\right), \\
\hat{\gamma}_1 &= \hat{\gamma}_2 + \hat{\gamma}_3,
\end{aligned}$$

with $\beta \in [0,1]$.

We consider a network $(\mathcal{I}, \mathcal{J})$ as defined in (4.1). Let $w = (w_1, \cdots, w_N)$ be a target function such that for any $i \in \{1, \cdots, N\}$, w_i is a stationary solution on each road/edge I_i. We consider the system

$$\begin{cases} \partial_t \rho^i(t,x) + \partial_x f^i(\rho^i(t,x)) = 0, \quad (t,x) \in \mathbb{R}^+ \times I_i, \\ \rho^i(0,x) = \rho_0^i(x), \quad x \in I_i \\ \rho(t, j_i) \in \mathcal{G}^{J_i}(F_i), \quad t \in \mathbb{R}^+, \end{cases} \tag{7.2.7}$$

where j_i is the position of the junction J_i, $F_i \in \mathbb{R}^{n_i \times m_i}$ is the feedback controller applied at the junction J_i of the network and the germ $\mathcal{G}^{J_i}(F_i)$ is identified from a real-work junction (see Section (4.2.2) replacing D^i and S^i by $D^i_{F_i}$ and $S^i_{F_i}$). We have the following open-questions :

1. Can we construct N feedback controllers $F = (F_i)_{i=1,\cdots,N}$ that stabilize (7.2.7) around the target function w, i.e for any initial data $\rho_0 = (\rho_0^1, \cdots, \rho_0^N)$, the $\mathcal{G}$-solutions $\rho(t,\cdot)$ of (7.2.7) converges to $w(\cdot)$ in $(L^1(0,L))^N$ as $t \to \infty$.
2. If we only have a limited number of controllers, can we find their optimal locations so as to steer the $\mathcal{G}$-solutions $\rho(t,\cdot)$ of (7.2.7) as close as possible to $w(\cdot)$ in $(L^1(0,L))^N$ as $t \to \infty$?
3. Can we replace the first-order equation LWR by the second order GARZ in (7.2.7)?

The target function can be either a classical shock (ρ_L, ρ_R) with $f(\rho_L) = F(\rho_R)$ and $\rho_L < \rho_R$ or a constant function. We denote by $\mathcal{S} = (\mathcal{S}_1, \cdots, \mathcal{S}_n)$ the finite set of possible stationary solutions of (7.2.7). We can choose a target function that solves the following optimization problem

$$\min_{w=(w_1,\cdots,w_n) \in \mathcal{S}} \sum_{i \in J} \int_{a_i}^{b_i} \mathcal{F}(w(x))\, dx \tag{7.2.8}$$

where J is a subset of $\{1, \cdots, N\}$ and $\mathcal{F}$ may represent the total travel time, the pollution or the congestion. For instance, in (6.1.3), the cost function $\mathcal{F}$ stands for total fuel consumption and in [14] the cost function $\mathcal{F}$ stands for road evacuation in an urban environment. In [71], the feedback controllers depend on the number of vehicles on the road, an observation that can be reconstructed using pneumatic road tubes.

Open problem 2 : optimal control problem on road networks using AVs.
We want to dissipate a traffic jam or reduce pollution through the use of controlled autonomous vehicles operating on a network $(\mathcal{I}, \mathcal{J})$ defined in (4.1). We consider the following system

$$\begin{cases} \partial_t \rho^i(t,x) + \partial_x f^i(\rho^i(t,x)) = 0, \quad (t,x) \in \mathbb{R}^+ \times I_i, \\ \rho^i(0,x) = \rho_0^i(x), \quad x \in I_i \\ f\left(\rho^{i(k)}(t, y_k(t))\right) - \dot{y}_k(t) \rho^{i(k)}(t, y_k(t)) \le F_\alpha\left(\dot{y}_k(t)\right), \quad t \in \mathbb{R}_+,\, k = 1, \cdots, N \\ \dot{y}_k(t) = \min\{V_k(t), v(\rho^{i(k)}(t, y_k(t)+))\}, \quad t \in \mathbb{R}_+,\, k = 1, \cdots, N, \\ y_k(0) = y_k^0, \quad k = 1, \cdots, N, \\ \rho(t, j_k) \in \mathcal{G}^{J_k}(F^k), \quad t \in \mathbb{R}^+, \quad k = 1, \cdots, N, \end{cases} \tag{7.2.9}$$

where $(y_k)_{i=k,\cdots,N}$ stands for the trajectory of N autonomous vehicles, the function $F_\alpha(\dot{y}_k(t))$ with $\alpha \in (0,1)$ stands for the maximal road capacity reduction due to the presence of the k^{th} autonomous vehicle, $i(k)$ denotes the index of the road on which the autonomous vehicle is operating and the controller V_k is the maximum speed of the k^{th} AV. We assume that each autonomous vehicle follows a predefined route through the network. We have the following optimization problem

$$\inf_{\substack{(V_i)_{i=1,\cdots,N}\in[0,V_{\max}]^N \\ \|V_i\|_{BV}\leq C}} J(V) = \sum_{i\in J}\int_0^{T_f}\int_{a_i}^{b_i}\mathcal{F}(\rho^i(t,x))dtdx, \tag{7.2.10}$$

where J is a subset of $\{1,\cdots,N\}$, $(\rho, y_1,\cdots,y_N)$ is the solution of (7.2.9) associated to $(\rho_0, y_1^0,\cdots,y_N^0)$ and $\mathcal{F}$ may represent the total travel time, the pollution or the congestion. Solving the optimization problem (7.2.10) leads to the following open-questions :

1. Can we prove existence of solutions for (7.2.9)?
2. Can we solve the optimization problem (7.2.10)? Existence? optimality conditions?

To prove existence of solutions for (7.2.9), we must account for interactions between AVs. The authors in [52] analyze such interactions on a highway and show, in particular, that two non-classical shocks cannot interact. To prove the convergence of the approximate solutions (ρ^n, y^n), constructed using wave-front tracking method, to the solution (ρ, y), we must modify the total variation functional (3.1.2) to account for the new waves generated by AV interactions, which is essential for establishing Lemma 3.1.1. We also need to analyze the interactions between the autonomous vehicles and the network junctions. To this end, we select as the road Riemann solver RS_{road} the moving-constrained Riemann solver introduced in Section 3.1, and then apply the strategy described in Section 4.1.

Since ρ^i may develop discontinuities in finite time, the cost function in (7.2.10) is not differentiable with respect to V (see [74] or Section 6.1). To get first-order optimality conditions, the derivative of the cost function J_0 in $(\mathcal{O}_T)$ can be regarded in a weak sense by requiring strong conditions on the set of initial data as in [16, 17, 20, 21]. We may also apply a spatial semi-discretization of the LWR equation on each road to make the cost functional J differentiable and use an adjoint-based method as in [14]. Nevertheless, directly tackling the optimization problem (7.2.10) remains challenging. Another approach consists in learning near-optimal decision-making strategies through interactions with an environment. More precisely, the agents are the autonomous vehicles, the environment is the network model (4.1), the actions correspond to the vehicles' speeds, the states are given by the vehicles' positions and the traffic densities on the network roads, and the reward is defined by the cost functional J. Our objective is to combine reinforcement learning methodologies with mathematical analysis in order to extract explicit feedback controllers, as proposed in [1]. We can then compare the efficiency of the feedback controllers constructed in Open Problems 1 and 2 when the cost function in (7.2.8) and (7.2.10) represent the same objective, such as pollution reduction or travel time minimization.

Bibliography

[1] Kala Agbo Bidi, Jean-Michel Coron, Amaury Hayat, and Nathan Lichtlé. A novel approach to feedback control with deep reinforcement learning. *Systems and Control Letters*, 202:106102, August 2025.

[2] Navid Allahverdi, Alejandro Pozo, and Enrique Zuazua. Numerical aspects of large-time optimal control of burgers equation. *ESAIM: Mathematical Modelling and Numerical Analysis*, 50(5):1371–1401, 2016.

[3] Juan J Alonso and Michael R Colonno. Multidisciplinary optimization with applications to sonic-boom minimization. *Annual Review of Fluid Mechanics*, 44:505–526, 2012.

[4] Boris Andreianov, Paola Goatin, and Nicolas Seguin. Finite volume schemes for locally constrained conservation laws. *Numerische Mathematik*, 115(4):609–645, 2010.

[5] Boris Andreianov, Kenneth H. Karlsen, and Nils Henrik Risebro. A theory of l^1-dissipative solvers for scalar conservation laws with discontinuous flux. *Archive for Rational Mechanics and Analysis*, 201(1):27–86, 2011.

[6] A. Aw, A. Klar, M. Rascle, and T. Materne. Derivation of continuum traffic flow models from microscopic follow-the-leader models. *SIAM Journal on Applied Mathematics*, 63(1):259–278, 2002.

[7] A. Aw and M. Rascle. Resurrection of "second order" models of traffic flow. *SIAM Journal on Applied Mathematics*, 60(3):916–938, 2000.

[8] Nail Baloul, Amaury Hayat, Thibault Liard, and Pierre Lissy. Traffic Flow Reconstruction from Limited Collected Data. accepted to 2025 IEEE 64th Conference on Decision and Control (CDC), 2025.

[9] M. Bando, K. Hasebe, A. Nakayama, A. Shibata, and Y. Sugiyama. Dynamical model of traffic congestion and numerical simulation. *Phys. Rev. E*, 51:1035–1042, Feb 1995.

[10] Matthieu Barreau, Miguel Aguiar, John Liu, and Karl Henrik Johansson. Physics-informed learning for identification and state reconstruction of traffic density. In *2021 60th IEEE Conference on Decision and Control (CDC)*, pages 2653–2658, 2021.

[11] Matthieu Barreau, John Liu, and Karl Henrik Johansson. Learning-based state reconstruction for a scalar hyperbolic PDE under noisy lagrangian sensing. In *Proceedings of the 3rd Conference on Learning for Dynamics and Control*, volume 144 of *Proceedings of Machine Learning Research*, pages 34–46. PMLR, 07 – 08 June 2021.

[12] Georges Bastin and Jean-Michel Coron. *Stability and boundary stabilization of 1-d hyperbolic systems*, volume 88. Springer, 2016.

[13] Julian Berberich, Anne Koch, Carsten W. Scherer, and Frank Allgöwer. Robust data-driven state-feedback design. In *2020 American Control Conference (ACC)*, pages 1532–1538, 2020.

[14] Mickael Bestard, Emmanuel Franck, Laurent Navoret, and Yannick Privat. Optimal scenario for road evacuation in an urban environment. *Zeitschrift für angewandte Mathematik und Physik*, 75(146), 2024. Published: 16 July 2024.

[15] Sébastien Blandin, Xavier Litrico, Maria Laura Delle Monache, Benedetto Piccoli, and Alexandre Bayen. Regularity and lyapunov stabilization of weak entropy solutions to scalar conservation laws. *IEEE Transactions on Automatic Control*, 62(4):1620–1635, 2016.

[16] François Bouchut and François James. One-dimensional transport equations with discontinuous coefficients. *Nonlinear Analysis*, 32(7):891, 1998.

[17] François Bouchut and François James. Differentiability with respect to initial data for a scalar conservation law. In *Hyperbolic problems: theory, numerics, applications*, pages 113–118. Springer, 1999.

[18] A. Bressan. *Hyperbolic systems of conservation laws: the one-dimensional Cauchy problem.* Oxford university press, 2000.

[19] Alberto Bressan and Philippe G. Lefloch. Structural stability and regularity of entropy solutions to hyperbolic systems of conservation laws. *Indiana University Mathematics Journal*, 48(1):43–84, 1999.

[20] Alberto Bressan and Andrea Marson. A maximum principle for optimally controlled systems of conservation laws. *Rendiconti del Seminario Matematico della Universita di Padova*, 94:79–94, 1995.

[21] Alberto Bressan and Andrea Marson. A variational calculus for discontinuous solutions of systems of conservation laws. *Communications in partial differential equations*, 20(9):1491–1552, 1995.

[22] G. Bretti, M. Briani, and E. Cristiani. An easy-to-use algorithm for simulating traffic flow on networks: Numerical experiments. *Discrete and Continuous Dynamical Systems - Series S*, 7(3):379–394, 2014.

[23] M. Briani and E. Cristiani. An easy-to-use algorithm for simulating traffic flow on networks: Theoretical study. *Networks and Heterogeneous Media*, 9(3):519–552, 2014.

[24] Pierre Cardaliaguet. A microscopic derivation of a traffic flow model on a junction with two entry lines. *ESAIM: Mathematical Modelling and Numerical Analysis*, 59(4):2021–2054, 2025.

[25] Pierre Cardaliaguet, Nicolas Forcadel, and Régis Monneau. A class of germs arising from homogenization in traffic flow on junctions. *Journal of Hyperbolic Differential Equations*, 21(2):189–254, 2024.

[26] Carlos Castro, Francisco Palacios, and Enrique Zuazua. An alternating descent method for the optimal control of the inviscid burgers equation in the presence of shocks. *Mathematical Models and Methods in Applied Sciences*, 18(03):369–416, 2008.

[27] Carlos Castro, Francisco Palacios, and Enrique Zuazua. Optimal control and vanishing viscosity for the burgers equation. In *Integral Methods in Science and Engineering, Volume 2*, pages 65–90. Springer, 2010.

[28] Mladen Čičić and Karl Henrik Johansson. Traffic regulation via individually controlled automated vehicles: a cell transmission model approach. In *2018 21st International Conference on Intelligent Transportation Systems (ITSC)*, pages 766–771. IEEE, 2018.

[29] Robin Olav Cleveland. *Propagation of sonic booms through a real, stratified atmosphere.* PhD thesis, Citeseer, 1995.

[30] G. M. Coclite, M. Garavello, and B. Piccoli. Traffic flow on a road network. *SIAM Journal on Mathematical Analysis*, 36(6):1862–1886, 2005.

[31] R. M. Colombo and P. Goatin. A well posed conservation law with a variable unilateral constraint. *J. Differential Equations*, 234(2):654–675, 2007.

[32] Rinaldo M Colombo and Vincent Perrollaz. Initial data identification in conservation laws and hamilton–jacobi equations. *Journal de Mathématiques Pures et Appliquées*, 138:1–27, 2020.

[33] Jean-Michel Coron. *Control and nonlinearity*, volume 136 of *Mathematical Surveys and Monographs.* American Mathematical Society, Providence, RI, 2007.

[34] Jean-Michel Coron, Sylvain Ervedoza, Shyam Sundar Ghoshal, Olivier Glass, and Vincent Perrollaz. Dissipative boundary conditions for $2\times$ 2 hyperbolic systems of conservation laws for entropy solutions in bv. *Journal of Differential Equations*, 262(1):1–30, 2017.

[35] Emiliano Cristiani and Smita Sahu. On the micro-to-macro limit for first-order traffic flow models on networks, 2016.

[36] Shumo Cui, Benjamin Seibold, Raphael Stern, and Daniel B. Work. Stabilizing traffic flow via a single autonomous vehicle: Possibilities and limitations. In *IV 2017 - 28th IEEE Intelligent Vehicles Symposium*, IEEE Intelligent Vehicles Symposium, Proceedings, pages 1336–1341. Institute of Electrical and Electronics Engineers Inc., July 2017.

[37] Constantine M Dafermos. Polygonal approximations of solutions of the initial value problem for a conservation law. *Journal of Mathematical Analysis and Applications*, 38:33 – 41, 1972.

[38] Constantine M. Dafermos. *Hyperbolic Conservation Laws in Continuum Physics*, volume 325 of *Grundlehren der Mathematischen Wissenschaften*. Springer-Verlag, Berlin, 4 edition, 2016.

[39] Maria Laura Delle Monache and Paola Goatin. Scalar conservation laws with moving constraints arising in traffic flow modeling: an existence result. *Journal of Differential equations*, 257(11):4015–4029, 2014.

[40] Maria Laura Delle Monache, Thibault Liard, Benedetto Piccoli, Raphael Stern, and Dan Work. Traffic reconstruction using autonomous vehicles. *SIAM Journal on Applied Mathematics*, 79(5):1748–1767, 2019.

[41] Maria Laura Delle Monache, Thibault Liard, Anaïs Rat, Raphael Stern, Rahul Bhadani, Benjamin Seibold, Jonathan Sprinkle, Daniel B. Work, and Benedetto Piccoli. *Feedback Control Algorithms for the Dissipation of Traffic Waves with Autonomous Vehicles*, pages 275–299. Springer Optimization and Its Applications. Springer International Publishing, 2019. Publisher Copyright: © Springer Nature Switzerland AG 2019.

[42] M. Di Francesco and M. D. Rosini. Rigorous derivation of nonlinear scalar conservation laws from follow-the-leader type models via many particle limit. *Arch. Rational Mech. Anal.*, 225:129–166, 2017.

[43] Carlos Esteve and Enrique Zuazua. The inverse problem for hamilton–jacobi equations and semiconcave envelopes. *SIAM Journal on Mathematical Analysis*, 52(6):5627–5657, 2020.

[44] Shimao Fan, Michael Herty, and Benjamin Seibold. Comparative model accuracy of a data-fitted generalized aw-rascle-zhang model. *Networks and Heterogeneous Media*, 9(2):239–268, 2014.

[45] M. Di Francesco, S. Fagioli, and M. D. Rosini. Many particle approximation of the Aw–Rascle–Zhang second order model for vehicular traffic. *Mathematical Biosciences and Engineering*, 14(1):127–141, 2017.

[46] Marco Di Francesco and Graziano Stivaletta. Convergence of the follow-the-leader scheme for scalar conservation laws with space dependent flux, 2020.

[47] José Ramón Domínguez Frejo and Eduardo Fernández Camacho. Global versus local mpc algorithms in freeway traffic control with ramp metering and variable speed limits. *IEEE Transactions on Intelligent Transportation Systems*, 13(4):1556–1565, 2012.

[48] Mauro Garavello, Paola Goatin, Thibault Liard, and Benedetto Piccoli. A multiscale model for traffic regulation via autonomous vehicles. *Journal of Differential Equations*, 2020.

[49] Mauro Garavello and Benedetto Piccoli. *Traffic flow on networks*, volume 1. American institute of mathematical sciences Springfield, 2006.

[50] Denos C. Gazis, Robert Herman, and Richard W. Rothery. Nonlinear follow-the-leader models of traffic flow. *Operations Research*, 9(4):545–567, 1961.

[51] P. Goatin, S. Göttlich, and O. Kolb. Speed limit and ramp meter control for traffic flow networks. *Engineering Optimization*, 48(7):1121–1144, July 2016.

[52] Paola Goatin, Chiara Daini, Maria Laura Delle Monache, and Antonella Ferrara. Interacting moving bottlenecks in traffic flow. *Networks and Heterogeneous Media*, 18(2):930–945, 2023.

[53] G. Gomes and R. Horowitz. Optimal freeway ramp metering using the asymmetric cell transmission model. *Transportation Research Part C: Emerging Technologies*, 14(4):244–262, 2006.

[54] Laurent Gosse and Enrique Zuazua. Filtered gradient algorithms for inverse design problems of one-dimensional burgers equation. In *Innovative algorithms and analysis*, pages 197–227. Springer, 2017.

[55] S. Göttlich, M. Herty, and U. Ziegler. Modeling and optimizing traffic light settings in road networks. *Computers & Operations Research*, 55:36–51, March 2015.

[56] S. Göttlich and U. Ziegler. Traffic light control: A case study. *Discrete and Continuous Dynamical Systems - Series S*, 7:483–501, 2014.

[57] Amaury Hayat, Thibault Liard, and Benedetto Piccoli. A multiscale second order model for the interaction between AV and traffic flows: analysis and existence of solutions. Preprint, January 2025.

[58] Amaury Hayat, Benedetto Piccoli, and Sydney Truong. Dissipation of traffic jams using a single autonomous vehicle on a ring road. *SIAM Journal on Applied Mathematics*, 83(3):909–937, 2023.

[59] J. C. Herrera, D. B. Work, R. Herring, X. J. Ban, Q. Jacobson, and A. M. Bayen. Evaluation of traffic data obtained via gps-enabled mobile phones: The mobile century field experiment. *Transportation Research Part C: Emerging Technologies*, 18(4):568–583, 2010.

[60] Juan C. Herrera and Alexandre M. Bayen. Incorporation of lagrangian measurements in freeway traffic state estimation. *Transportation Research Part B: Methodological*, 44(4):460–481, 2010.

[61] M. Herty and A. Klar. Modeling, simulation, and optimization of traffic flow networks. *SIAM Journal on Scientific Computing*, 25(3):1066–1087, 2003.

[62] H. Holden and N. H. Risebro. The continuum limit of follow-the-leader models — a short proof. *SIAM Journal on Mathematical Analysis*, 51(2):1771–1786, 2019.

[63] D. Inzunza and P. Goatin. A pinn approach for traffic state estimation and model calibration based on loop detector flow data. In *8th International Conference on Models and Technologies for Intelligent Transportation Systems (MT-ITS)*, pages 1–6, 2023.

[64] D. Jacquet, C. C. de Wit, and D. Koenig. Optimal ramp metering strategy with extended lwr model, analysis and computational methods. In *Proceedings of the 16th IFAC World Congress*, pages 100–104, Prague, 2005. IFAC.

[65] Stanislav N Kružkov. First order quasilinear equations in several independent variables. *Mathematics of the USSR-Sbornik*, 10(2):217, 1970.

[66] Jean-Patrick Lebacque. The godunov scheme and what it means for first order traffic flow models. In Jeffrey B. Lesort, editor, *Proceedings of the 13th International Symposium on Transportation and Traffic Theory*, pages 647–677, Lyon, France, 1996. Pergamon.

[67] Jean-Patrick Lebacque and M. Khoshyaran. First order macroscopic traffic flow models for networks in the context of dynamic assignment. In Michael Patriksson and Kurt A. P. M. Labbe, editors, *Transportation Planning State of the Art*, pages 119–140. Kluwer Academic Publishers, Norwell, MA, 2002.

[68] Jean-Patrick Lebacque and M. M. Khoshyaran. Modelling vehicular traffic flow on networks using macroscopic models. In R. Vilsmeier, F. Benkhaldoun, and D. Hanel, editors, *Finite Volumes for Complex Applications II*, pages 551–558. Hermes Science Publications, Paris, France, 1999.

[69] Hugo Lhachemi, Christophe Prieur, and Emmanuel Trélat. Pi regulation of a reaction–diffusion equation with delayed boundary control. *IEEE Transactions on Automatic Control*, 66:1573–1587, 2021.

[70] Thibault Liard, Ismaïla Balogoun, Swann Marx, and Franck Plestan. Boundary sliding mode control of a system of linear hyperbolic equations: A lyapunov approach. *Automatica*, 135:109964, 2022.

[71] Thibault Liard and Vincent Perrollaz. Stabilization of conservation laws for g-solutions with application to traffic flow. *Work in progress.*

[72] Thibault Liard and Benedetto Piccoli. Well-posedness for scalar conservation laws with moving flux constraints. *SIAM Journal on Applied Mathematics*, 79(2):641–667, 2019.

[73] Thibault Liard and Benedetto Piccoli. On entropic solutions to conservation laws coupled with moving bottlenecks. *Accepted to Communications in Mathematical Sciences*, 2020.

[74] Thibault Liard, Raphael Stern, and Maria Laura Delle Monache. A pde-ode model for traffic control with autonomous vehicles. *Networks and Heterogeneous Media*, 18(3):1190–1206, 2023.

[75] Thibault Liard and Enrique Zuazua. Initial data identification for the one-dimensional burgers equation. *IEEE Transactions on Automatic Control*, 67(6):3098–3104, 2022.

[76] Thibault Liard and Enrique Zuazua. Analysis and numerical solvability of backward-forward conservation laws. *SIAM Journal on Mathematical Analysis*, 55(3):1949–1968, 2023.

[77] M. J. Lighthill and G. B. Whitham. On kinematic waves. ii. a theory of traffic flow on long crowded roads. *Proceedings of the Royal Society of London. Series A, Mathematical and Physical Sciences*, 229:317–345, 1955.

[78] M. L. Delle Monache, B. Piccoli, and F. Rossi. Traffic regulation via controlled speed limit. *SIAM Journal on Control and Optimization*, 55(5):2936–2958, 2017.

[79] Régis Monneau. Structure of Riemann solvers on networks. Manuscript in preparation, 2025.

[80] E. Moulay and W. Perruquetti. Finite time stability of nonlinear systems. In *42nd IEEE International Conference on Decision and Control (IEEE Cat. No.03CH37475)*, volume 4, pages 3641–3646 vol.4, 2003.

[81] A. Muralidharan and R. Horowitz. Optimal control of freeway networks based on the link node cell transmission model. In *Proceedings of the American Control Conference (ACC)*, pages 5769–5774. IEEE, 2012.

[82] Vincent Perrollaz. Asymptotic stabilization of entropy solutions to scalar conservation laws through a stationary feedback law. In *Annales de l'IHP Analyse non linéaire*, volume 30, pages 879–915, 2013.

[83] Vincent Perrollaz. Asymptotic stabilization of stationnary shock waves using a boundary feedback law. *arXiv preprint arXiv:1801.06335*, 2018.

[84] Giulia Piacentini, Paola Goatin, and Antonella Ferrara. Traffic control via moving bottleneck of coordinated vehicles. *IFAC-PapersOnLine*, 51(9):13–18, 2018.

[85] Rabie A Ramadan and Benjamin Seibold. Traffic flow control and fuel consumption reduction via moving bottlenecks. *arXiv preprint arXiv:1702.07995*, 2017.

[86] J. Reilly, W. Krichene, M. L. D. Monache, S. Samaranayake, P. Goatin, and A. Bayen. Adjoint-based optimization on a network of discretized scalar conservation law pdes with applications to coordinated ramp metering. *Journal of Optimization Theory and Applications*, 167:733–760, 2015.

[87] Paul I. Richards. Shock waves on the highway. *Operations Research*, 4:42–51, 1956.

[88] Walter Rudin. *Functional analysis, 2nd edition.* McGraw-Hill, 1991.

[89] Toru Seo, Alexandre M. Bayen, Takahiko Kusakabe, and Yasuo Asakura. Traffic state estimation on highway: A comprehensive survey. *Annual Reviews in Control*, 43:128–151, 2017.

[90] R. Shi, Z. Mo, K. Huang, X. Di, and Q. Du. A physics-informed deep learning paradigm for traffic state and fundamental diagram estimation. *IEEE Transactions on Intelligent Transportation Systems*, 2021.

[91] Raphael E Stern, Shumo Cui, Maria Laura Delle Monache, Rahul Bhadani, Matt Bunting, Miles Churchill, Nathaniel Hamilton, Hannah Pohlmann, Fangyu Wu, Benedetto Piccoli, et al. Dissipation of stop-and-go waves via control of autonomous vehicles: Field experiments. *Transportation Research Part C: Emerging Technologies*, 89:205–221, 2018.

[92] Yuki Sugiyama, Minoru Fukui, Macoto Kikuchi, Katsuya Hasebe, Akihiro Nakayama, Katsuhiro Nishinari, Shin-ichi Tadaki, and Satoshi Yukawa. Traffic jams without bottlenecks—experimental evidence for the physical mechanism of the formation of a jam. *New Journal of Physics*, 10(3):033001, mar 2008.

[93] Shin-ichi Tadaki, Macoto Kikuchi, Minoru Fukui, Akihiro Nakayama, Katsuhiro Nishinari, Akihiro Shibata, Yuki Sugiyama, Taturu Yosida, and Satoshi Yukawa. Phase transition in traffic jam experiment on a circuit. *New Journal of Physics*, 15(10):103034, oct 2013.

[94] Liudmila Tumash, Carlos Canudas-de Wit, and Maria Laura Delle Monache. Boundary control design for traffic with nonlinear dynamics. *IEEE Transactions on Automatic Control*, 67(3):1301–1313, 2022.

[95] Fangyu Wu, Raphael Stern, Miles Churchill, Maria Laura Delle Monache, Ke Han, Benedetto Piccoli, and Daniel B Work. Measuring trajectories and fuel consumption in oscillatory traffic: experimental results. In *TRB 96th Annual Meeting Compendium of Papers*, page 14, Washington, DC, United States, January 2017.

[96] H. M. Zhang. A non-equilibrium traffic model devoid of gas-like behavior. *Transportation Research Part B: Methodological*, 36(3):275–290, March 2002.

[97] A. K. Ziliaskopoulos. A linear programming model for the single destination system optimum dynamic traffic assignment problem. *Transportation Science*, 34(1):37–49, 2000.